NORTHWESTERN UNIVERSITY

Building and Crack Response to Blasting, Construction Vibrations and Weather Effects

A Thesis

Submitted to the Graduate School in Partial Fulfillment of the Requirements

For the Degree

MASTER OF SCIENCE

Field of Civil and Environmental Engineering

By

Pierre-Alexandre Abeel

Evanston, IL

December 2012

TABLE OF CONTENTS

ACKNOWLEDGEMENTS

This thesis is the result of collaborative work amongst several individuals who deserve much more than a simple acknowledgement. Without the assistance of these gracious and patient people, this project could not have been accomplished.

First and foremost, I would like to thank my advisor, Professor Charles Dowding, for his guidance, expertise, support, and motivation, without which this thesis would certainly not have been possible. I would also like to thank Professor Richard Finno and Professor Giuseppe Buscarnera for their geotechnical instruction, as well as the rest of the faculty for allowing me to pursue my degree at Northwestern University.

I would like to extend a special thanks to Dr. Catherine Aimone-Martin of the New Mexico Institute of Mining and Technology for her extraordinary assistance and patience throughout the entire scope of the projects presented here.

The long-term financial support of the Infrastructure Technology Institute, funded by a block grant from the U.S. Department of Transportation, is also gratefully acknowledged. I must thank the ITI staff members, particularly Dave Kosnik, Mat Kotowski, and Dan Marron for their technical support and incredible patience.

I would also like to thank my fellow geotechnical graduate students and dear friends at Northwestern University for taking me in and helping me get through many evenings in the office.

Above all else, a final thanks to my parents and family for being the best support anyone could ever wish for.

ABSTRACT

This thesis summarizes the findings from two new developments of the Autonomous Crack Monitoring [ACM] research effort, along with an example of further development of techniques to estimate strains through use of 3D models.

The ACM studies compare micro-inch crack response to construction vibrations with those induced by climatological effects. One study in Illinois compares blast induced response with climatological response over a two year period, while the other in New Mexico compares response of an adobe structure to heavy vibratory road compaction with daily temperature response. Specialized instrumentation was employed to measure the response of a 5-story building to contiguous blasting and 3D model simulation was employed to estimate the imposed strains.

Measurements and analysis show that crack response to climatological variation is overwhelmingly larger than that produced by blast or construction induced vibrations. Seasonal variations, weather fronts passing or even turning the house heating off can produce crack response that is larger by an order of magnitude. Occupant activity and wind gusts can produce crack response as large as that produced by blast or construction induced vibrations.

Despite high particle velocity excitation, blasting immediately adjacent and below large buildings does not induce large responses. These low responses are likely a result of the ultra-high excitation frequencies. Low responses thus result in low shear strains as calculated with 3D models.

LIST OF FIGURES

LIST OF TABLES

Chapter I – INTRODUCTION

This thesis summarizes findings from two differing approaches to assessing response of structures to construction induced vibrations: micro-inch crack response and strains induced in structures. The micro-inch crack response measurements were facilitated through the Autonomous Crack Monitoring (ACM) system. While the instrumented structures differed in location construction, and source of vibrations, they both involved comparison of micro-inch crack response to the construction vibrations to that produced by climatological effects. The Illinois wood frame structure was subjected to aggregate quarry blasting vibrations while the New Mexico adobe structure was subjected to heavy roller compaction induced ground motions.

The strain study leveraged building response data obtained through the use of specialized instrumentation. This study was unique because of its construction, excavation of contiguous rock. The structure was a 5 story, load bearing masonry wall building where rock was excavated some 10s of feet adjacently below. Special, reusable transducers were employed to measure the "in-rock" motions to allow amplification to be calculated in a fashion employed in more rural studies.

Responses of the Sycamore Illinois house have been measured for more than two years and are presented and analyzed in Chapter II. The same transducers that monitor long-term, climatologically induced micro-inch crack response also measure dynamic responses induced by blast induced ground motions, occupant activities and wind gusts. The two-story house has been expanded several times, is founded on an irregular basement, framed in wood and clad with wood siding and clapboard. The unusually long monitoring period allows observation of two maximum, climatologically induced peak crack responses, and as such represents one of the longest periods of continuous observation in the literature. These once a year peak climatological responses are compared with unusually intensive ground motions in excess of that allowed by regulation. Intense

ground motions were legally possible because the test house is owned by the quarry and located on the quarry property. These comparisons show that climatic and environmental variations cause greater crack response than ground motions that exceed regulatory limits.

The response of the Albuquerque, New Mexico house to construction vibrations during road compaction was recorded and analyzed in terms of structure displacements, wall strains and micro inch crack displacement response. Results are presented in Chapter III. The purpose of this study is to evaluate the impact of construction activities using compaction vibratory rollers on wall cracking potential in an 80 year old native adobe house, and compare this with the cracking potential from the influence of long-term changes in weather. The hose is a slab on grade structure with adobe brick walls coated on the outside with stucco. A comparison is made of the construction-induced dynamic crack displacements with displacements induced by changes in temperature and humidity expected to take place in the house.

Chapter IV presents the dynamic response of a 5-story building to very-high frequency excitation from blasting vibrations originating from immediately adjacent rock excavation. The building was constructed in the early 1900s and is composed of a 3-wythe load-bearing exterior brick wall. The blast excavated rock is a metamorphic. Geophones located in the rock and on the structure are used to measure the dynamic displacement response of the building to blasting. Structural response was compared to rock motions to determine if there any unusual amplification of the rock motion. A 3D model is used to compute inter floor drift displacements and the resulting inter story strains employing three differing methods of idealized displacement excitation. These inter story strains were then compared with the gross building strain.

Chapter II – Long Term Field Measurement Of Micro-Inch Crack Response To Climatological And Blast Vibration Induced Effects

Introduction

This chapter presents structural response and the resulting crack response of a two-story residential structure situated on the property of an aggregate quarry in Sycamore, Illinois. It is part of an ongoing research project on Autonomous Crack Monitoring [ACM] at the Infrastructure Technology Institute [ITI] at Northwestern University in Evanston, IL, and expands the work presented in the Installation Report (Meissner, 2010).

Focus of study

This chapter compares the structural response and resulting crack response produced by:

- Ground motions from blasting
- Environmental conditions (weekly and long-term changes in temperature and humidity)
- Occupant activity
- Wind gusts

The instrumented house is a two-story wood-framed structure with a basement foundation. It is located approximately 300 feet (91m) away from the edge of the blasting zone of Vulcan Material, Co. Sycamore #397 Quarry. The house and its location are shown in Figure II-1.

The ITI research engineering group installed the wired eDAQ system on June 16th and June 17th, 2010. Data collection began on July 2nd, 2010, and has continued since. The air overpressure

transducer and the indoor temperature and humidity gauge were installed on July 21st, 2010. The air overpressure transducer did not begin recording properly until November of 2010.

During the study period (from July 1st, 2010 to October 27th, 2012), the quarry generated blasts 36 times. Table II-1 describes the blast vibration environment. Blasts were initiated at varying distances from the house: between 300ft and 1400ft (90- 425m) away. These distances were evaluated by triangulation using distances between the blasts and surrounding houses, provided by Vulcan Materials.

On some occurrences (indicated in Table II-1 by a star), data were not recorded by the ITI system. However, Vulcan Materials compliance monitoring would have recorded ground motions where necessary.

Figure II-1 - Overall view of Vulcan Materials, CO. Sycamore Quarry and photograph and location of the instrumented house

Date	Recorded PPV (in/s)			Distance to blast (ft)	Air blast		Crack response (μin)		
	[L]	[T]	[V]		[10^-4 psi]	[dB SPL]	Shear	Seam	Ceiling
09/01/10	0.108	0.134	0.239	1200	-	-	53	59	215
09/13/10	0.172	0.16	0.262	1300	-	-	82	82	427
09/20/10	0.157	0.12	0.219	1300	-	-	255	84	459
09/22/10 (*)	-	-	-	-	-	-	47	54	205
09/30/10	0.389	0.307	0.371	1300	-	-	401	242	509
10/08/10	0.452	0.34	0.636	900	-	-	274	211	444
10/19/10	0.16	0.128	0.224	1400	-	-	218	102	76
04/20/11	1.341	0.491	0.976	400	48.2	127.6	1120	532	486
04/22/11	0.817	0.792	0.646	300	50.2	128.0	2050	448	1260
05/11/11	0.197	0.189	0.201	600	27.2	122.7	154	86	201
05/19/11	0.516	0.523	0.417	400	34.4	124.7	807	439	1094
05/26/11	1.642	0.905	0.797	700	33.1	124.4	3277	1666	2162
06/03/11	0.454	0.275	0.301	1200	30.3	123.6	283	213	567
06/15/11 (*)	-	-	-	-	-	-	-	-	-
06/30/11	0.61	0.529	0.389	900	31.7	124.0	387	243	648
07/12/11 (*)	-	-	-	-	-	-	-	-	-
07/22/11	-	-	-	-	-	-	-	-	-
08/02/11	0.701	0.758	0.741	-	23.4	121.4	253	329	3032
08/10/11 (*)	-	-	-	-	-	-	-	-	-
08/18/11 (*)	-	-	-	-	-	-	-	-	-
09/07/11 (*)	-	-	-	-	-	-	-	-	-
09/14/11	1.137	0.749	0.665	400	36.6	125.3	1107	550	2363
09/22/11 (*)	-	-	-	-	-	-	-	-	-
10/03/11 (*)	-	-	-	-	-	-	-	-	-
10/10/11	0.443	0.291	0.215	-	64.3	130.1	279	170	536
06/28/12	0.847	0.452	0.662	-	65.7	130.3	918	414	2125
07/17/12	1.011	0.750	0.554	-	40.8	126.2	591	382	1630
07/23/12	1.023	0.683	0.559	-	41.5	126.3	433	314	1812
07/27/12	0.760	0.465	0.730	-	52.6	128.4	754	284	946
08/13/12	0.514	0.507	0.752	-	63.4	130.0	335	324	1203
08/17/12	0.384	0.349	0.495	-	45.1	127.1	327	200	1135
08/18/12	0.570	0.367	0.373	-	30.4	123.6	495	256	797
08/27/12	0.719	0.621	0.539	-	42.5	126.5	580	515	1059
09/05/12	0.746	0.598	0.671	-	55.5	128.9	426	483	2108
09/19/12	0.614	0.539	0.638	-	100.0	134.0	413	387	1058
09/24/12	0.468	0.319	0.233	-	37.3	125.4	512	579	1141
Average	0.628	0.457	0.500	879	44	126	601	345	1061

Table II-1 - Characteristics of blasts producing the vibrations throughout the study period

Instrumentation

Structural and crack response is autonomously measured by the combination of sensors listed in Table II-2. The crack sensors are described in more detail in the section below. All the other sensors are described in the Installation Report (Meissner, 2010).

Although the house was equipped with both a wired and a wireless monitoring system, the present report is mainly based on data gathered from the wired system. Wireless response is documented in two ITI reports by Dowding et al. (2011).

The sensor installation plan is shown in Figure II-2. Photographs of the crack sensors in their context are also shown in Figure II-3. Details of the installation of the velocity transducers are documented in the Installation Report (Meissner, 2010).

Two types of data are recorded: long-term and dynamic:

- Long-term response is obtained by measuring crack response, temperature and humidity once every hour. These single points are the average of 1000 samples obtained in one second.
- Dynamic response is obtained by measuring crack response, ground and structural velocity, and air overpressure. These values are recorded at 1000 samples per second for 3 seconds when triggered during dynamic events above 0.1 in/s of amplitude, with a 0.5 second pre-trigger.

LVDT displacement sensors have been installed to monitor the in-plane responses of three cracks. Table II-2 also describes the locations, purposes and sensors used for each crack.

Sensor	Channel Name	Description/Location
Triaxal Geophone (buried)	Geo_L_1 Geo_T_2 Geo_V_3	Buried outside the house - south-east corner
Air Overpressure	Air_Blast_4	Located on the outside wall
Temperature and Humidity	InTemp_5 InHumid_6	Indoor climatic data
Linear Variable Differential Transformer (LVDT)	LVDT_9_Shear	Shear crack, South wall, 1st floor
	LVDT_10_Null	Null sensor, uncracked area adjacent to Shear crack
	LVDT_11_Seam	Addition Seam crack, South wall, 1st floor
	LVDT_12_Ceil	Ceiling crack, Bedroom ceiling, 2nd floor
Horizontal Wall Geophone	HG_13_Bot1f HG_14_Top1f HG_15_Top2f HG_16_MidW	Wall-mounted

Table II-2 - Description of sensors, channel designation and location

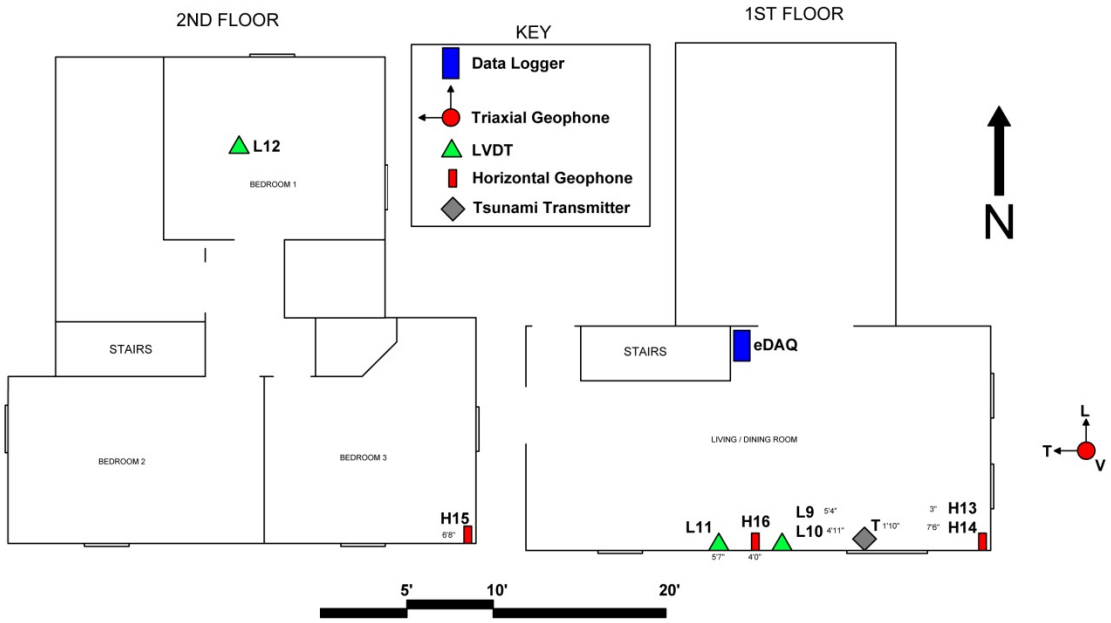

Figure II-2 - Exact sensor and equipment locations in the house

↑ **a - Close-up of ceiling crack monitored by LVDT_12**

← **b - Interior view of Node 3 in upstairs bedroom. Crack sensor connected to eKo Mote**

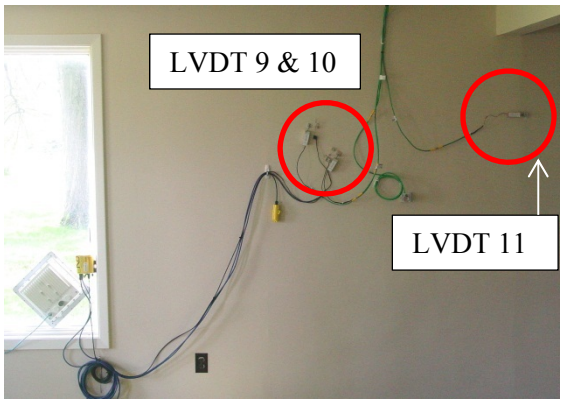

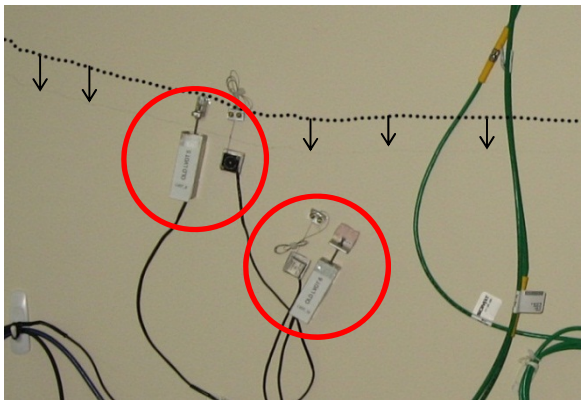

↑ **c - Overall view of sensor suite on south wall (first floor)**

↗ **d - Close-up of Shear crack monitored by LVDT_9 and Null gauge LVDT_10.**

→ **e - Close-up of Addition Seam Crack monitored by LVDT_11**

(NB : The crack paths are indicated by the offset parallel dotted lines)

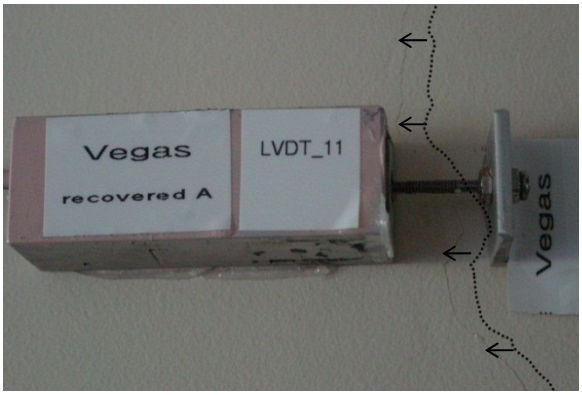

Figure II-3 - Overall views of the wall-mounted crack sensors

Crack response is the *change* in crack width, not total crack width, and is called *response* in this report. Figure II-4 (Siebert, 2000) illustrates this definition. All transducers have been installed so that positive response indicates crack opening and negative indicates crack closing. All measurements are made in micro-inches. A null sensor placed on an adjacent uncracked area provides a record of any drift or thermal effects on sensor metal or electronics. It has been shown that the null sensors' responses are small relative to the cracks' (Kosnik, 2008).

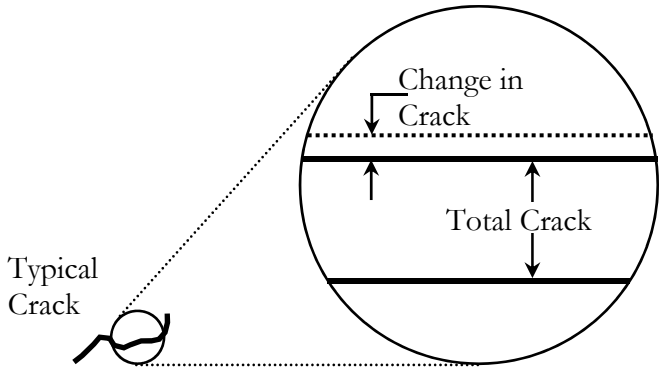

Figure II-4 - Crack response is change in crack width, not total crack width (Siebert, 2000)

RESULTS – CRACK RESPONSE

Long-term climatological effects

Long-term crack response is measured every hour as the average of a burst of 1000 sample in one second. This hourly data is represented by the red, highly variable line in Figure II-5 and Figure II-6. The less variable blue line is a 24-hour central moving average (CMA) of the hourly data, which shows the response to weather fronts. The even less variable black line is a 30-day CMA of the hourly data, which shows the response to seasonal trends as it varies about the 2 year average green horizontal line.

Climatic responses are defined in Figure II-5 to clarify the time scales of these influences. Daily response is defined as the difference between the hourly data and the 24-hour CMA (red arrow). Frontal response is defined as the difference between the 24-hour CMA and the 30-day CMA (blue arrow). Seasonal response is the difference between the black, 30-day CMA curve and the green overall average curve (green arrow). Finally, the maximal response is the sum of the daily, frontal and seasonal effects, which is the difference between the red hourly data and the overall average curve (black arrow). The maximum values are presented in Table II-3.

Response (µin, zero-to-peak)	Shear crack	Null	Seam	Ceiling crack
Max Daily	3276	258	2791	1849
Max Frontal	3840	122	3459	5182
Max seasonal	10485	285	2757	9157
Maximal	12064	745	4861	11726

Table II-3 - Maximum crack response to weather effects (1µin=0.0254µm).
All measurements are zero-to-peak.

Figure II-5 presents a two months fragment of the whole project that will be seen again later in this chapter. Long-term response to date (28 months) is compared for all three cracks in Figure II-6 with indoor temperature and humidity.

The unusual longevity of this study (28 months) allows measurement and observation of yearly responses. As described elsewhere (Dowding, 2008), such long-term obersvations show the dominance of seasonal response, which produce the largest of the responses. The yearly maximum shown by the black arrows on Figure II-8 occurs once per year when all three factors (daily, frontal and seasonal) combine.

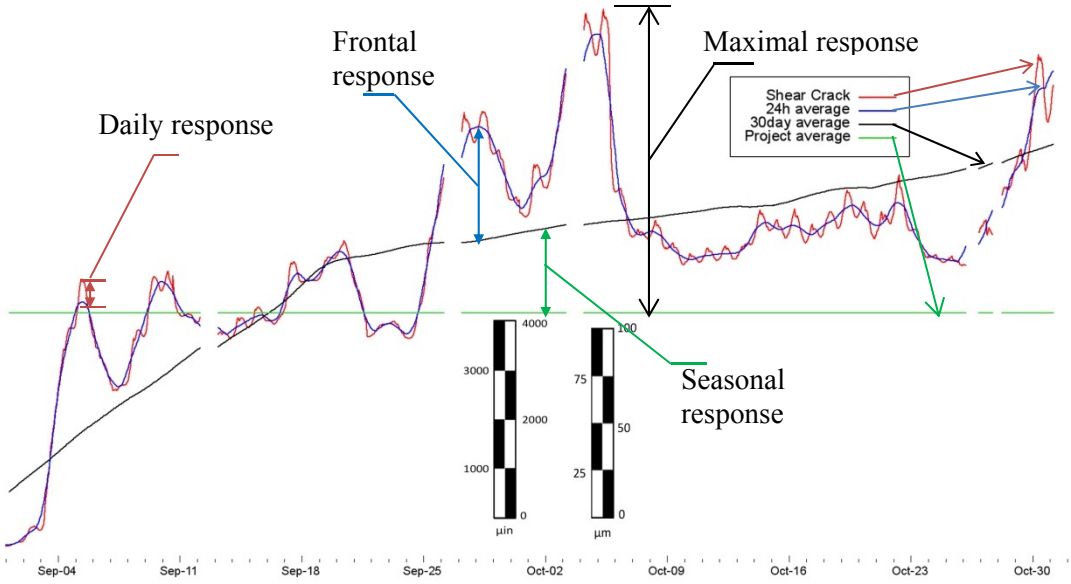

Figure II-5 - Crack response caused over the course of two months as shown in Figure II-6

Blast induced (dynamic) ground motion crack response

Table II-1 compares the zero-to-peak crack responses with the maximum peak particle velocities and the air overpressures over the course of the 28 month study. The ceiling crack response is larger than the south wall responses (shear and seam). This difference is a function of surface orientation with respect to vertical, location of the surface, construction details such as spacing of studs or joists, and construction materials (drywall, plaster, and lath). The seam has the least response with the thinnest crack width but located across a transition between an addition and the original structure.

Time histories for both crack and structural responses are presented in Figure II-7 for two blasts. The first (top graph) was recorded on September 20, 2010 with a maximum PPV of 0.219ips (5.6mm/s) in the vertical direction. The second (bottom graph) was recorded on May 19, 2011 with a maximum PPV of 0.523ips (13.3mm/s) in the transverse direction. The air blast was recorded only for the May event and is shown in the figure.

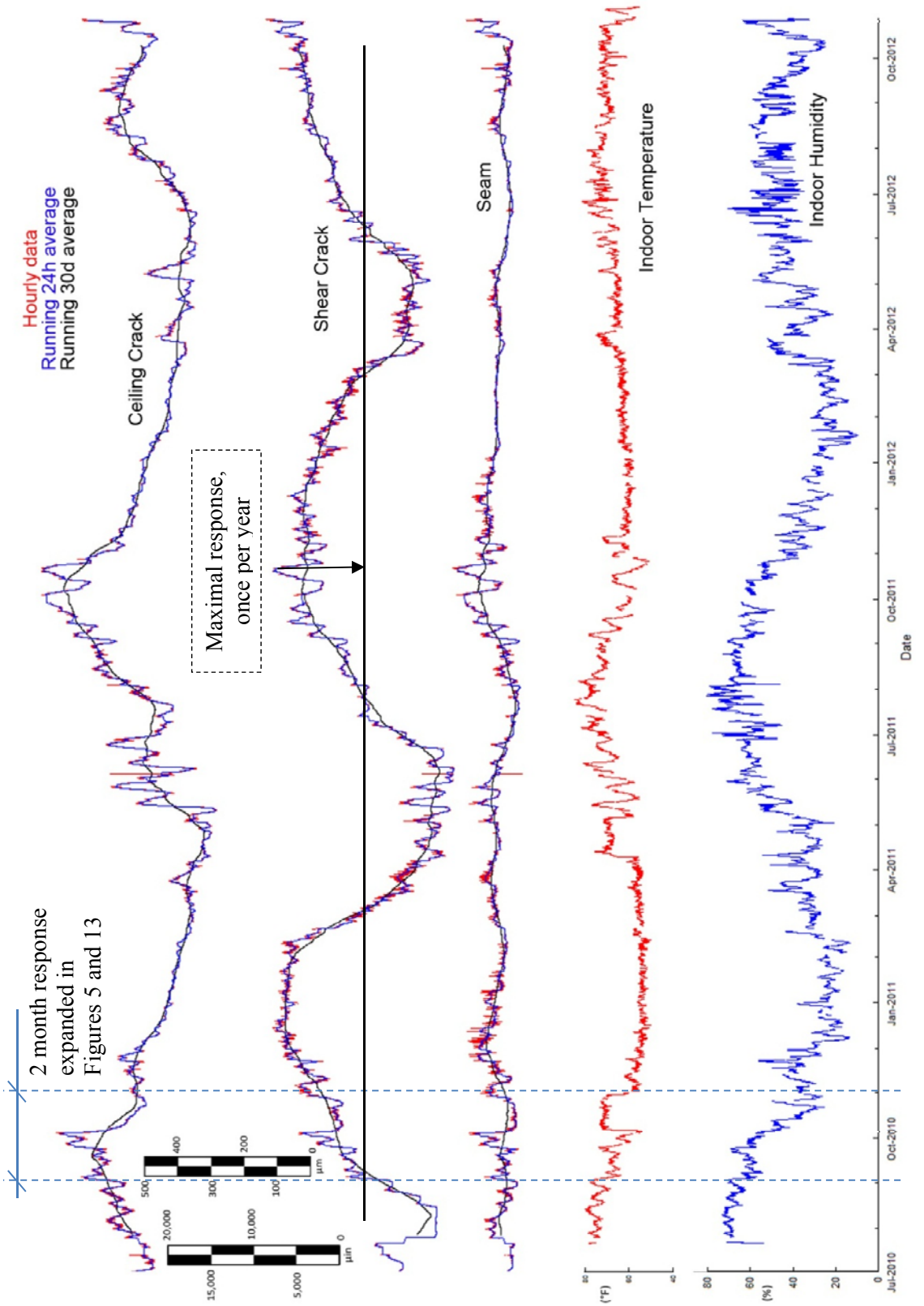

Figure II-6 – Comparison of the crack response with the variation in indoor temperature and humidity

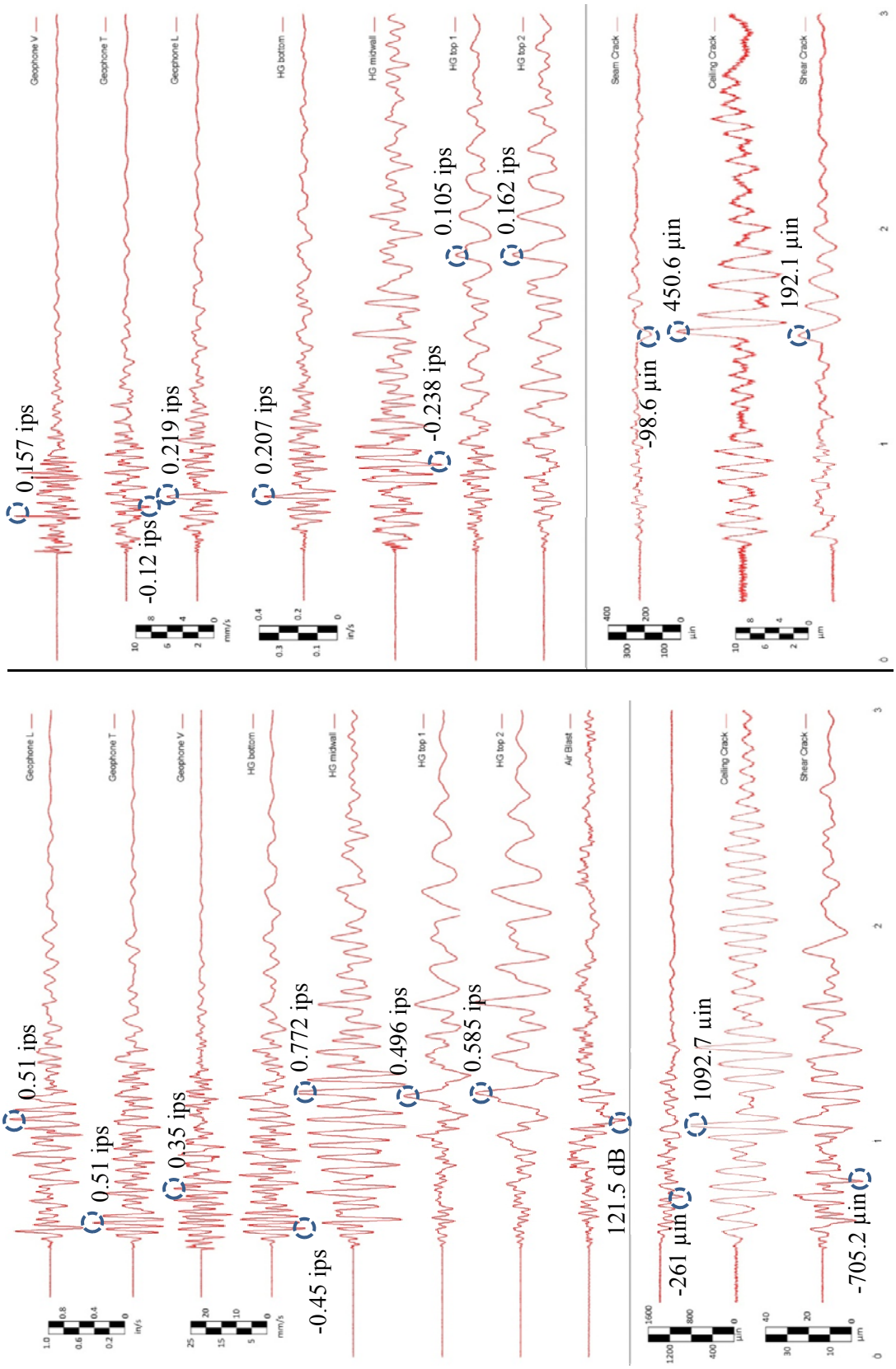

Figure II-7 - Structural and crack response time histories to blast events on Sep 20, 2010 (top) and May 19, 2011 (bottom). All measurements are zero-to-peak.

As shown in Figure II-8, the air overpressure can cause a significant crack response, especially when the ground vibrations are low. The late arrival of that air overpressure can even be responsible for a larger crack response than the ground vibrations themselves, as presented for the blast, on May 11, 2011 (Max PPV = 0.201 ips = 5.1 mm/s).

High PPVs in the ground are recorded because the house is located on mine property and will eventually be dismantled as the rock is mined out underneath it. As will be discussed later, even peak particle velocities (PPVs) above 0.5ips (12mm/s) produce crack responses that are only fractions of the seasonal, frontal, or even the daily "maximum" responses.

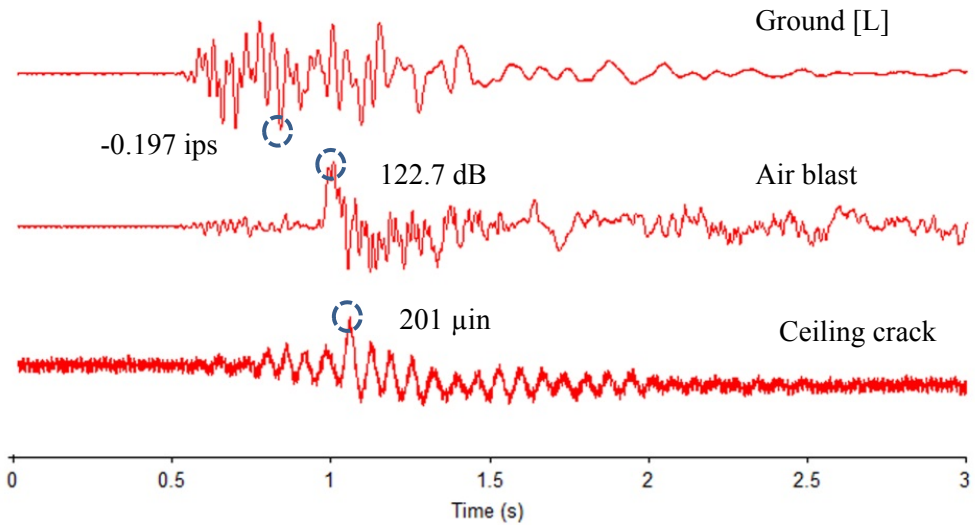

Figure II-8 - Influence of late arrival of air overpressure – Blast event on May 11, 2011. Measurements are zero-to-peak.

Occupant activity

Crack responses to the unplanned entrance of someone into the house are shown in Figure II-9. Comparison with planned events shows that the entrance was probably by the front door.

Maximum values for the crack responses to this door opening are tabulated in Table II-4.

The signal noise is high for the ceiling crack because of line losses due to a greater distance between the data logger and the transducer.

Structural and crack responses to 7 different planned occupant induced activities from the Installation Report (Meissner, 2010) are summarized below. Records in this chapter show that even if the average crack response for a single occupant induced excitation is rather small (less than 40μin or 1μm), one single event such as closing or slamming the bedroom door can induce an important response from the ceiling crack, located on the bedroom ceiling. Slamming the bedroom door produces a response of 2036μin (51.7μm).

These 7 occupant induced activities are listed and compared in Table II-4, and their time histories can be found in the Installation Report (Meissner, 2010).

Blast events must produce PPVs greater than 0.75ips (10mm/s) to produce larger ceiling crack response than the one produced when slamming the bedroom door. Moreover, the unplanned front door opening produced crack responses that are on the same order of magnitude of the responses produced by blast events such as those that occurred on Sep 01, 2010 or on May 11, 2011. These blast events produced ground motions slightly above 0.2ips.

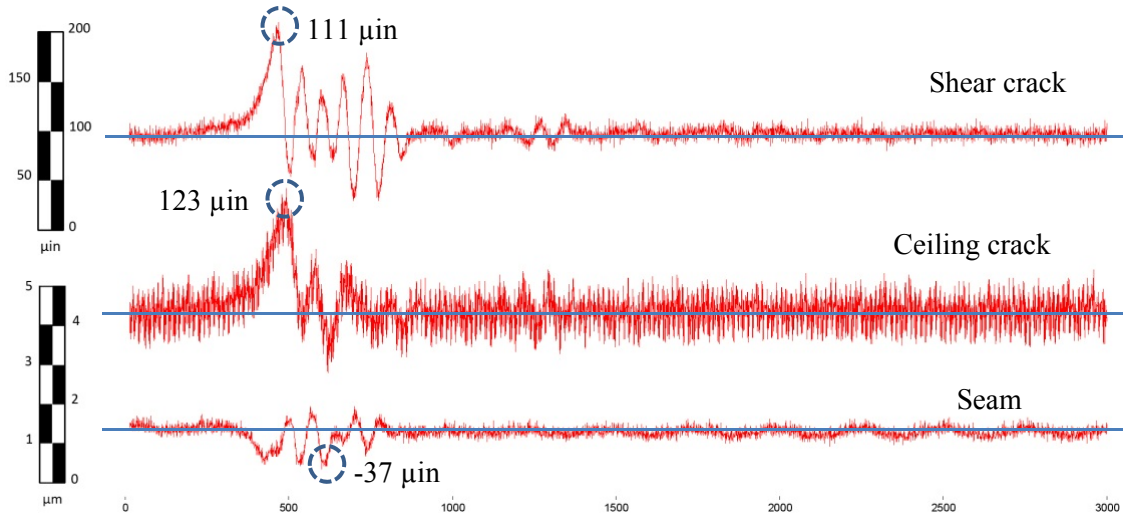

Figure II-9 - Crack response from opening the front door on the first floor

	Crack response (µin)				Structural response (in/s)			
Event	Shear	Null	Seam	Ceiling	HG 13 (Bottom)	HG 14 (Top 1)	HG 15 (Top 2)	HG 16 (Midwall)
Unplanned front door opening	111	18	37	123	0.008	0.02	0.03	0.12
Slam front door	18	14	39	190	0.013	0.02	0.031	0.128
Run down stairs	17	14	13	30	0.005	0.01	0.013	0.055
Close bedroom door	18	15	13	518	0.005	0.007	0.012	0.015
Slam bedroom door	13	14	13	2036	0.015	0.028	0.055	0.043
Slam garage door	15	14	23	150	0.009	0.025	0.038	0.123
Close window	17	13	12	38	0.028	0.014	0.01	0.07
Heel drop	18	20	15	39	0.003	0.003	0.004	0.025

Table II-4 - Crack and structural responses to 7 occupant activities (1µin = 0.0254µm)

Influence of inside temperature regulation

During the fall of 2012, the house thermostat was turned off, thus ending the temperature regulation inside the house.

As shown in Figure II-10, the inside temperature had a 13°F drop in one day on October 26th. After that, the temperature kept varying following a daily cycle, but at values much lower than when the heat was on.

Peak values of the crack response can be measured relative to average values during the 5 week period presented on Figure II-10 to show that the absence of inside temperature regulation caused a response comparable to the largest seasonal response observed during the 30 month study, as shown in Table II-5 and Figure II-12.

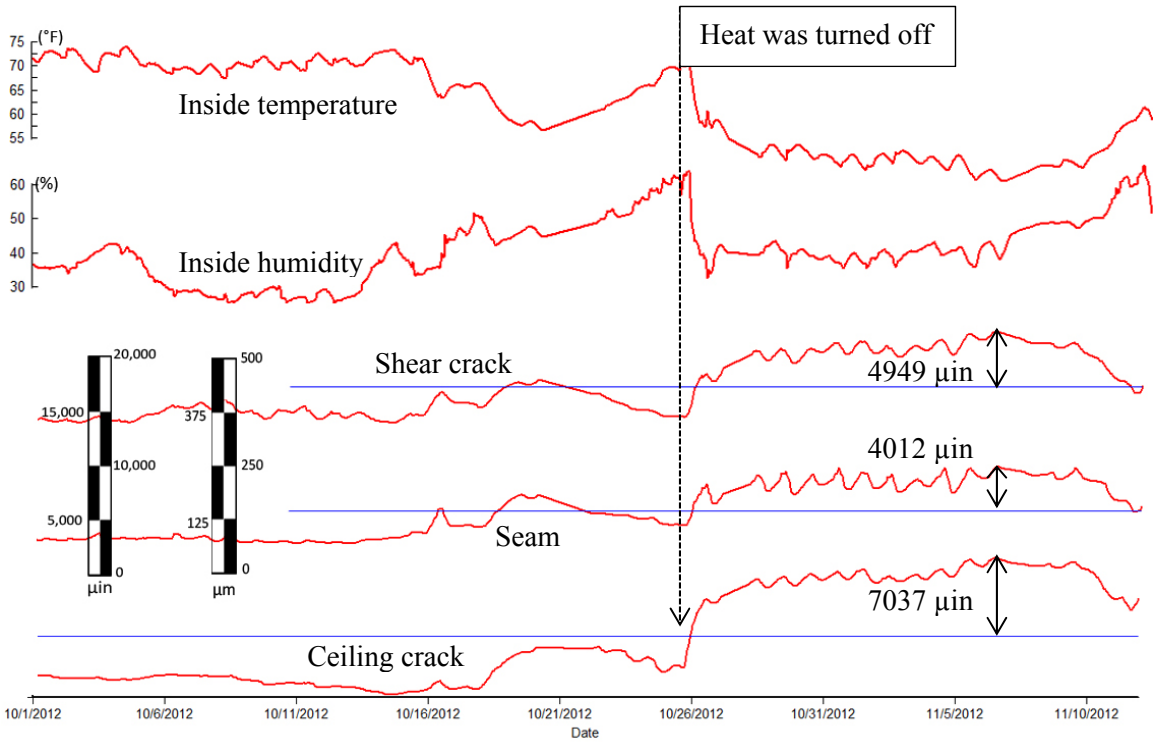

Figure II-10 - Influence of the inside temperature regulation during the fall of 2012

Wind response

Weather patterns, particularly involving wind, induced crack responses that were often just as strong as the responses induced by blasting. Wind gusts triggered disturbances in the Air Overpressure sensor. Figure II-11 shows an example of a response in the Air Overpressure sensor and the simultaneous crack displacements for all 3 cracks. Any crack displacements with corresponding activity of the Air Overpressure sensor were categorized as "wind events".

This wind gust event produced crack responses that are significant. As was observed with the occupant activity, the crack responses are on the same order of magnitude of the ones produced by blast events such as those which occurred on Sep 01, 2010 or on May 11, 2011. These blast events produced ground motions slightly above 0.2ips.

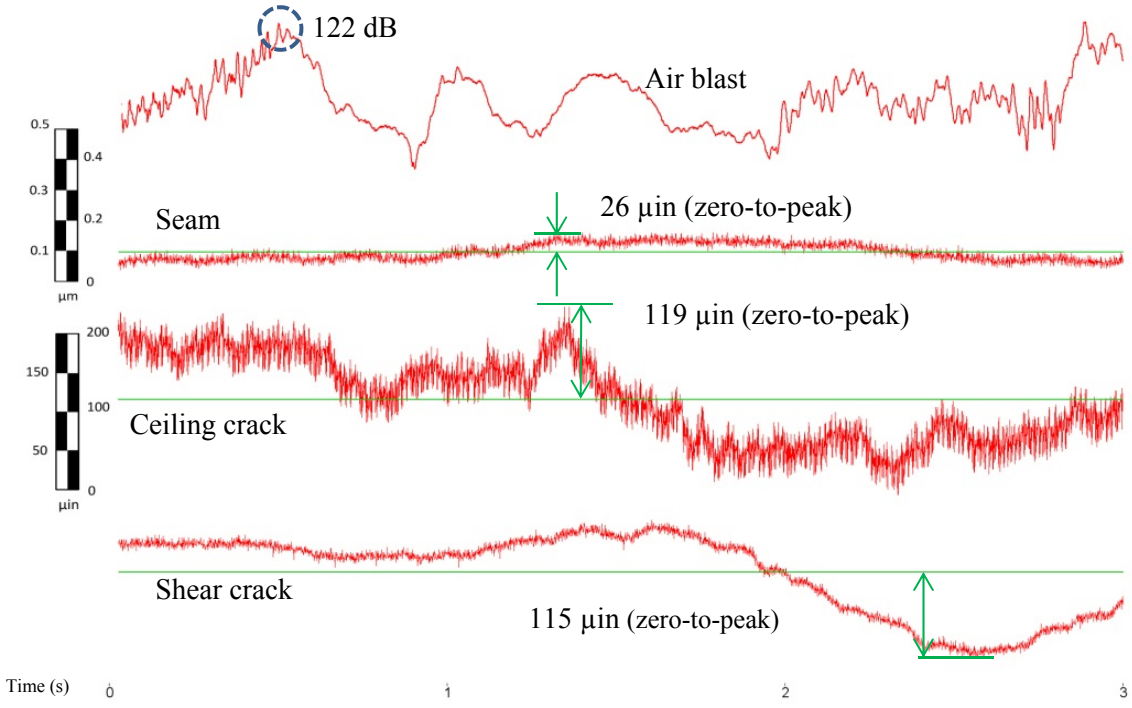

Figure II-11 - Example wind event on May 15, 2011 showing Air Overpressure and Crack Responses (1µin = 0.0254µm). Measurements are zero-to-peak

ANALYSIS

Comparison of crack response to climatological and vibration effects

Blast induced crack responses are compared to long-term environmental effects and occupant induced activities in Table II-5.

Long-term response is at least an order of magnitude larger than any of the dynamic responses, even those produced by ground motions as high as 0.5ips (12.7mm/s). Figure II-12 compares the tabulated responses in graphical form.

In general, the greater the climatologically induced long term response, the greater the dynamic response. Overall, the shear crack and the ceiling crack respond more than the seam. This difference is shown by the overall maximum response of the seam, which is less than half that of the shear or ceiling cracks. These ratios are consistent regardless of the source: occupant or blast, or the magnitude of ground motion: low (0.219ips) or high (0.523ips).

Response (μin)	Shear crack	Null	Seam	Ceiling crack
Max Daily	3276	258	2791	1849
Max Frontal	3840	122	3459	5182
Max seasonal	10485	285	2757	9157
Maximal	12064	745	4861	11726
Ground motion (09/20/11) Max PPV = 0.219ips	192	22	99	451
Ground motion (05/19/11) Max PPV = 0.523ips	705	30	261	1093
Occupant activity (front door open)	111	18	37	123
Wind event (May 15, 2011)	115	20	27	119
Turning off the heat inside the house (on Oct. 26, 2012)	4949	117	4012	7037

Table II-5 - Maximum crack response to all observed sources of vibrations. All measurements are zero-to-peak (1μin = 0.0254μm)

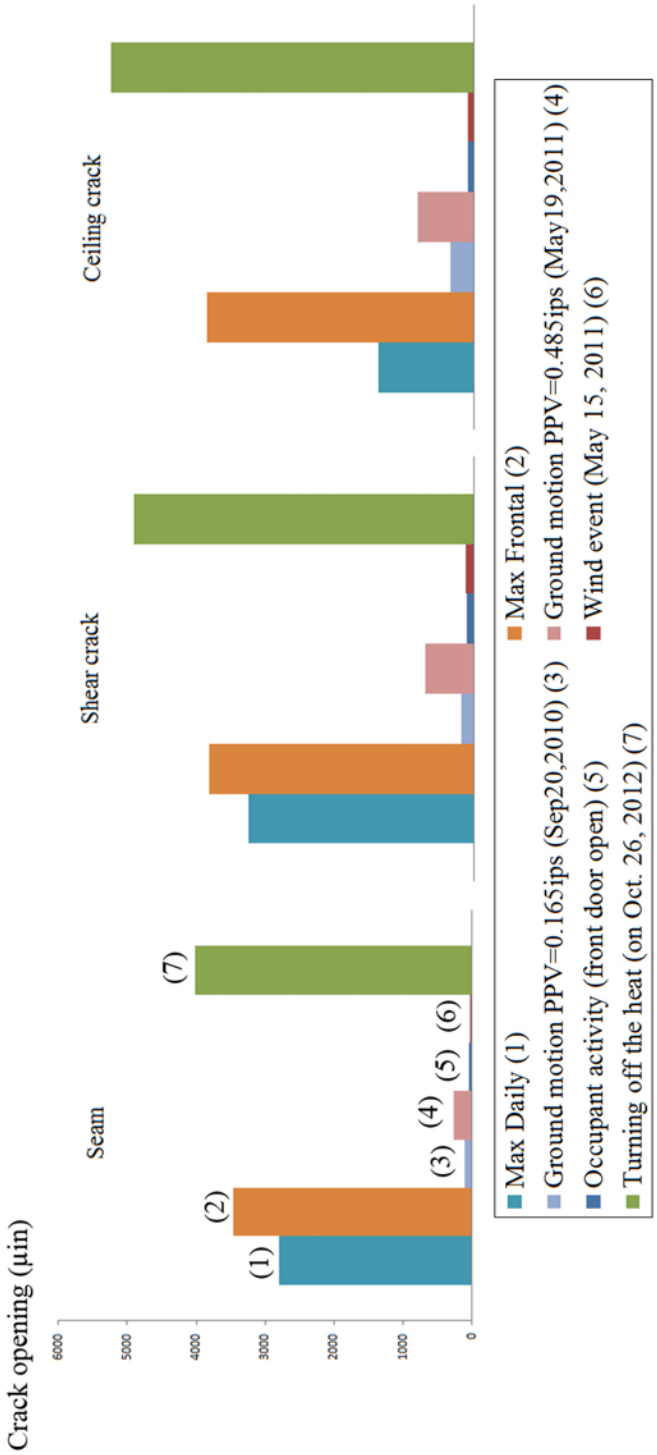

Figure II-12 - Comparison of crack response magnitudes as presented numerically in Table II-5

Time histories of daily climatological and blast induced response

Time histories of crack responses to the 0.219ips blast in Figure II-13 can be compared with the long-term climatic response in Figure II-6. This comparison is made with the two-month timespan bounded by the vertical dashed lines in Figure II-6. Two months of data illustrate the large effect of the passage of large weather systems/fronts. Blast responses are compared to the week of climatic response delimited by the dashed blue rectangle on Figure II-13 (top). This week-long comparison illustrates the daily environmental fluctuations that are superimposed over the longer term effects.

Long-term and dynamic responses are plotted on the same vertical scale for both comparisons. The small black vertical bar on September 20th represents the maximum magnitude of the dynamic response, which is expanded in the rectangular box below the graph. It can be seen in Figure II-13 that the environmentally induced response during the week surrounding the blast event is approximately an order of magnitude larger than the blast induced response. A similar conclusion was reached by Kosnik (2008) and Meissner & Dowding (2009).

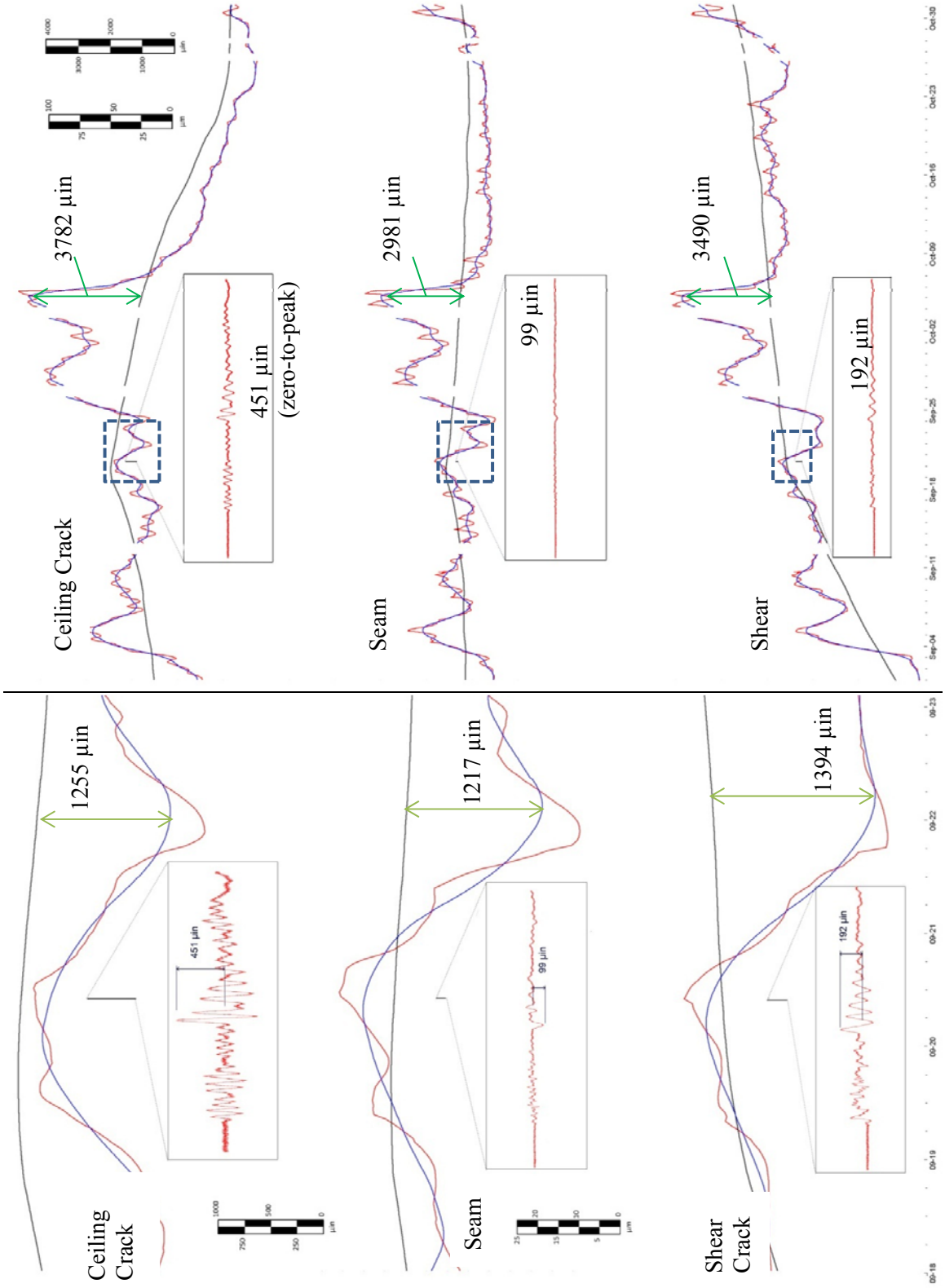

Figure II-13 - Comparison of zero-to-peak crack response to environmental effects over the course of two months (top) and one week (bottom, delimited in dashed boxes) with that produced by the PPV=0.219in/s event. (1µin=0.0254µm, 1in/s=25.4mm/s)

CONCLUSIONS

Data provided herein are a compilation of one of the longest continuously recorded crack responses to date. More than 28 months of continuous crack response have been recorded, including several periods of many months without blasting, thus showing that large crack response occurs without blasting. The unusually long period of observation provided the opportunity to observe response to two seasonal variations.

As has been observed before, crack response to environmental variations is overwhelmingly larger than that produced by blast induced ground motion and associated air overpressure pulses. Seasonal variations and even the passing of weather fronts can produce crack response that is larger by at least an order of magnitude. Turning off the heat inside the house in the fall can cause crack response of that order of magnitude as well, but over periods of time as short as a week.

Observation of occupant activity and wind gust events shows that both can produce crack response as large as that produced by blast induced ground motions.

Chapter III – STRUCTURE AND CRACK RESPONSE OF A ONE-STORY ADOBE HOUSE TO CONSTRUCTION ACTIVITIES USING VIBRATORY ROLLERS

INTRODUCTION

This report presents the structural and crack response of a one-story adobe house to construction activities involving vibratory rollers. The instrumented house was located at 324 Wellesley Rd. in Albuquerque, NM.

House description

The response of the 324 Wellesley house to construction vibrations during road compaction was recorded and analyzed in terms of structure displacements, wall strains, and existing crack displacements. The purpose of this study is to evaluate the impacts of construction activities on existing structure wall cracking potential and compare this with the cracking potential from the long-term changes in weather.

The south wall on the ground floor was selected for exterior measurements. It presented a wall crack ideally suited for monitoring along the window frame, facing the construction site.

To record long-term effects of weather on crack motions, instrumentation was deployed on April 7, 2011 and remained in place for a total of 248 hours until April 18, 2011, with some occasional stops in recording for maintenance of the installation.

This report summarizes the findings of structure response to construction as well as the response of crack displacements to changes in weather and construction. A comparison is made of the construction-induced dynamic cracks displacements with displacements induced by changes in temperature and humidity that are expected to take place in the house.

STRUCTURE RESPONSE STUDY

Figure III-1 shows a photo of the 324 Wellesley house, located on the corner of Wellesley Dr. and Coal Ave. in Albuquerque, NM. The structure is an 80-year old adobe one-story house. The structure walls exhibit few surface defects.

The structure was instrumented with single-axis velocity geophones to measure whole structure and mid-wall vibratory motions during road compaction. Displacement-type gauges were used to measure the movement of the existing interior wall crack and a section of un-cracked wall material. A single exterior tri-axial geophone was buried in the ground outside the structure to record ground motions. Data analyses for vibration-induced motions were conducted to

- compute differential displacements at the top of the structure to determine global shear, in-plane tensile, and vertical wall strains used to evaluate wall cracking potential,
- compute bending strains in mid-walls,
- compare dynamic construction-induced crack displacements with weather-induced opening and closing of cracks from changes in ambient temperature and humidity, and
- compare tensile failure strains of construction materials that were experimentally cracked with the maximum computed tensile strains from construction activities to evaluate cracking potential.

Figure III-1 - West side of the 324 Wellesley House

Vibration Instrumentation

Figure III-2 shows instrumentation at the structure. LARCOR™ multi-component seismographs were used to digitally record four channels of seismic data from velocity transducers. The locations of the single component transducers placed in the upper corner (S2), lower corner (S1), and at the mid-wall (MW) are indicated. Two horizontal components, radial (R) and transverse (T) along with a vertical (V) component, were mounted at S1 and S2. A fourth horizontal sensor was mounted at the center of the south wall (mid-wall, MW).

The exterior (master) unit consisted of a tri-axial geophone buried in the ground near the southeast structure corner 22ft from the road. The geophone, buried 6 inches deep, was oriented so that the R component was perpendicular to the south wall.

Seismographs were connected in series, with the exterior master seismograph acting as the triggering unit and all other systems as slave units, generically shown in Figure III-2. Transducers were affixed to the walls using hot glue. Two corner transducers measured whole structure motions in the horizontal directions (R and T) and were used to calculate in-plane tensile strains. The mid-wall transducer measured horizontal motions during wall flexure and was used to calculate bending strains.

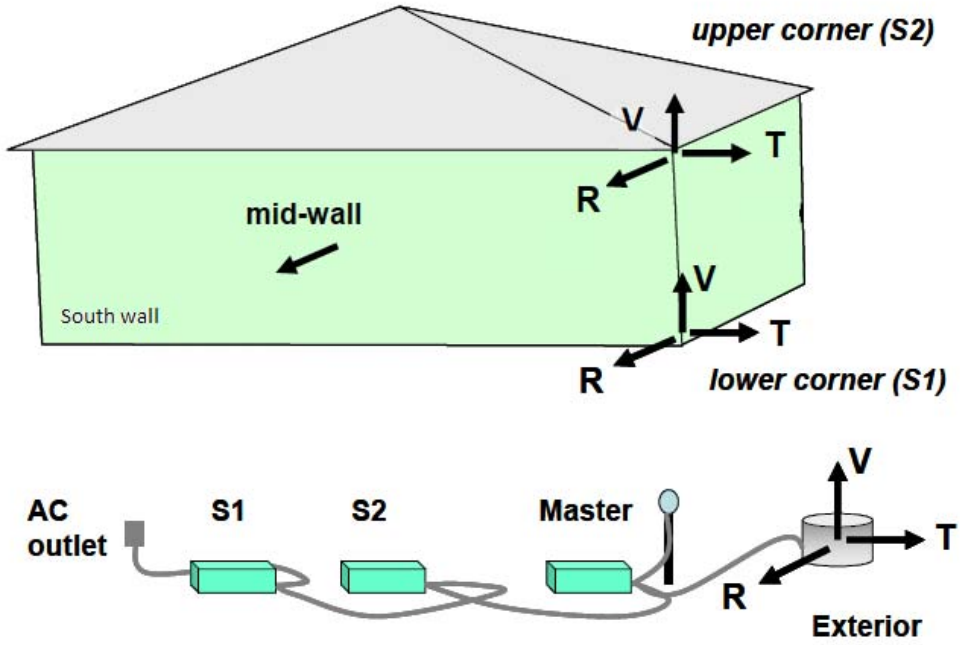

Figure III-2 - General positions of transducers and serial connection of seismographs used to measure time-correlated structure response

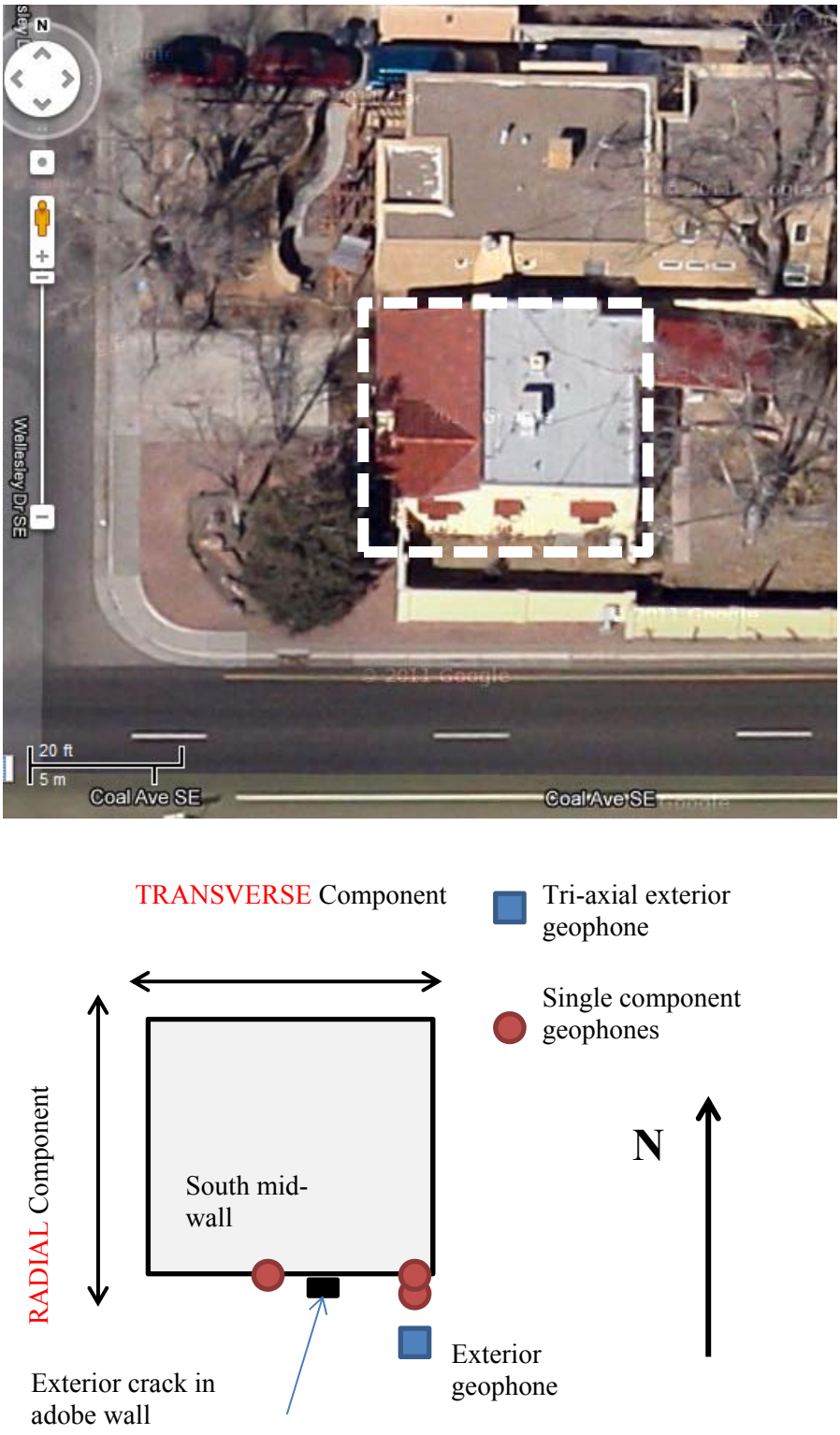

Figure III-3 - Specific instrumentation locations on south wall of the 324 Wellesley house

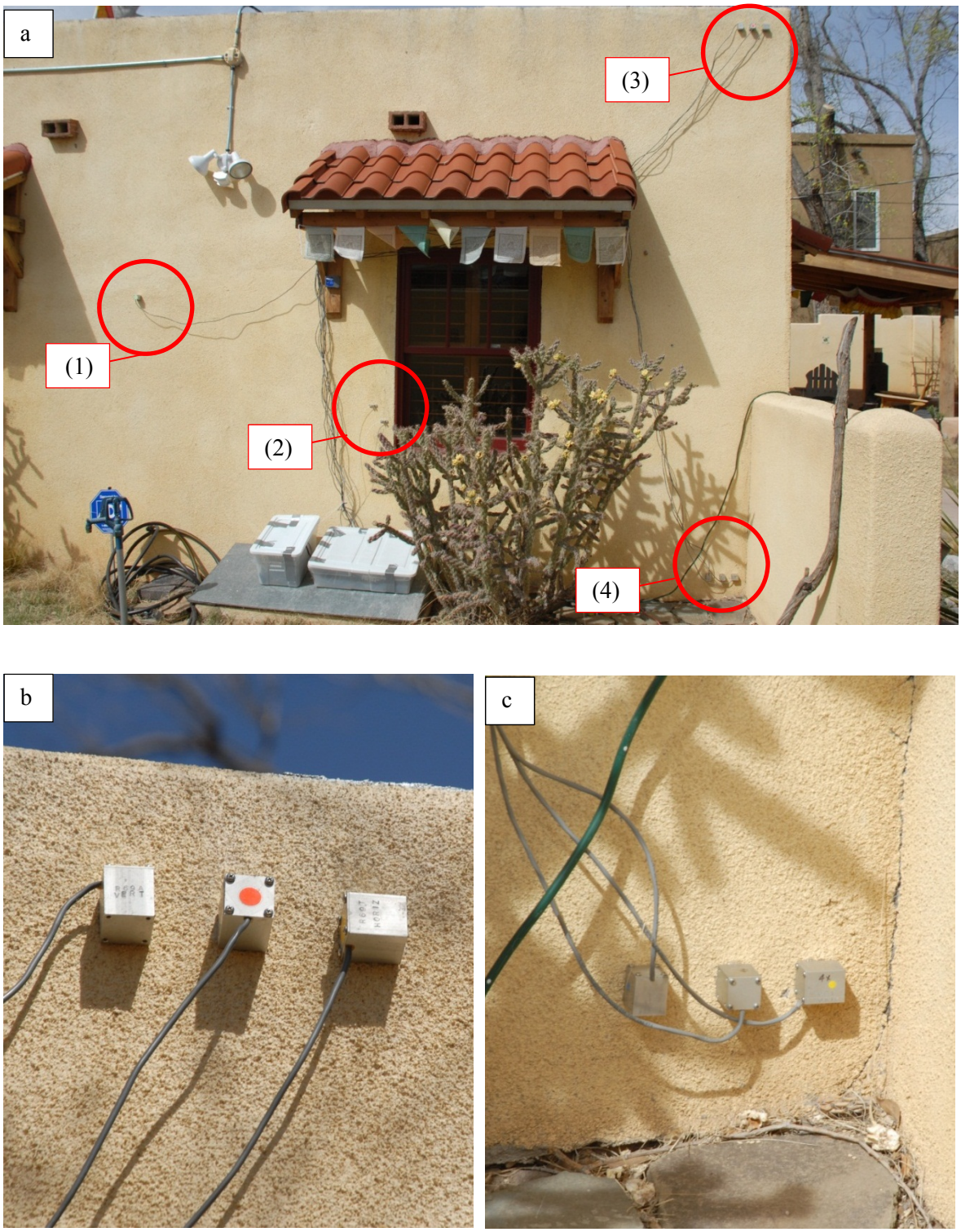

Figure III-4 - Exterior south wall instrumentation (a), with Midwall sensor (1), Crack gauges (2) and upper (3)(b) and lower (4)(c) cluster of single axis motions sensors

Figure III-5 - Crack displacement gauges mounted over an existing crack and un-cracked wall section

To measure the effects of construction activities and variations in climate conditions (temperature and humidity) on changes in the width of the interior crack, Kaman™ eddy-current displacement gages were installed and data collected using a SOMAT™ field computer. Mounted gauges are shown in Figure III-5 and a schematic of the data acquisition system is shown in Figure III-6.

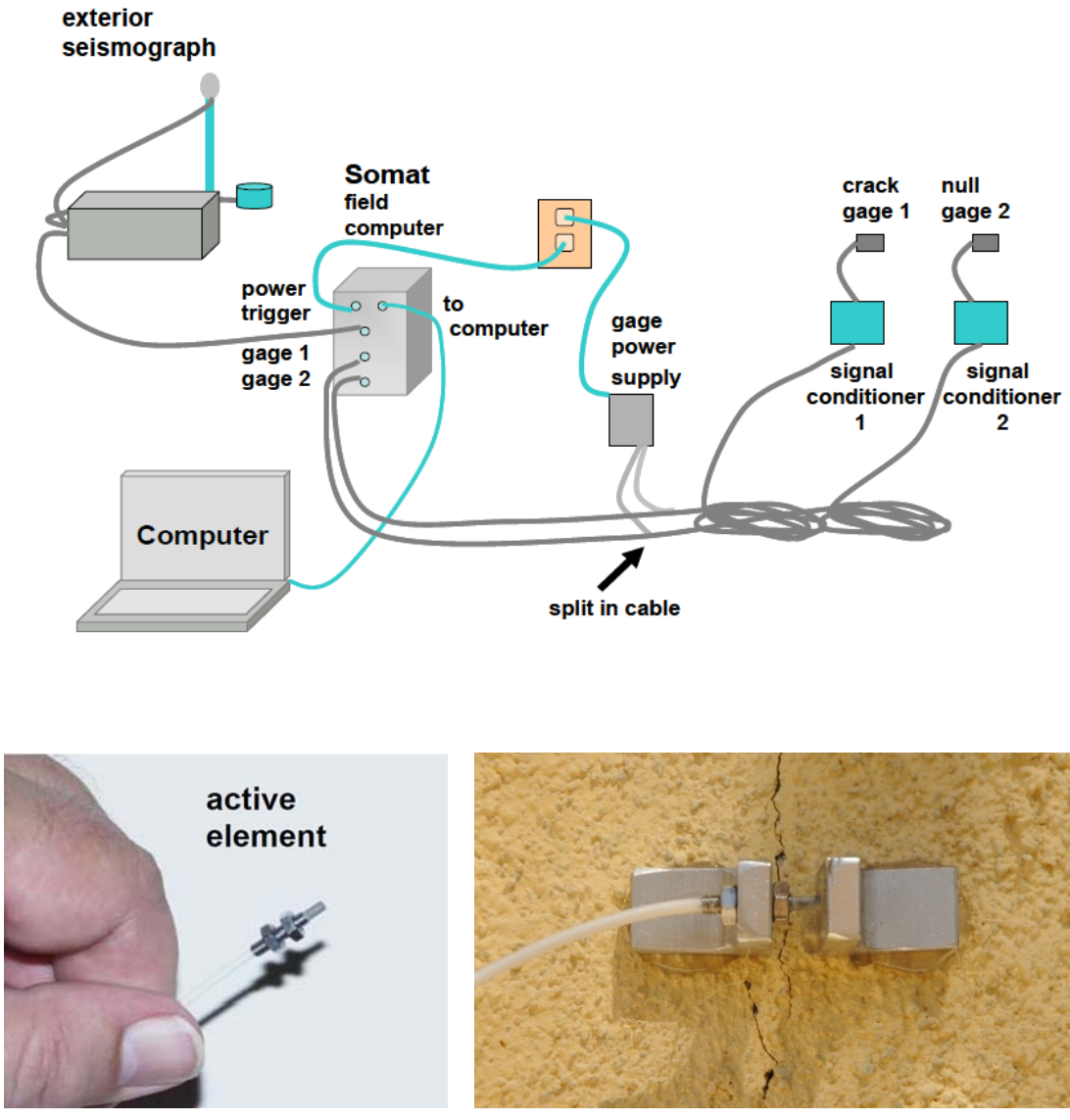

Figure III-6 - Displacement gage system used to measure opening and closing of an existing wall crack (top) and close-up of mounted crack gage (bottom) (Aimone-Martin, 2011)

Each Kaman gage consisted of mounting brackets, one of which served as a target plate and the other an active element. Mounting brackets were placed on either side of the crack (crack gage) and on an un-cracked surface (null gage) such that the active element was secured against the target plate at a sufficient gap distance to allow the gage to function properly. Displacement data for the null gage was subtracted from the crack gage data to obtain net crack motions without the influence of the construction material.

Operation of eddy-current gages relies on the property of electrical induction. The sensor consists of a coil of wire driven by a high frequency current that generates a magnetic field around the coil. If a non-magnetic conductive target material is introduced into the coil field, eddy-currents are induced in the surface of the target material. These currents generate a secondary magnetic field in the target, inducing a secondary voltage in the sensor coil (active element), resulting in a decrease in the inductive reactance in the coil. This type of system is also known as variable impedance because of the significance of the impedance variations in defining its complex nature (Welsby & Hitz, 1997).

The three seismographs and Somat field computer were connected in series. Upon triggering, the master seismograph delivered a 1 volt pulse via the serial cable to activate and begin recording dynamic data during blasting events. This produced seismograph and dynamic crack/null gage records that were time-correlated. Time correlated data is critical for analysis of structural and crack response. This issue and the solutions considered are presented more in depth in Appendix A.

The master and slave seismographs each had a range of available settings for recording data. These settings include:

- trigger level for the master unit set to 0.03 in per second (ips) for ground velocity as recommended in industry practice
- sample rate set at 1024 samples per second
- a sampling duration of 2.5 seconds

These settings ensured the full data record was preserved with sufficient resolution and detail. The Kaman gage system was programmed to sample crack opening and closing every hour in response to diurnal environmental changes. In the dynamic or 'burst' mode, data was acquired every 0.001 seconds. Temperature and relative humidity were recorded using a SUPCO™ data logger. A sample interval of 10 minutes was used. Operating parameters of the Kaman gages are as follows:

- displacement monitoring range of 0.02 in
- output voltage range ± 5 volts
- resolution of 3.94 micro-inch. (0.00000394 in)
- frequency response of 10,000 Hertz (Hz)

Data Analysis

Velocity data were analyzed using White 2000™ software to plot and integrate velocity time histories to obtain displacement time histories, and then compiled to account for the length of the events. Crack gage data were downloaded from the SOMAT™ field computer and analyzed using SOMAT WINTCS v.2.1.5 and v.2.1.4 and SOMAT™ DataXplorer v. 3 softwares.

Construction Activities

Ground and structure motions were recorded during roller compaction of the road adjacent to the house on April 18, 2011. Photos of the compaction activities are given in Figure III-7 showing the location of the house adjacent to the road and the equipment used for the compaction.

Figure III-7 - Road during compaction process (a) and equipment used: Dynapac CA260 (b), Ingersoll-Rand DD10 (c), CAT CB534D (d)

RESULTS

Attenuation of Ground Vibration

The decrease of ground vibrations away from the road was measured earlier in the year and less than a mile away, using an array of seismographs placed to the north of the road from 11 to 70ft away, as shown on Figure III-8.

Figure III-8 - Seismograph array placed at 2020 Coal Ave. on Feb. 23, 2011

The attenuation of ground vibration for representative data is given in Figure III-9. Regression analysis was used to obtain the best-fit (50-percentile) equation describing the decrease in PPV with distance. This was obtained by plotting the peak particle velocity (PPV) of the largest of the three components (R, V, or T) against distance, D, on log-log axes and computing the "power" curve fit through the data. The equation takes on the form

$$PPV = a * D^{-b} \tag{3}$$

where 'a' is the y-intercept value at D =1 and 'b' is the attenuation exponent that describes the rate of decay in PPV. The parameter 'a' is the energy term that represents the relative magnitude of

energy coupled into the ground at the road site and dependent on equipment type, operating mode, and density of the soils. It is often referred to as the "site" factor in the literature.

The attenuation slope term 'b' is a function of geology transmitting the energy between the trench site and the seismograph in the form of motion within a shallow layer of ground surface. The slope term 'b' and, to a lesser extent, 'a' are good indicators of directional geology and can be used to determine azimuthal or directional difference of ground motion characteristics as energy propagates from the site.

The best-fit or 50-percentile equation for the data is

$$PPV = 1.75 * D^{-0.85} \tag{4}$$

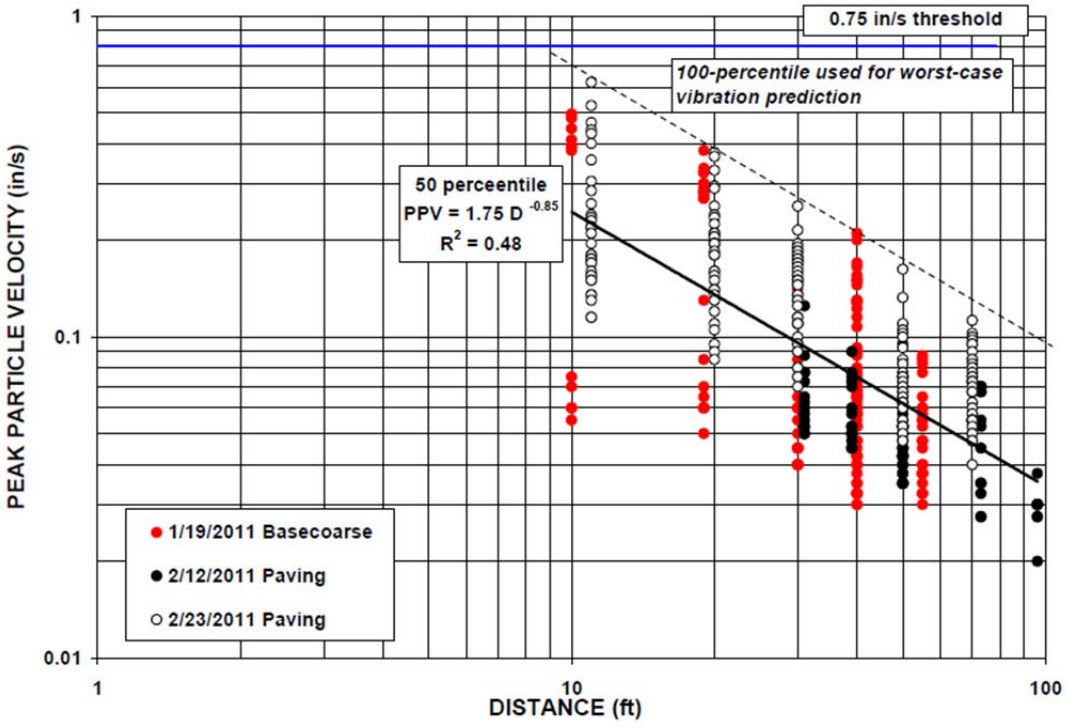

Figure III-9 - Peak particle velocity (PPV) of ground vibration plotted against distance

Ground Vibrations at the Structure

The highest amplitude of ground vibrations at the structure was measured to be 0.48 in/s with a frequency of 32 Hz. The amplitude was recorded only once and is considered to be quite low and unlikely to generate significant structure response to allow computation of dynamic structure characteristics. Furthermore, structure threshold cracking or extensions of existing cracks do not occur until ground vibrations are far greater than 0.75 ips, depending on the frequencies of the vibrations. Therefore, it was not possible to obtain dynamic structure properties for the 324 Wellesley house

Damage Potential to the house based on PPV

Figure III-10 is a plot of the peak particle velocities (PPV) and frequency of ground motion at the PPV (peak frequency) as measured using the exterior seismograph closest to the house. This type of plot is used to show compliance with safe vibration standards used to predict damage potential in residential structures.

A comparison is made between data recorded near the structure and the safe blasting criteria recommended by the U.S. Bureau of Mines (Siskind, Stagg, Kopp, & Dowding, 1980) indicated by the black line that represents the upper bound lines for threshold wall cracking in Figure III-10. Threshold cracking (often referred to as cosmetic damage) is defined as hairline cracking or existing crack extensions in the weakest material in structures assumed to be plaster, gypsum board, or drywall interior surfaces. The upper solid black line represents the lowest possible values for PPV and frequency that will not cause hairline (or threshold) cracking with a 100% level of assurance or probability. Values above this line increase the probability of cracking while for values below the upper line cracking in structures is not possible.

Additional lower bounds for minor and major structure damage (represented by struck or mortar materials and concrete, respectively) require higher amplitude of ground vibrations in excess of 3.0 in/s (for minor damage) and 8.0 in/sec (for major damage).

The maximum ground velocities recorded near the structure fall well below the limit at which cosmetic cracking may begin as shown in Figure III-10. Using the U.S. Bureau of Mines criteria for frequencies just below 40Hz, the factor of safety (FOS) against crack damage in the structure is 1.72/0.5 or 3.45. This FOS indicates it is not possible for the low levels of ground motions and associated frequencies during compaction using a roller compactor to cause threshold cracking or any higher levels of damage in structure.

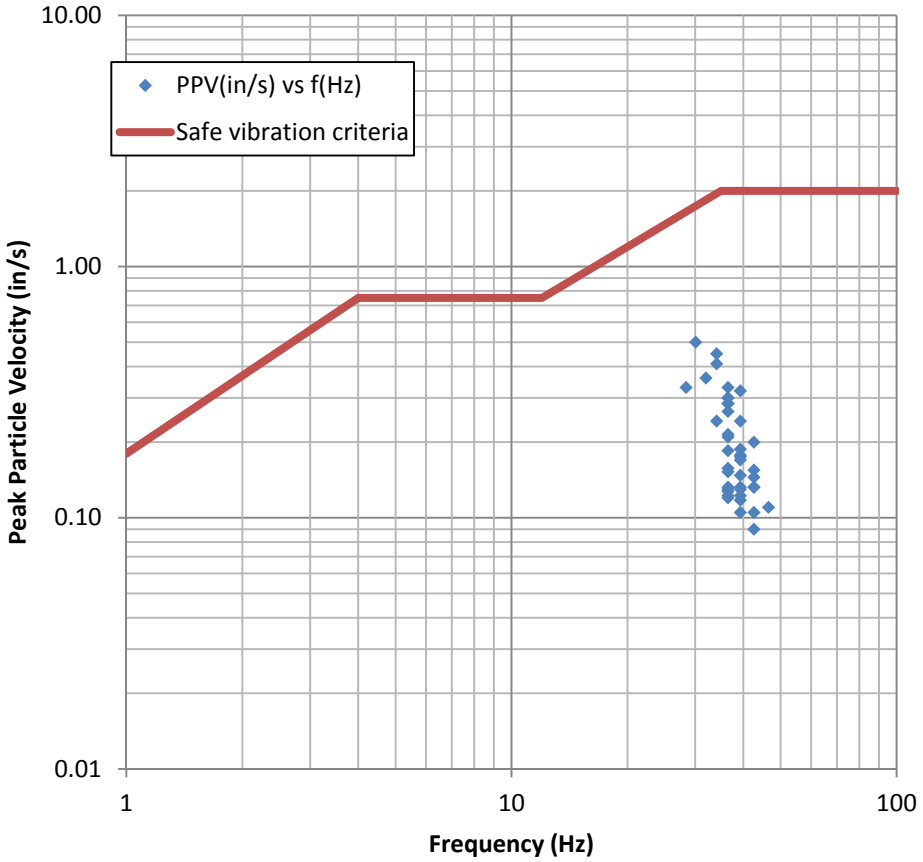

Figure III-10 - Peak particle velocity versus frequency at the peak velocity showing threshold damage limits

Velocity Amplification

Figure III-11 presents the velocity time histories that were recorded during the first event (#1), which presents the highest level of ground vibrations. Table III-1 presents the values for peak particle velocity for each sensor (S2 top of the wall, S1 bottom of the wall, Master in ground).

Attenuation in the particle velocity is observed in both directions when the wave propagates from the ground into the structure. There is an opposite phenomenon of amplification caused by the structure between the bottom of the wall and the top of the wall. The largest peak particle velocities are recorded in the ground.

	Transverse PPV (in/s)	**Radial PPV (in/s)**
S2 sensor (Top of the wall)	0.12	0.26
S1 sensor (Bottom of the wall)	0.09	0.11
Master sensor (In-ground)	0.11	**0.48**

Table III-1 - Peak particle velocity values during event #1 for velocity amplification study. All values are zero-to-peak.

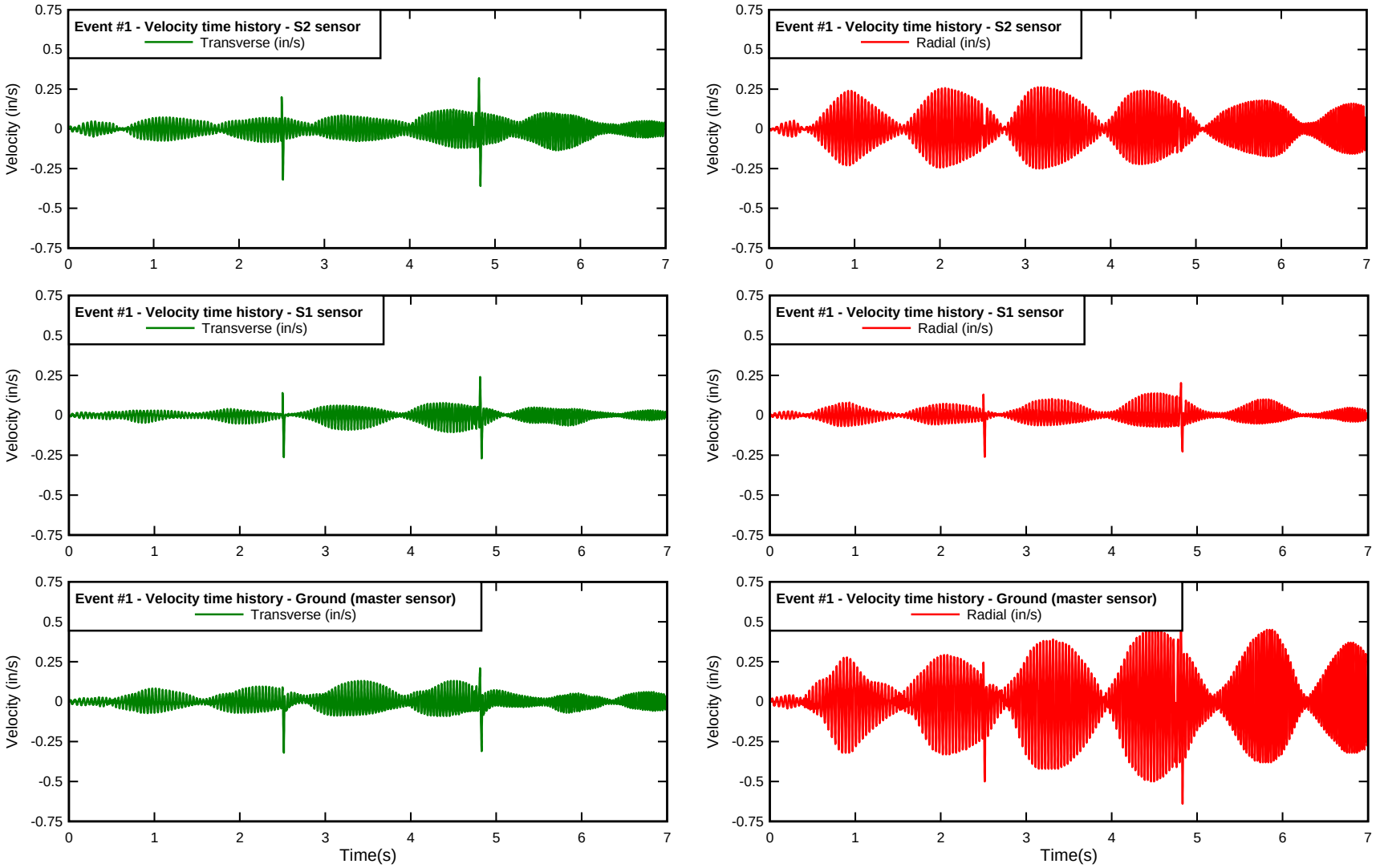

Figure III-11 - Velocity amplification between the ground and the top and the bottom of the structure

Crack Motions induced by road vibratory compaction events

Event #	Date	Time	Maximum crack	Maximum ground velocity (in/s) (zero-to-peak)			Excitation frequency
			(μinches) (peak to peak)	Transverse	Radial	Vertical	(Hz)
1	04/18/11	10:40	595.5	0.11	0.48	0.14	32
2	04/18/11	10:44	108.6	0.12	0.13	0.08	32
3	04/14/11	12:40	103.6	0.024	0.116	0.055	36.5
4	04/14/11	12:47	255.7	0.040	0.085	0.070	36.5

Table III-2 - Summary of crack motions for vibration events relative to ground motion excitations

A total of 54 triggered events occurred during compaction using several types of vibratory rollers. Of these events, 4 typical occurrences were studied in depth. Table III-2 presents the correlation between the crack response and the ground vibrations for these 4 events. These events present the clearest dynamic response all around, as well as the largest crack displacements. They account for the use of two different machines, as evidenced by the change in excitation frequency.

The event #1 presents both the highest level of ground vibration and the largest crack displacement: 0.48 in/s ground vibration in the radial direction and 595.5 micro-in opening of the crack. These values are compatible with previous observation and analysis performed by Snider (2004), presented in Figure III-12.

This study was performed on a one-story residential structure located in Las Vegas, Nevada. Crack response resulted from ground motion triggered by backhoe excavation, trenching, as well as vibratory rolling compaction. The plan-view geometry of the monitored house is presented in Figure III-12.

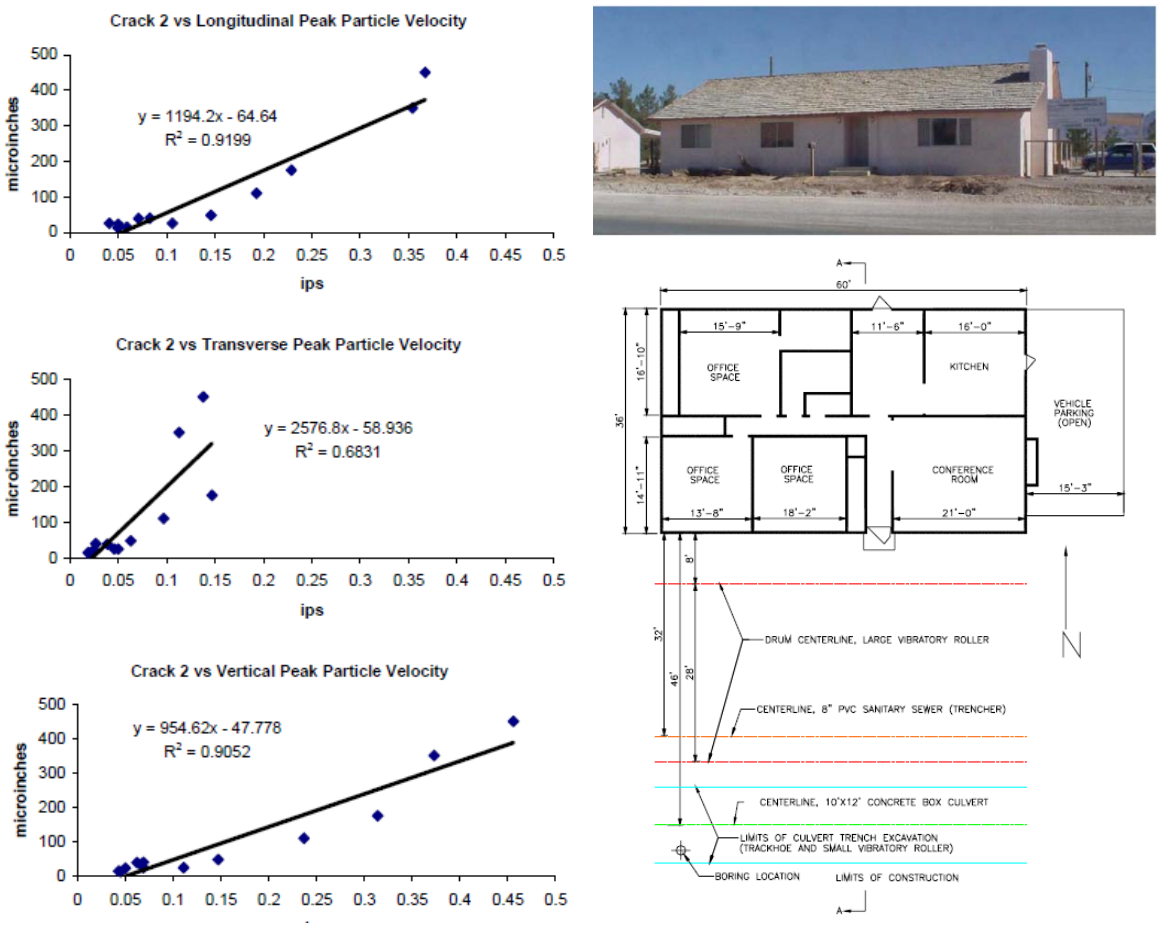

(a) **(b)**

Figure III-12 - (a) Crack displacement vs. particle velocity for vibratory roller compaction events and (b) Picture and plan view geometry of the monitored house. (Snider, 2003)

In the Las Vegas project, a level of ground vibrations on the order of 0.5 in/s in the longitudinal (radial) direction would cause a dynamic opening of the crack on the order of 550 micro-in, which is compatible with the values observed during this New Mexico study.

Strains induced by road vibratory compaction events

Table III-3 presents the strain levels that were caused in the structure by the ground vibration excitation events. The values of strains are compared to the crack opening as well as the differential wall displacement and the ground vibration velocities. It can be observed that the highest levels of strains were caused by the vibration on April 18th (events #1 and #2).

Event #	Shear (μstrains)		In-plane tensile (μstrains)		Bending (μstrains)	Maximum crack opening	Maximum differential wall displacement, S2-S1 (10^{-3}in)		Maximum ground velocity (in/s) (zero-to-peak)		
	South wall	East wall	South wall	East wall	South wall	(μinches) (peak to peak)	Radial (NS)	Transverse (EW)	[T]	[R]	[V]
1	33.72	28.87	14.93	11.79	13.95	595.5	2.934	2.512	0.11	0.48	0.14
2	27.88	26.00	12.34	10.62	11.53	108.6	2.425	2.262	0.12	0.13	0.08
3	6.68	2.83	2.96	1.16	2.76	103.6	0.581	0.246	0.024	0.116	0.055
4	3.78	7.25	1.68	2.96	1.57	255.7	0.329	0.631	0.040	0.085	0.070

Table III-3- Summary of wall strains and maximum crack motions for vibration events relative to excitations ground motions

Equations used to calculate in-plane tensile and mid-wall bending strains using velocity time histories are given in Appendix B. Complete displacement time histories for upper and lower corners used to compute strains along with crack displacement time histories are found in Appendix C for compacting events.

Crack motions induced by weather: changes in temperature and humidity

The width of existing wall cracks is highly sensitive to changes in ambient temperature and humidity. Although existing exterior and interior cracks in structures near construction are often attributed to the operation of vibratory equipment, it is often the case that the construction- induced crack motions are small compared with the static, or slow, opening and closing of existing cracks with diurnal (or 24-hour) fluctuations in temperature and humidity.

To show this comparison, long-term changes in the crack width were measured and recorded on an hourly basis throughout the week between April 13th, 2011 and April 18th, 2011. Changes in crack width were plotted against time and shown in Figure III-13 (bottom plot) in comparison to changes in temperature (top plot) and relative humidity (middle plot). A positive increase in crack displacement corresponds with opening of the crack.

In general, crack movement follows the trend in the ambient humidity and temperature. When humidity increases, the crack opens and this occurs most predominately very early in the mornings, well before dawn. During the day, as temperature increases and humidity decreases, cracks tend to close. It is this daily cycle that produces high stresses on existing cracks and in particularly, at the tips or ends of the cracks, causing the crack to grow slowly over time under the right conditions.

The largest variations in crack width over the entire monitoring period and for a one-half day cycle (12-hour) were determined and shown in Figure III-14 and Figure III-15. Given the oscillatory nature of the excitation, the comparisons are peak-to-peak. The largest half-day movement was 8081.5 micro-in, and overall movement was 9227 micro-in. These daily crack width changes are far greater than 595.5 micro-in, the largest dynamic change during any compacting event. The influence of temperature and humidity is 15.5 times greater than the influence of the largest wall motion driving the crack during vibration work.

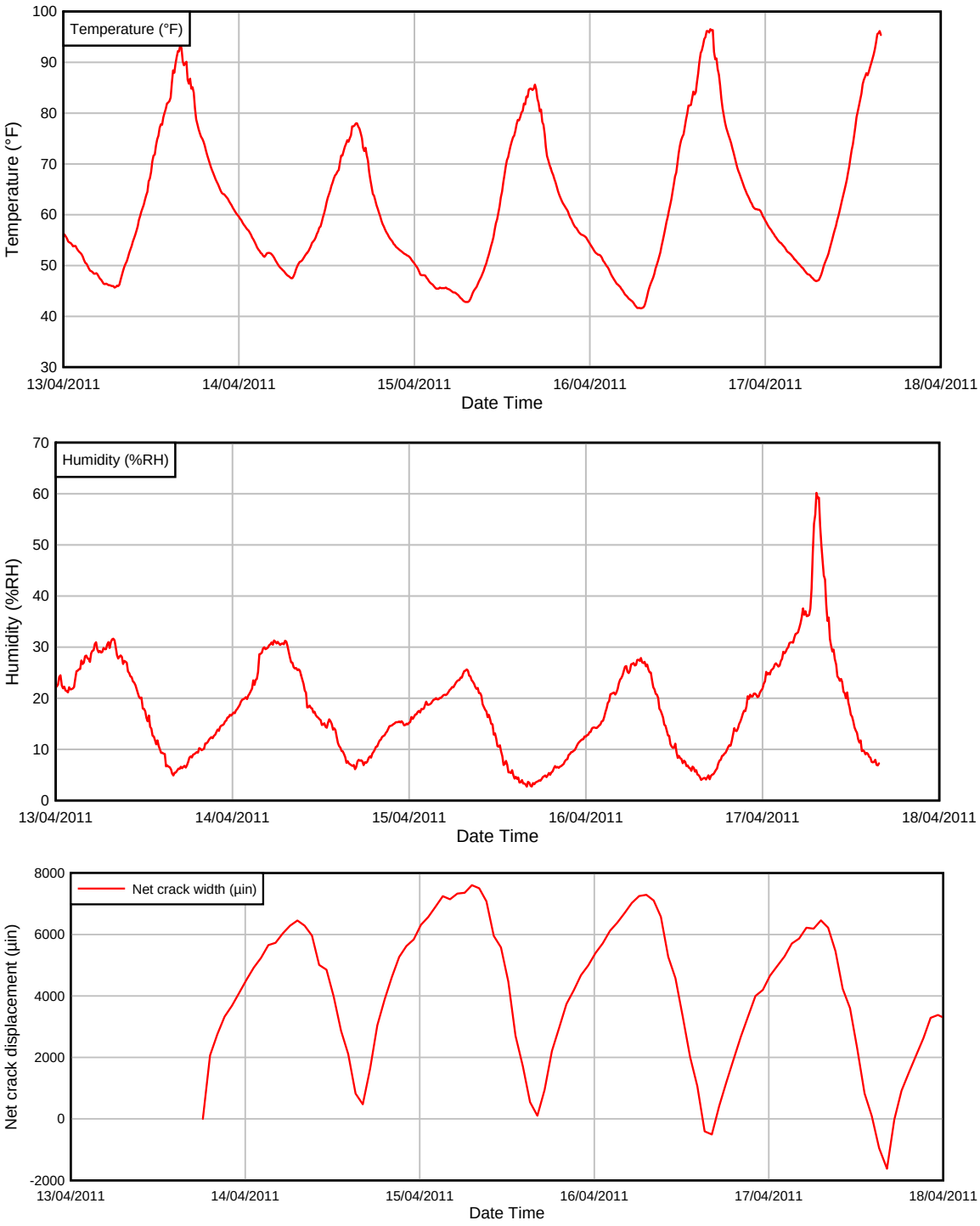

Figure III-13 - Variations in ambient temperature, humidity, and corresponding net crack displacement over 6 days

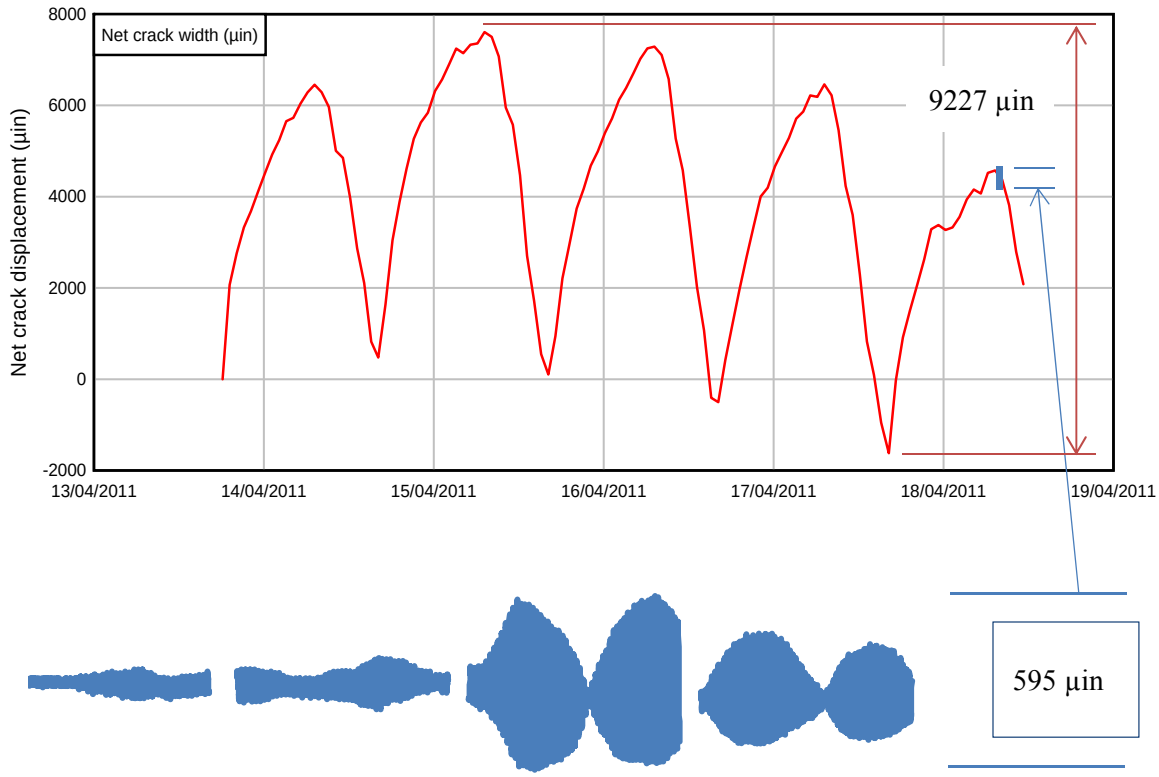

Figure III-14 - Comparison of dynamic crack displacement time history for vibratory compaction with overall static crack movement of 9227 micro-in responding to climate changes over a 6-day period

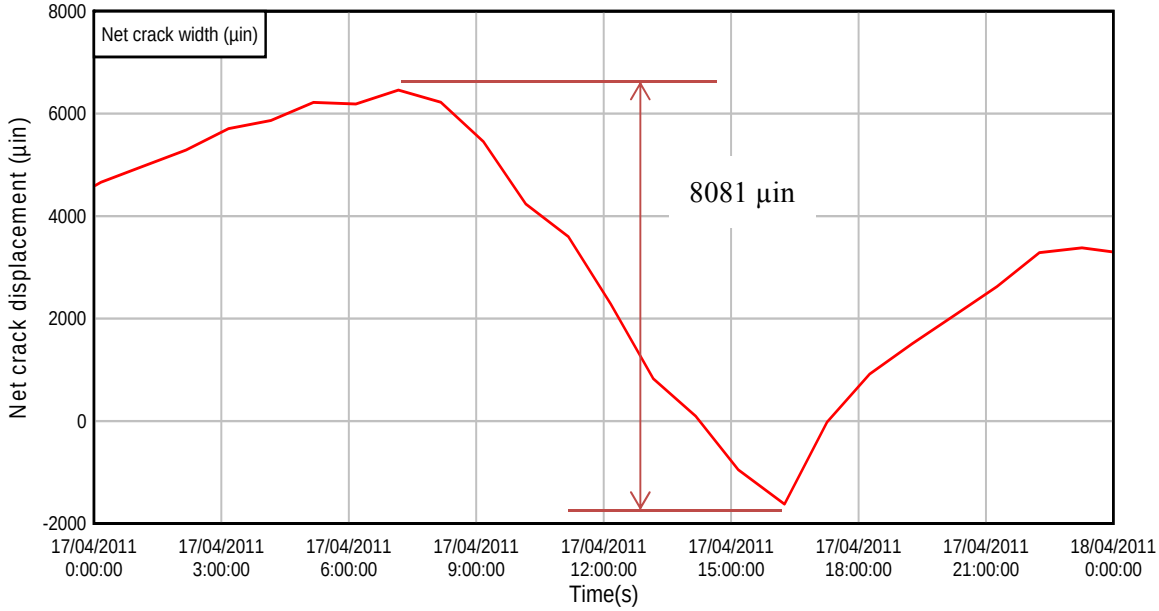

Figure III-15 - Static crack movement for largest 12-hour change in weather conditions (night to day)

Peak Strains Compared with Failure Strains

Calculated strains based on wall displacements are valid within the elastic range of the construction materials comprising walls. Within the elastic range, deformations are fully recovered and permanent displacements in the walls do not occur. The upper limit to this elastic range is the start of material failure. The failure strains of construction materials under dynamic loading are well known. The range of failure strains in the gypsum core of drywall existing in both structures is 300 to 500 micro-strains (Dowding, 1985) while for plaster it can be as low as 200 micro-strains. Exterior fire brick façade does not fail before 500 to 1000 micro-strains. Concrete mortar joints in basements generally start to crack at 1200 micro-strains and require at least 3.0 ips PPV before cracking occurs. Concrete slabs start to crack at 8 to 10 ips, based on damage observations during earthquakes.

The maximum observed in-plane tensile strain of 14.93 micro-strains in the south wall during vibration is well within the safe limits to prevent cracking. The minimum factor of safety against plaster cracking is 20.

CONCLUSIONS

The instrumentation of the 324 Wellesley house and the observation of the structural and crack response over a period of a week during which vibratory rollers were used to compact an adjacent road showed that the influence of temperature and humidity is more than 15 times greater than any motion that occurred during vibration work. The strain study also showed that the measured strains are 20 times lower than the documented failure strains.

It is concluded that large weather-induced changes in crack width are the greatest contributing factor to crack extension and widening over time. Compaction vibration influences on changes in crack widths and the potential formation of cracks in structures are negligible compared with cracking potential from the influence of climate changes.

Chapter IV – NEW DEVELOPMENTS IN MONITORING STRUCTURE RESPONSE TO CLOSE-IN BLASTING IN URBAN SETTING: 3D MODEL SIMULATION OF BUILDING RESPONSE TO HIGH-FREQUENCY EXCITATION

INTRODUCTION

Project Overview

This chapter presents the dynamic response of an elderly five-story building to high frequency vibrations produced by immediately adjacent blasting. A 3-dimensional model was used to compare computed expected displacements of the structure to those measured.

Description of structure and setting

The five-story test structure was constructed in the early 1900s. It is believed to be a masonry load bearing structure with a 3-wythe exterior brick wall. Its dimensions are 7m [W] x 19.5m [L] x 19.8m [H] (276in x 768in x 780in). Figure IV-1 is a photograph of the building and the immediately adjacent rock. The lower back building on the left is not attached to the instrumented structure.

Blasting environment

The adjacent excavation is approximately 80ft by 200ft, as shown in Figure IV-2. The excavated rock was predominately metamorphic.

While variable from shot to shot, a typical blast consisted of approximately 10 to 20 holes arranged in two rows with an 8x8 pattern or S/B = 1. Each hole was detonated separately with 4 to 8lbs of explosive per hole.

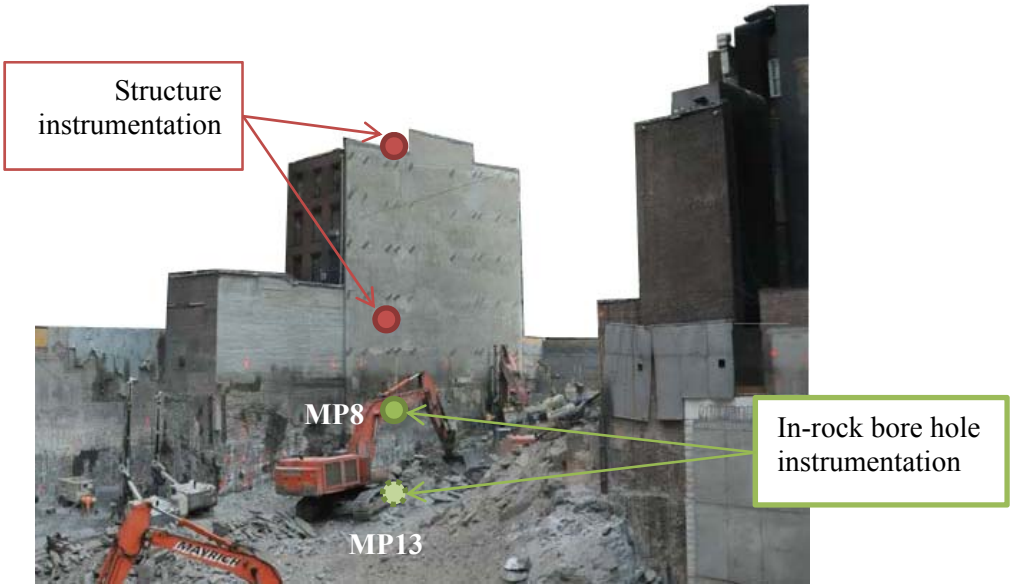

Figure IV-1 - View of the excavation and the instrumented building

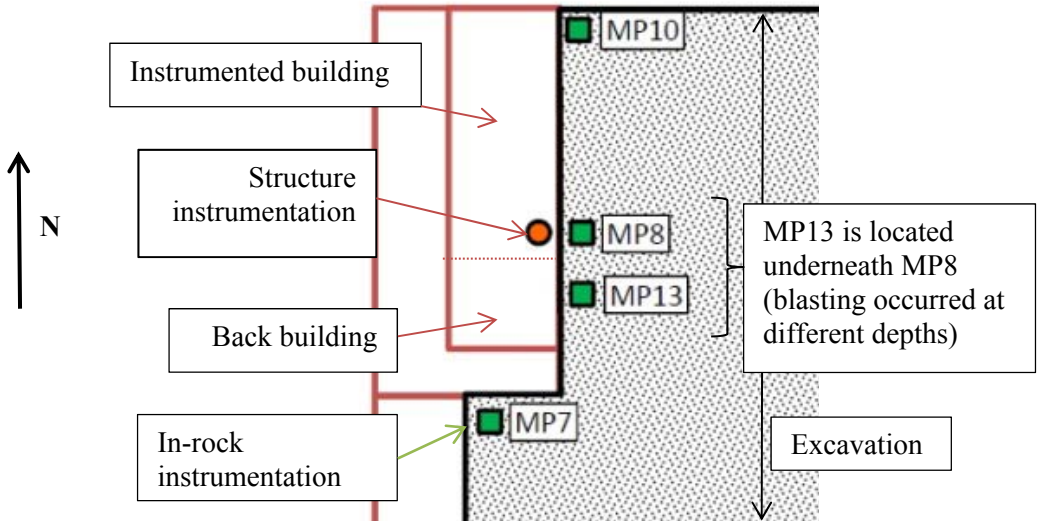

Figure IV-2 – Plan view of the excavation and location of the various measurement points and the building instrumentation

The blasting progressed west to east from south to north, which means that the source location of the blast differed for every detonation. Thus each blast occurred at different distance and angle to the building and fixed instrument locations.

Focus of measurement and study

The objective of this paper is to compare the response of the structure with excitation as well as that in the literature. To do so, instrumentation was placed both on the structure and in holes drilled into rock adjacent to the structure.

Instrumentation

The in-rock instrumentation was located at several locations to account for the progressive advance of the blasting. Before every shot, a three-component geophone was inserted in a drilled hole close to the blasting area and adjacent to the structure as shown in Figure IV-2. Unlike what is often done on other projects, the in-rock geophones were placed in bore holes drilled in the foundation rock. Often the lack of space requires the excitation motion to be measured on the basement of the structure rather than the rock below. These in-rock geophones were designed to be reused and could be moved during excavation. The measurement point 7 (MP7) was the first in place before the structure instrumentation started, as blasting began in the tight northwestern corner south of the building.

The structure was instrumented with two sets of geophones, each of them composed of two horizontal transducers. One set was placed on the ground floor, while the other one was placed on the roof parapet.

The sensor located on the ground floor of the building was placed at street level, on the outside of the building and close to the back south-west corner of the structure. As shown in Figure IV-1, the ground level is one floor above the rock-building interface. The top structure sensor was vertically above the ground floor sensor. While at the roof level, the sensors were affixed to the base of a parapet extending from the upper roof line to preserve the integrity of the rooftop insulation.

These two-component geophones were oriented to record horizontal motions of the structure in both the radial –or longitudinal- direction, parallel to the length of the building, and in the transverse direction, or perpendicular to the length of the building. They were both located on the east wall, so that the radial component measures in-plane wall movement and the transverse component measures the out-of-plane wall movement.

MEASURED RESULTS

During the observation period, 9 blasting events were monitored. Only events with large excitation of MP8 were analyzed to coincide with the 3D model simulation performed later in this report. Peak particles velocities for these 9 events are presented in Table IV-1, and their time histories are presented in Appendix D. A typical suite of vibration records is presented in Figure IV-3, for both transverse and longitudinal directions (or perpendicular and parallel to the rear wall.

Comparison of these high frequency excitation time histories in Figure IV-1 and Table IV-1 describes a variety of phenomena. Dominant frequencies of these motions decline from the in-rock excitation (higher than 150Hz) to the structure response of 7Hz to 40Hz. This can be observed in Figures IV-3 and IV-5 as well as in Appendix E. Amplitude of the motion declines or increases only slightly when compared to those measured in the rock.

Such data comparing close-in rock excitation with building response are relatively rare. In rural areas, small distances between blast and structure are rare. In urban areas, adjacent excavations often preclude measurement of the motions in the rock itself. Thus compliance transducers are often placed on the structure at its lowest accessible floor. As the excavation deepens, this ground level or basement transducers become less and less equivalent to the excitation location.

Building Response Transducer Locations

Transducer attachment location affects their response. Responses are affected by both super structure and wall motion responses of the building, which differ in frequency. These differences are important in investigation of building response. In this study "ground level" transducers were placed on the outside of the building without exact knowledge of the interior shear wall locations. As such ground level measurements may be dominated by wall motions rather than superstructure motions. Normally walls will exhibit natural frequencies in the 10 to 20 Hz range as illustrated by the motions in Figure IV-3.

Top transducers were attached to the lowest portion of the parapet to avoid penetrating roof waterproofing membrane. As such they too may be responding to these parapet motions as well. The free response at the end of the top response time history may be more indicative of the super structure response than the earlier portion of the time history. More detailed study of the structure would be necessary to more precisely determine the exact nature of the response.

Low frequency rider on velocity time histories

The in-rock or building response from this study shed some light on the low frequency rider on high-frequency velocity measurement such as that in the ground level radial recording shown in Figure IV-3. Several reasons have been advanced for such low frequency events:

- actual displacements from poorly attached velocity transducers
- delayed gas pressure excitation
- velocity transducer response itself

Considering this case, the ground level transducers were bolted to the structure and are unlikely to have been displaced. The in-rock transducers, the most likely to be subjected to delayed gas pressure, show no such response. Furthermore only the motions parallel to the building (radial)

not perpendicular (transverse) display the low frequency rider. Thus in this case it appears that the most likely reason is the high frequency transducer response itself. While personal discussions with instrument manufacturers (Wheeler R., 2012; Turnbull R., 2012) showed that they have been able to reproduce these responses in the laboratory, the investigation of this phenomenon is continuing.

Estimation of the damping ratio and natural frequency of structure

Fourier frequency transfer functions (FFTs) of the time histories presented in Figure IV-3 can be employed to determine the fundamental dynamic characteristics of the structure. As shown in Figure IV-4 and the attached equations, if the building is idealized as a single degree of freedom (SDOF) system, its response characteristics can be reduced to its natural frequency, f, and its damping ratio, β.

Values of f and β can be found using a transfer function (Dowding C. H., 2008) equal to the ratio of the FFT of the time history at the top of the structure divided by the FFT at the ground level. This transfer function is shown in Figure IV-5. The values obtained, f = 7.5Hz and β = 3.2%, are compatible with values previously documented (Dowding C. H., 2008) and will be used as inputs in the SDOF model presented later in this paper. These results can also be compared with the free response of the building as shown in Figure IV-3.

PPV study - Amplification ratios and comparison to results from the United States Bureau of Mines

Table IV-1 presents the values of peak particle velocity (PPV) for all nine recorded blast events, in the rock and on the structure. It is particularly interesting to analyze the ratios of these PPVs between the top and the ground level of the structure, between the ground level of the structure and the rock, and between the top of the structure and the rock. The ratios presented in Table IV-1 were computed using peak values at each level, and not time-correlated values.

Comparisons will focus on the transverse direction, which describes the out-of-plane displacements. While not known for certain, it is presumed that the majority of the blasts that were recorded occurred near MP8 along the east side of the building. Not only is the building narrower in this direction, thus presenting a lower structure stiffness, but it is also the direction of the highest wall responses.

The transverse PPV ratios presented in can then be plotted against the transverse PPV in the rock in Figure IV-6. The trend in both of these plots shows that as the PPV in the rock increases the building response ratio decreases. This declination is most likely the result of the increased dominant excitation frequency of the rock as the blasts approach the building. Since the blasts were of a similar design; the higher the rock PPV, the smaller the distance to the structure.

These values of velocity amplification can be compared to response ratios previously measured by the United States Bureau of Mines (Siskind, et al., 1980). In this study it was decided that the ground-level (GL) motions were likely to be influenced by both the wall and super structure motions. They were analyzed as both. Amplification values of GL/rock in Table IV-1 were compared to USBM wall amplification values in Figure IV-7.

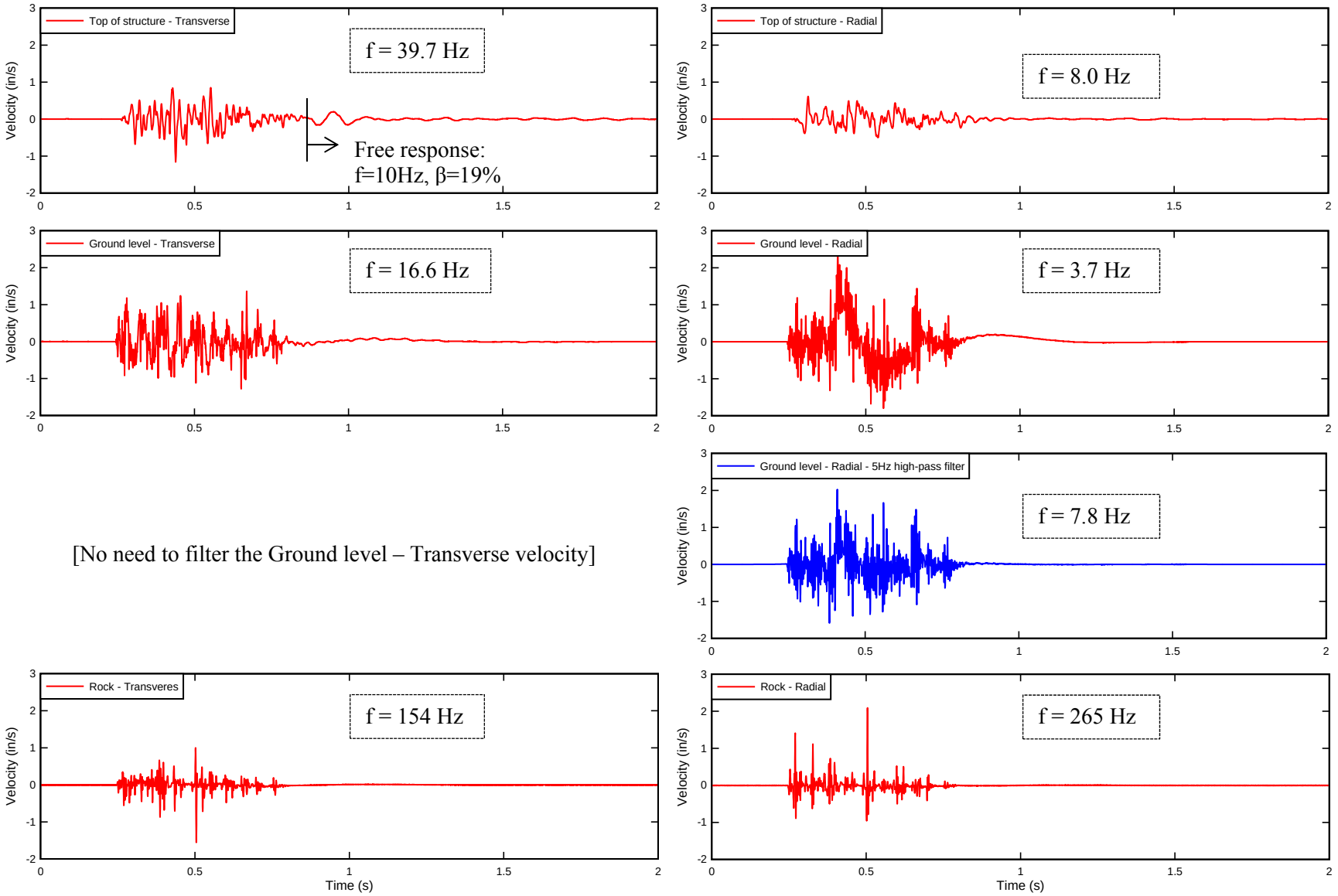

Figure IV-3 – Velocity time histories for a typical blast (Event 1) arranged from top to ground floor to in-rock, transverse direction (left) and radial (right).

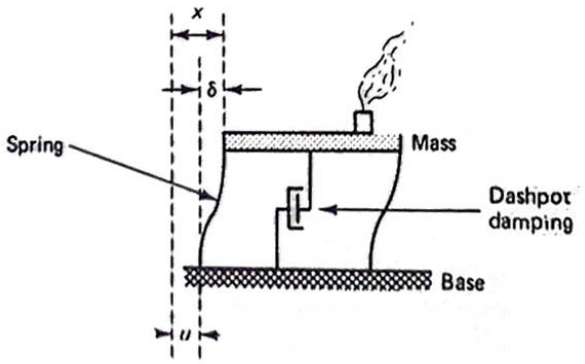

$$\ddot{\delta} + 2\beta p\dot{\delta} + p^2\delta = \ddot{u}$$

$$\frac{1}{f_s} = T = \frac{2\pi}{p_d} = \frac{2\pi}{p\sqrt{1-\beta^2}}$$

$$\beta = \frac{1}{2\pi}(-\ln\frac{\dot{u}_{n+1}}{\dot{u}_n})$$

Figure IV-4 - Single degree of freedom model (Dowding C. H., 1996)

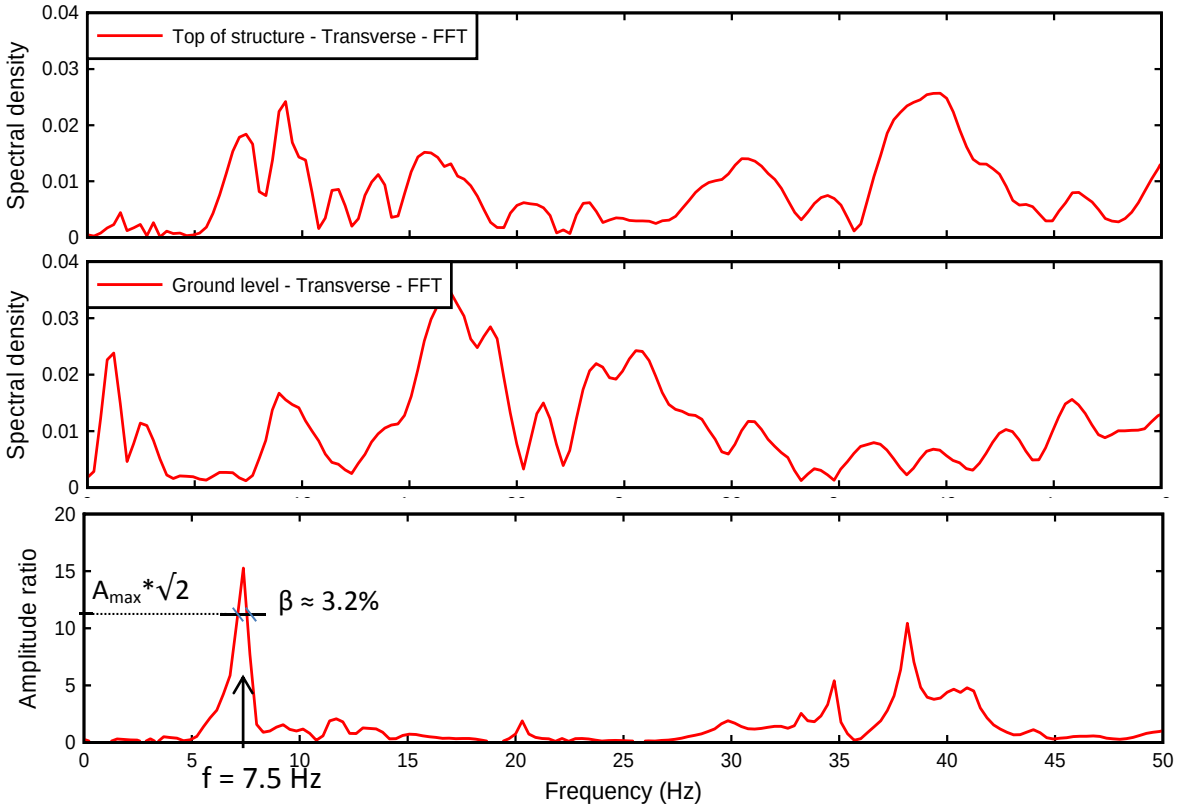

Figure IV-5 - Transfer function presenting the intrinsic characteristics of the building

In-rock measurement location		MP8		MP10						
	MAX PPVs (principal pulse)	**Event #1**	**2**	**3**	**4**	**5**	**6**	**7**	**8**	**9**
Structure	Radial Top	0.61	0.88	0.71	0.81	0.24	0.3	0.74	0.13	0.13
	Radial Ground floor	2.6	3.24	2.36	3.2	0.72	0.85	3.72	0.64	0.59
	Transverse Top	**1.16**	**1.32**	**1.64**	**1.68**	**0.49**	**0.54**	**1.6**	**0.25**	**0.23**
	Transverse Ground floor	**1.36**	**2.44**	**2.88**	**2.56**	**0.43**	**0.65**	**3**	**0.34**	**0.23**
Rock	Radial	2.09	1.11	2.13	2.26	1.87	2.07	2.44	1.30	0.75
	Transverse	**1.00**	**0.99**	**0.64**	**1.17**	**1.08**	**1.32**	**1.26**	**1.67**	**1.93**
RATIOS	**PPVtop/PPVgroundfloor**									
	Radial	0.23	0.27	0.30	0.25	0.33	0.35	0.20	0.20	0.22
	Transverse	**0.85**	**0.54**	**0.57**	**0.66**	**1.14**	**0.83**	**0.53**	**0.74**	**1.00**
	PPVtop/PPVrock									
	Radial	0.3	0.8	0.3	0.4	0.1	0.1	0.3	0.1	0.2
	Transverse	**1.2**	**1.3**	**2.6**	**1.4**	**0.5**	**0.4**	**1.3**	**0.1**	**0.1**
	PPVgroundfloor/PPVrock									
	Radial	1.2	2.9	1.1	1.4	0.4	0.4	1.5	0.5	0.8
	Transverse	**1.4**	**2.5**	**4.5**	**2.2**	**0.4**	**0.5**	**2.4**	**0.2**	**0.1**

Table IV-1 - Summary of PPV values and PPV ratios for all 9 blast events

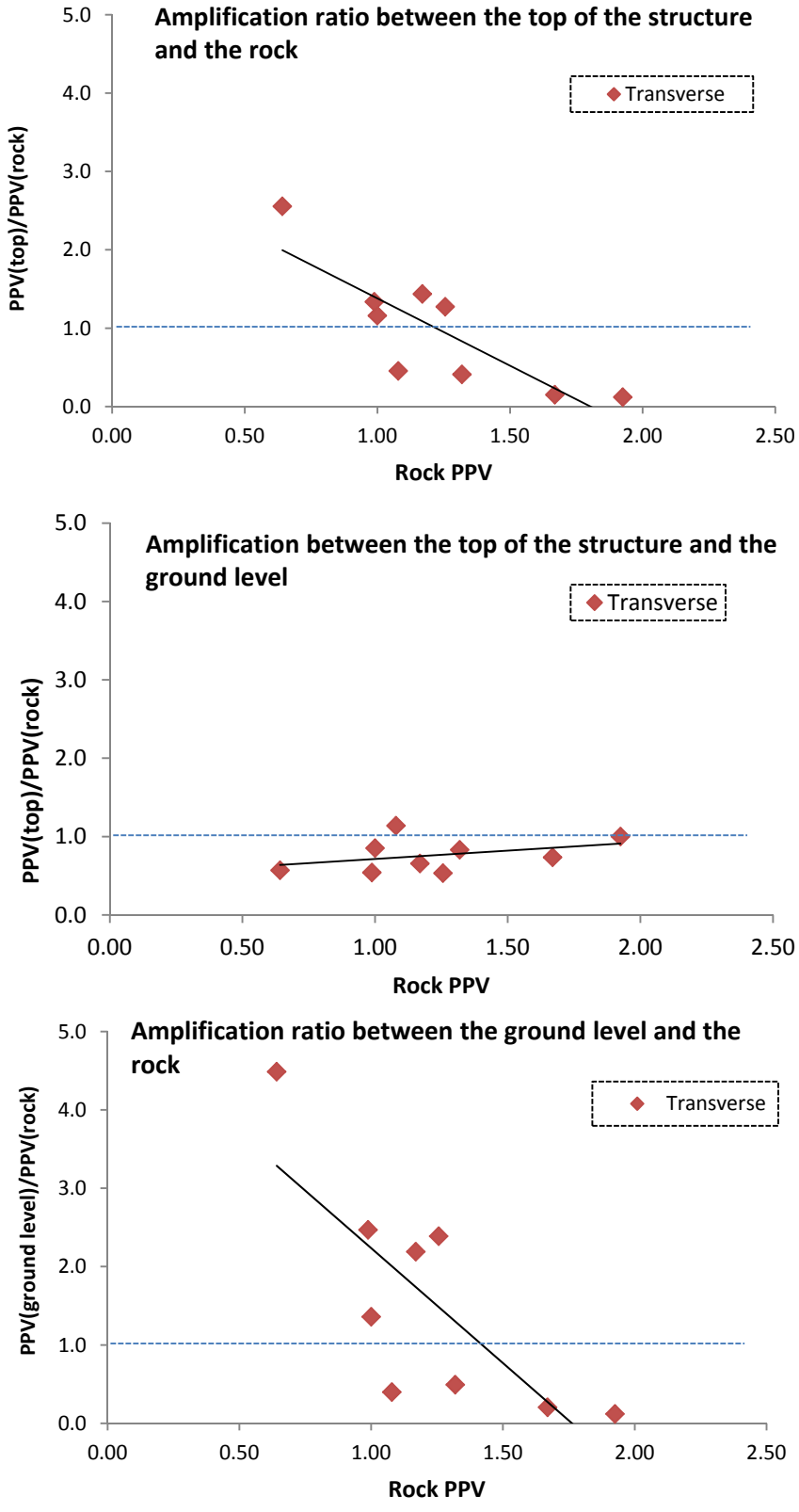

Figure IV-6 - Analysis of the PPV ratios as functions of the PPV in the rock

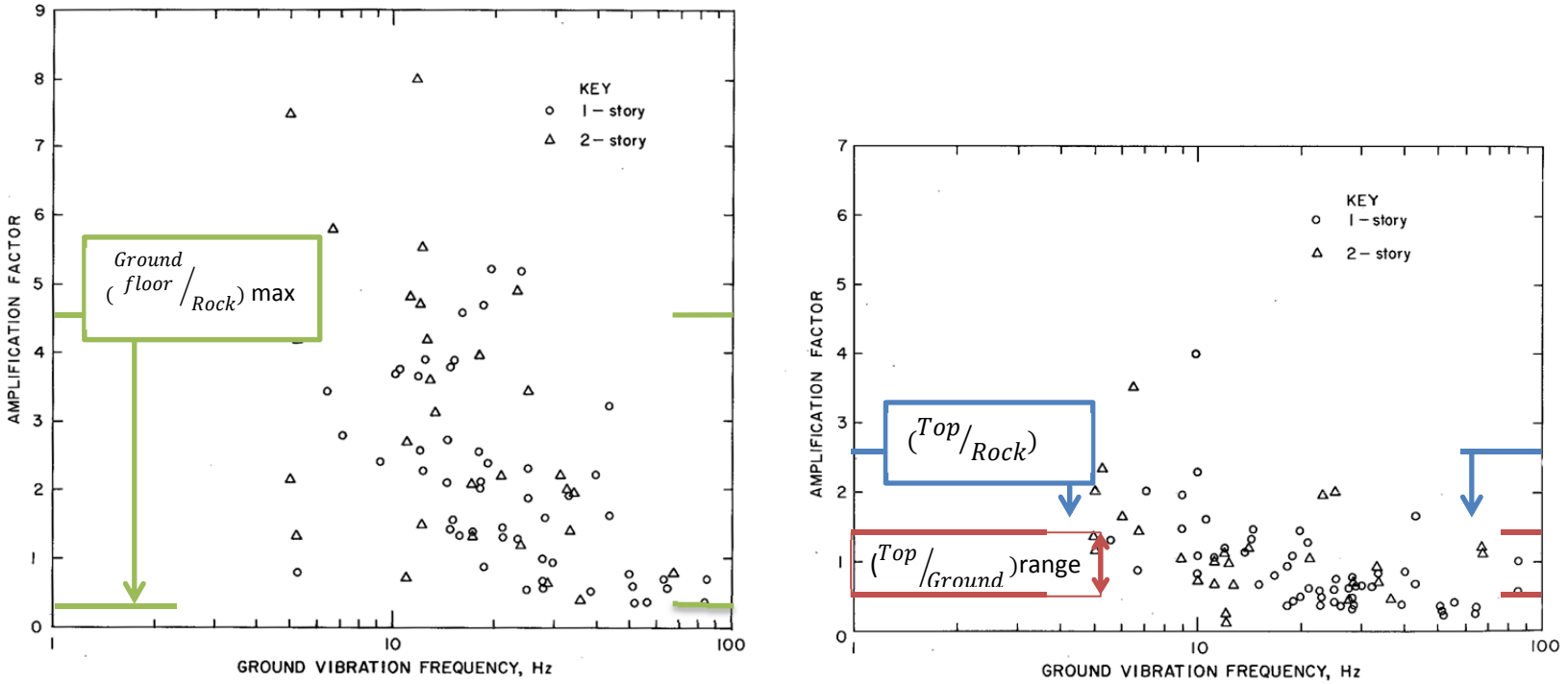

(Siskind, et al., 1980)

Figure IV-7 – Comparison of amplification ratios from this study to those measured by the U.S. Bureau of Mines (Siskind, et al., 1980); Wall response to the left and superstructure response to the right.

Displacement study and low-frequency filtering

To complement the velocity study, displacements were compared as well. They were computed from numerical integration of the velocity time histories. A 5Hz high-pass filter had to be applied to the velocity time histories to eliminate low frequency oscillation shown in the time histories in Figure IV-8. This filter was applied to all of the measurements.

Rock and lower structure displacements can then be used as inputs in the model presented in this paper, while measured top structure displacements were compared to the outputs of the model.

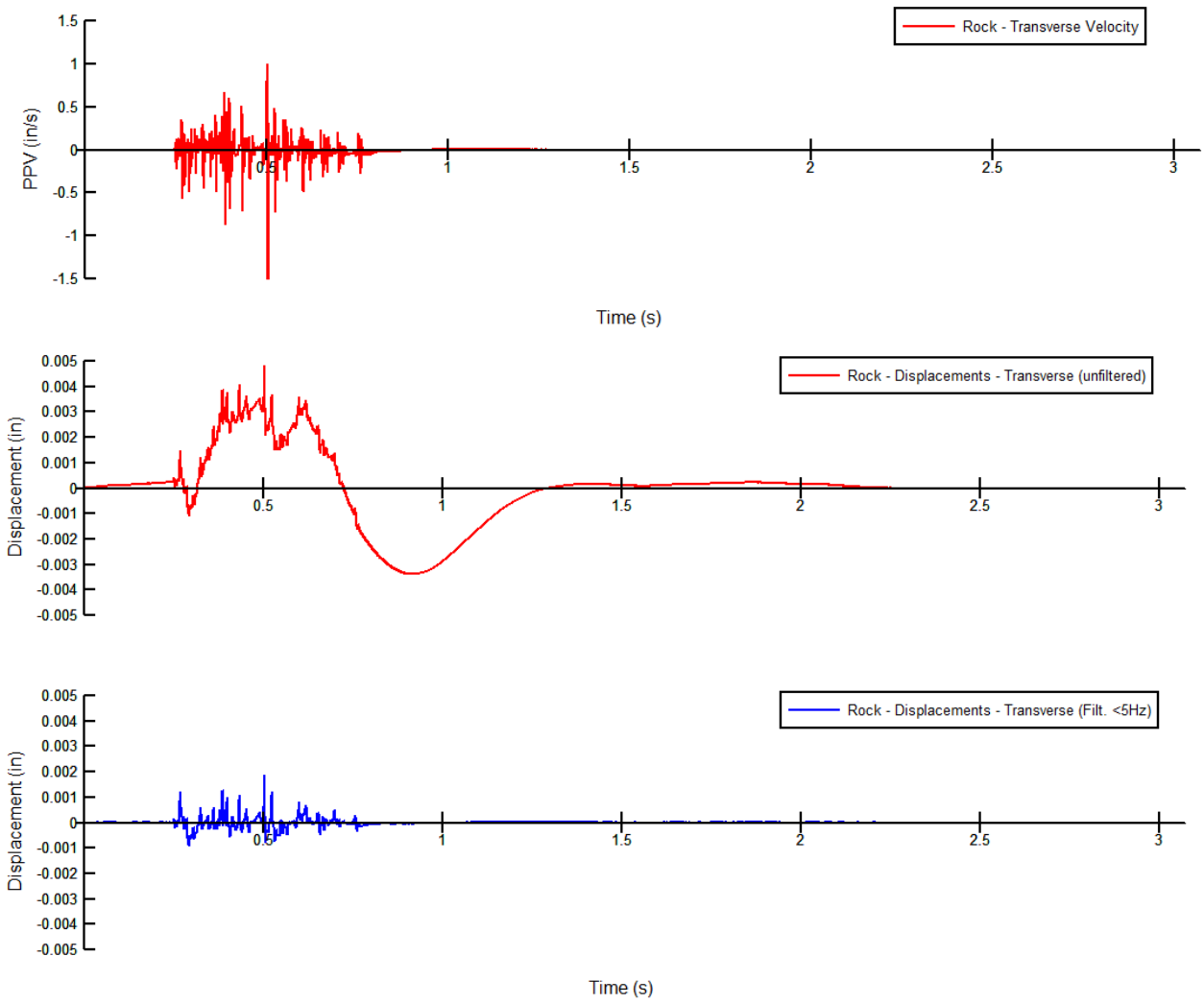

Figure IV-8 - Velocities and Displacements time histories in the Rock, before and after filtering, Transverse direction, Event 1

3D Model Of The Displacement And Strain Response Of The Structure

Presentation of software and model: parameters, inputs, outputs

A 3D model was employed to determine if "in-rock" excitation motions could be employed to estimate or predict building response. The applicability of this modeling is assessed by comparing various simulation approaches to calculate building displacements with those measured. The instrumented building was modeled with structural analysis software SAP 2000, and is presented in Figure IV-9. Building geometry was described earlier. Table IV-2 presents the building parameters that were employed in the model. Values were chosen because they were reasonable and typical. The model was not modified to fit the measured response. The contact nodes located at the base of the structure columns were modeled as fixed constraints.

Model response can either be deformation, displacement or stress at any point of the structure. Displacements of the nodes corresponding to the location of the instrumentation (shown by dots in Figure IV-9) were compared to those measured.

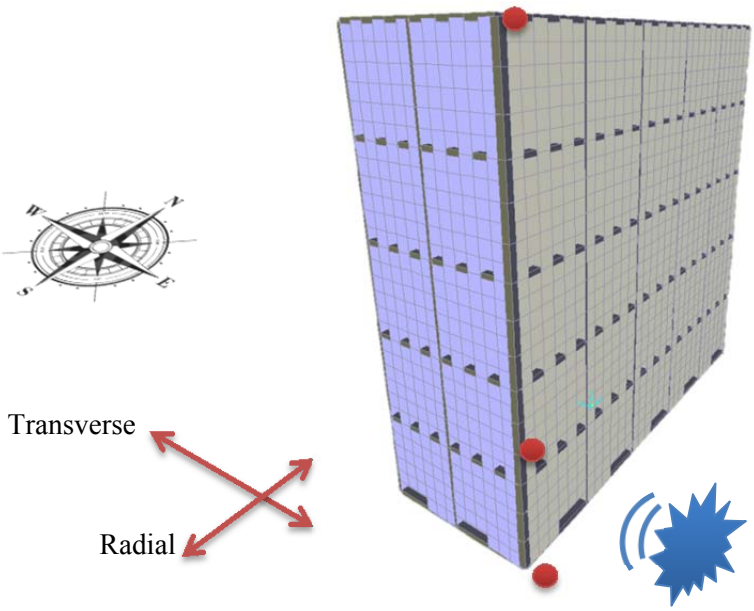

Figure IV-9 - Presentation of 3D model geometry

Parameter	Value
Building	
Width	376 in
Length	780 in
Height	768 in
Material	
Unit weight	125 pcf
Compressive strength f'c	4000 psi
Modulus E	$3.6x10^5$ psi
Poisson's Ratio U	0.2
Frame dimensions	
Beams (thickness x width)	8 x 12 in
Columns (width x width)	12 x 12 in
Material damping	5%
Slabs thickness	8 in
Walls thickness	14 in
Bay dimensions	138 x 154 x 156 in
Number of bays	50

Table IV-2 - Parameters used for the construction of the 3D model

Presentation of the different types of input

Excitation motions used to perturb the model can either be an acceleration time history or a displacement boundary condition applied to every node in contact with the ground. In the case of an acceleration input, a sample acceleration time history can be used to simulate any kind of vibration such as an earthquake or, in the case of this study, a blast. This excitation will however be the same across the whole structure, thus it cannot account for the attenuation and change in phase that occurs as the excitation vibration waves propagates through the rock.

Excitation by boundary node excitation allows more factors to be taken into account. As the waves propagate away from the source of the blast with a defined velocity, the amplitude should attenuate with distance, as is often observed. As this distance between blast and excitation node increases, the amplitude should decline. In addition, differences in travel distances between blast

and excitation node result in differences in arrival times. Differences in arrival time can be calculated by dividing the different travel distances by the propagation velocity (estimated to be 9000ft/s in the rock). These differences in amplitude and arrival times are illustrated in Figure IV-10, where the example of a blast occurring at the south west corner of the building yields different values of amplitude attenuation and time delay at different points of the building.

The SAP 2000 software allows the user to account for the attenuation and time delay by employing displacements of the ground nodes as an input. A different displacement time history for each bottom node can be specified at each point. Displacements were obtained by integrating the "in-rock" excitation particle velocity time histories. Two cases were computed with this displacement input:

- A non-attenuated displacement input, where only the displacement time measured at the "in-rock" location is employed. An example of a typical set of time histories for one blast is shown in Figure IV-12, with acceleration, velocity, and displacements plots. The event #1 acceleration time history was established by differentiating the velocity time history. This displacement time history is then used as an input to the model on every ground node, without any attenuation or delay.
- An attenuated displacement input, where the same displacement time history is entered in the software, but with attenuation and time delay such as that presented in Figure IV-10 and detailed in Figure IV-11 and Table IV-3.

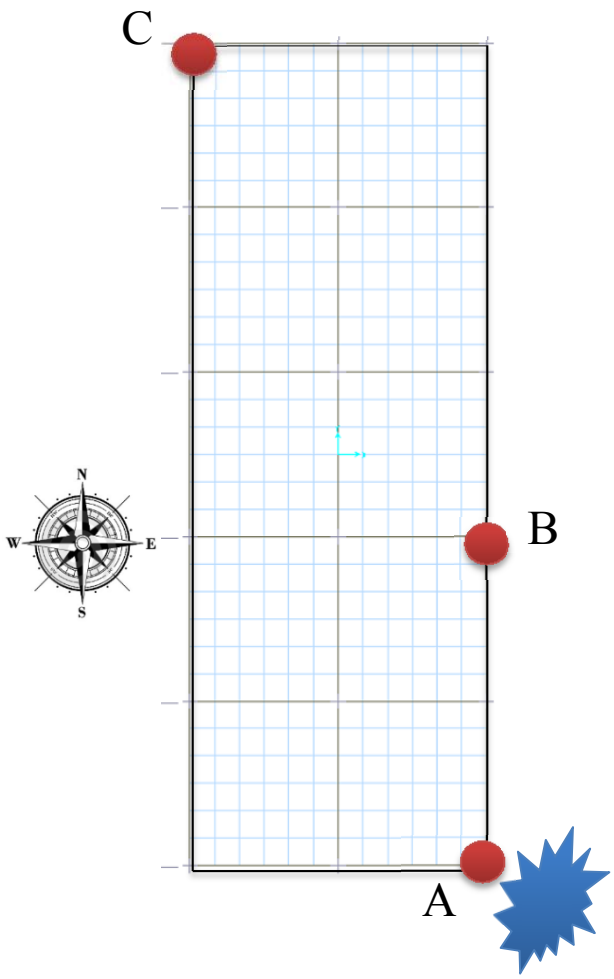

$$C_s = propagation.velocity = 9000\ ft/s$$

$$Delay = \frac{d}{C_s}$$

$$Amplitude = 100e^{-0.195d}$$

Point A:
Source of blast
Delay = 0 ms
Amplitude = 100%

Point B:
Distance = 308in
Delay = 2.85ms
Amplitude = 63%

Point C:
Distance = 818in
Delay = 7.57ms
Amplitude = 28%

Figure IV-10 - Attenuation ratio and time delay computation for some example points located at the base of the building, i.e. the interface between structure and rock

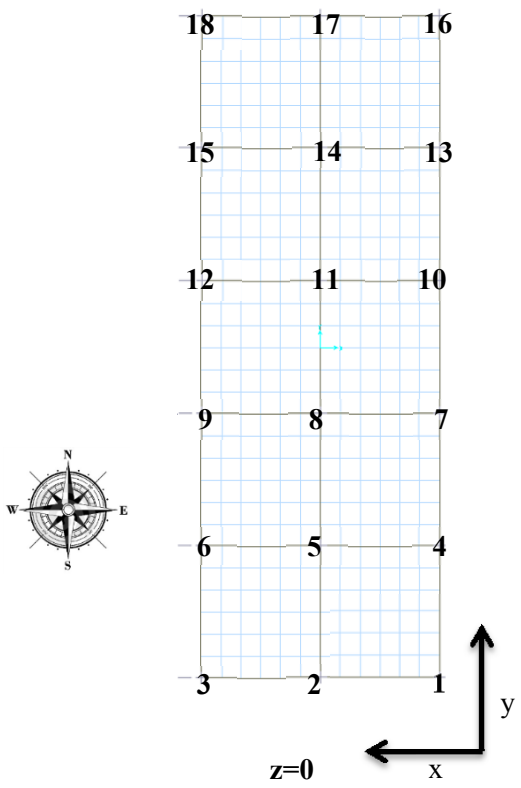

Figure IV-11 - Footprint of the 3D model of the building and numbering of columns

Column #	x (in)	y (in)	Distance from blast (in)	Propagation velocity (ft/s)	Delay (ms)	Amplitude (%)
1	0	0	0		0.00	100
2	138	0	138		1.28	79
3	276	0	276		2.56	63
4	0	154	154		1.43	79
5	138	154	206.8		1.91	72
6	276	154	316.1		2.93	60
7	0	308	308		2.85	63
8	138	308	337.5		3.13	59
9	276	308	413.6	9,000	3.83	52
10	0	462	462		4.28	50
11	138	462	482.2		4.46	48
12	276	462	538.2		4.98	43
13	0	616	616		5.70	39
14	138	616	631.3		5.85	38
15	276	616	675		6.25	35
16	0	770	770		7.13	31
17	138	770	782.3		7.24	30
18	276	770	818		7.57	28

Table IV-3 - Time delay and attenuation computation for the attenuated displacement input

Finally, a fourth model can be used to compute the expected deformation of the structure, idealizing the building as a single degree of freedom system (SDOF) as presented earlier in this report. The values of the natural frequency f and the damping ratio β obtained from the function transfer are used as building parameters: f_s = 7.5Hz and β = 3.4%. These values can be compared to the ones that were automatically computed by SAP 2000 from the structural parameters that were entered: f_s = 7.6Hz with an assumed damping ratio of 5%. The SDOF model compacts all geometry, mass, stiffness and damping into two parameters, f_s and β. In other words a single story residential structure with f_s = 7.5Hz and β = 3.4% will have the same computed SDOF response as this massive 5-story structure.

Output results from these four models (three multiple-degree-of-freedom models and one single-degree-of-freedom) can be compared to the measured displacements at the top of the structure, as shown in Figure IV-13. It appears that the results given by the acceleration excitation (top) correlate best with these measured (bottom). This correlation is better than that of either of the displacement input models. All of the multi-degree of freedom response correlated better than that of the SDOF response.

Inter-story displacement produced by the acceleration input and attenuated displacement excitation are presented in Figure IV-14 and compared to the measured displacements in Figure IV-15. In all cases the measured and calculated responses have similar dominant frequencies. The maximum amplitude of the model response with the acceleration input matches that of the measured most closely.

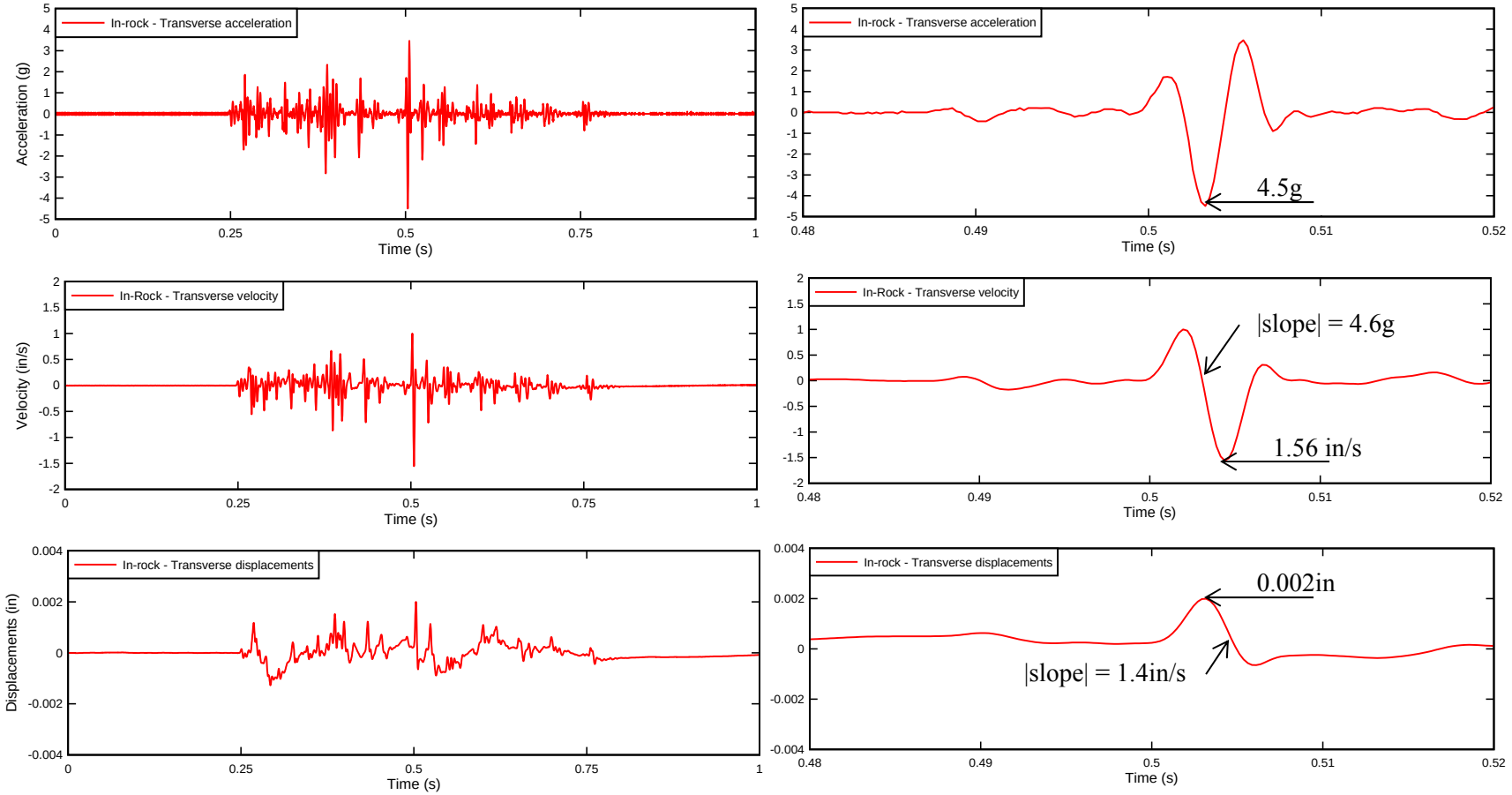

Figure IV-12 - Set of time histories in the rock used as inputs, for Event #1. The velocity is derived to obtain the acceleration, and integrated and filtered to obtain the displacements with no low-frequency trend. Principal peaks are expanded on the right.

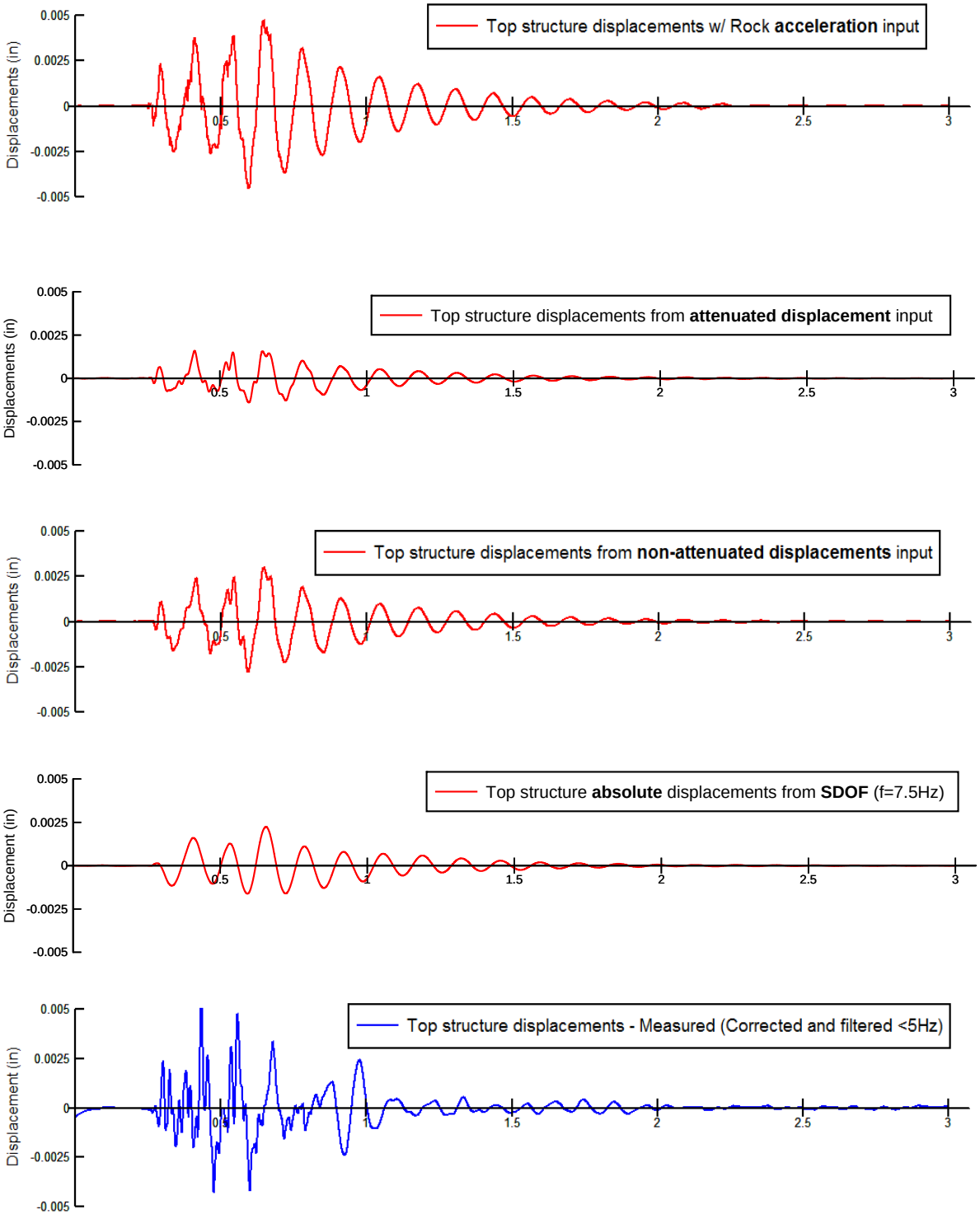

Figure IV-13 - Comparison of computed and measured displacements at the top of the structure. Attenuated displacement excitation was delayed by the propagation velocity

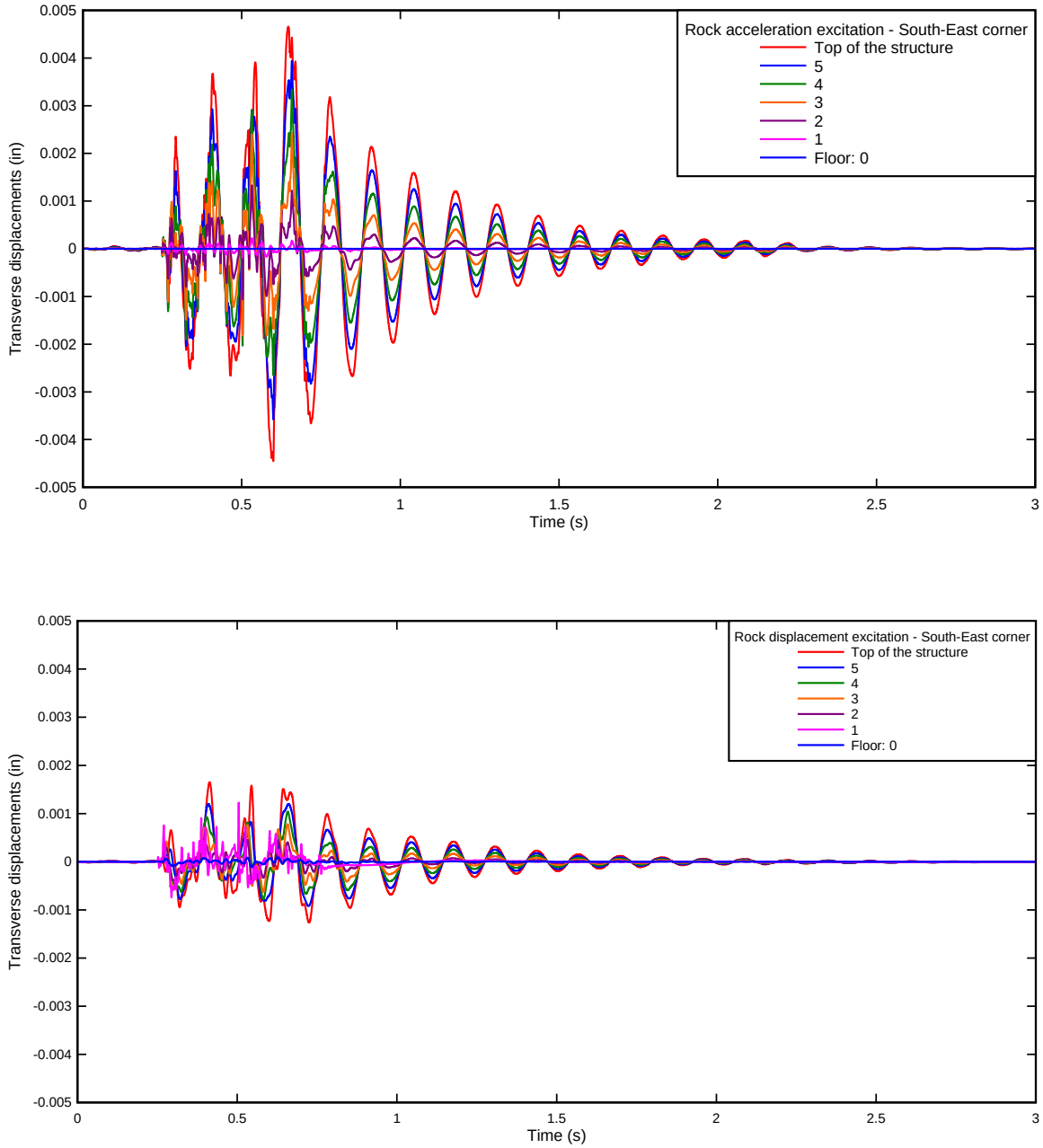

Figure IV-14 - Computed transverse displacements along the south-east corner of the building using the rock acceleration excitation (top) and the attenuated displacement excitation (bottom)

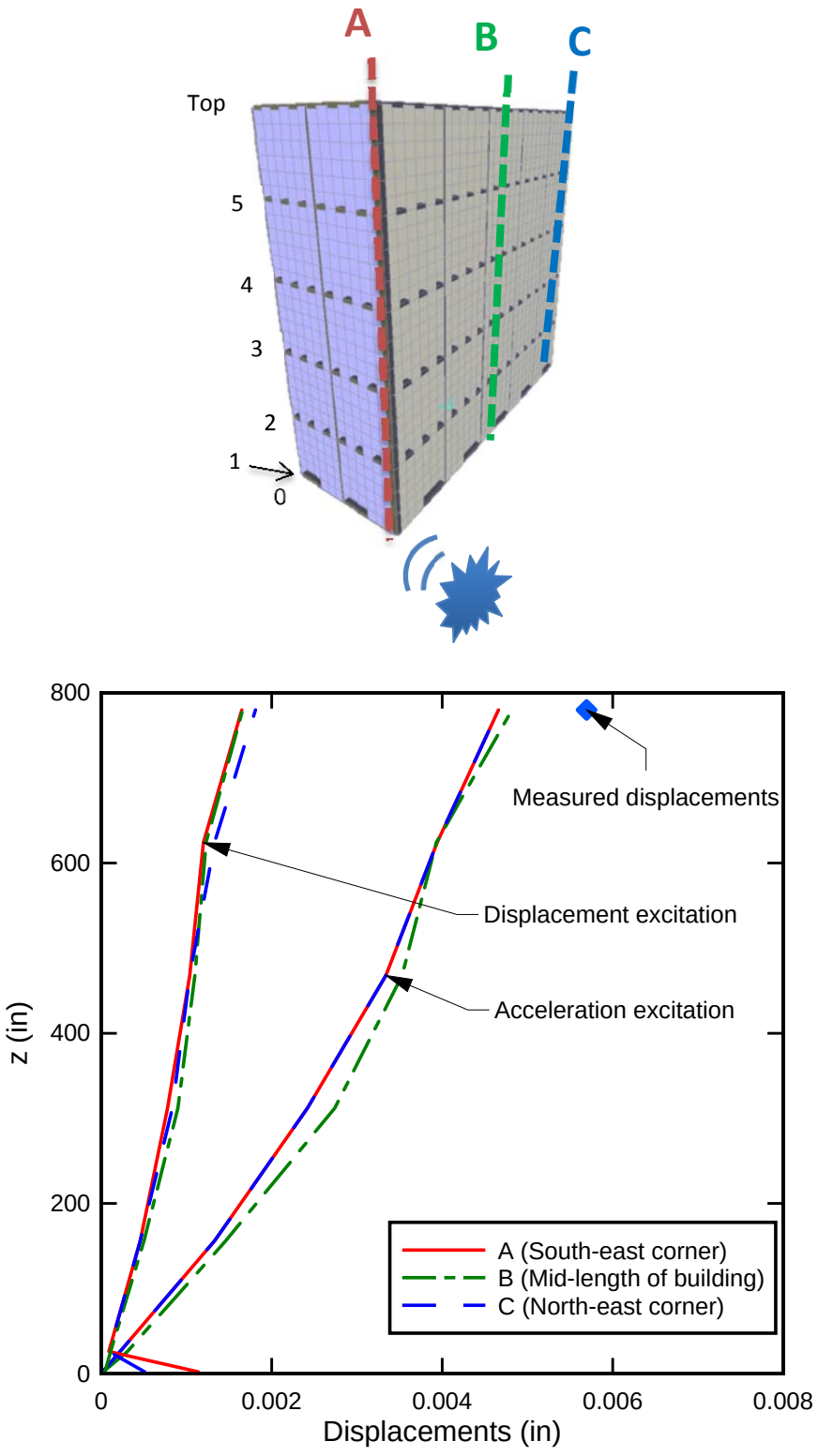

Figure IV-15 – Comparison between displacements results from acceleration and displacement excitations and those measured at the top of the structure

Strains calculation and representation

Inter-story shear strains acting on the inside transverse shear walls were calculated along the vertical line A in Figure IV-15 from the computed displacements. Figure IV-16 illustrates the method used to compute these shear strains, while Figure IV-18 compares them to the global shear strain computed from the measured displacements.

The global shear strain presented in Figure IV-18 was found by differentiating ground floor and top displacements, as shown in Figure IV-17, and was evaluated to 11.4 micro-strains.

Inter-story shear strains in Figure IV-16 were found from the peak displacement pulse produced by the acceleration perturbation shown on the right middle. These were the computed displacement on the south-east corner (vertical line A). They were determined at the same instant of time during the pulse at 0.66s. The strain distribution along vertical lines A, B and C are compared in the figure on the lower right. This procedure was also followed at 0.645s and the two strain distributions are compared at the bottom left.

This comparison shows that the strain distribution varies in amplitude and in shape as the wave propagates in the structure. Figure IV-17 presents a calculation of the propagation velocity in the structure as a function of the time delay between the measured displacement time histories as the top and the ground level. The propagation velocity of the wave in the structure was calculated to be 3440ft/s. This lag would not be observed in 1 to 2 story residential structures.

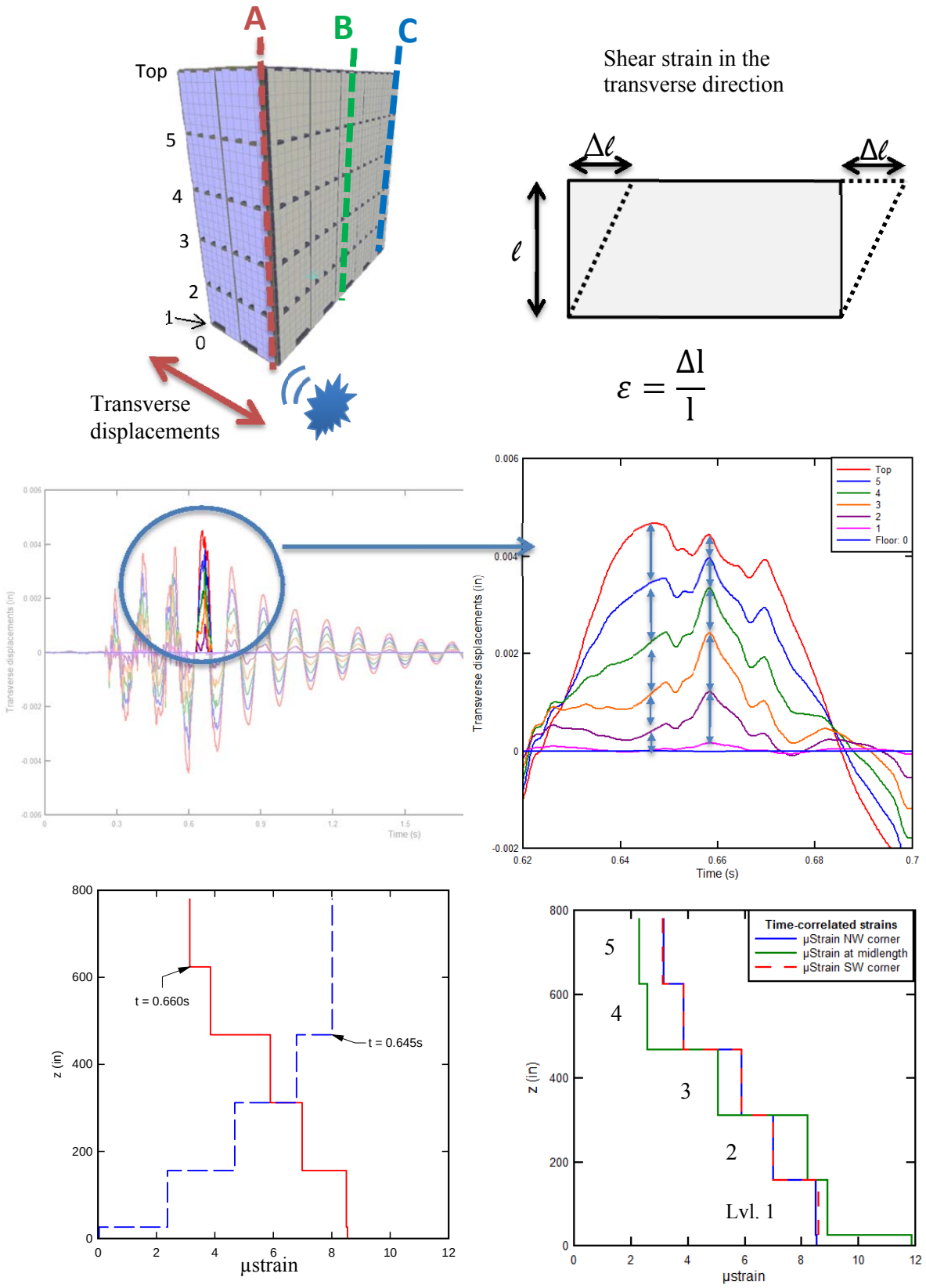

Figure IV-16 - Strains calculation using time-correlated relative displacements along vertical line A

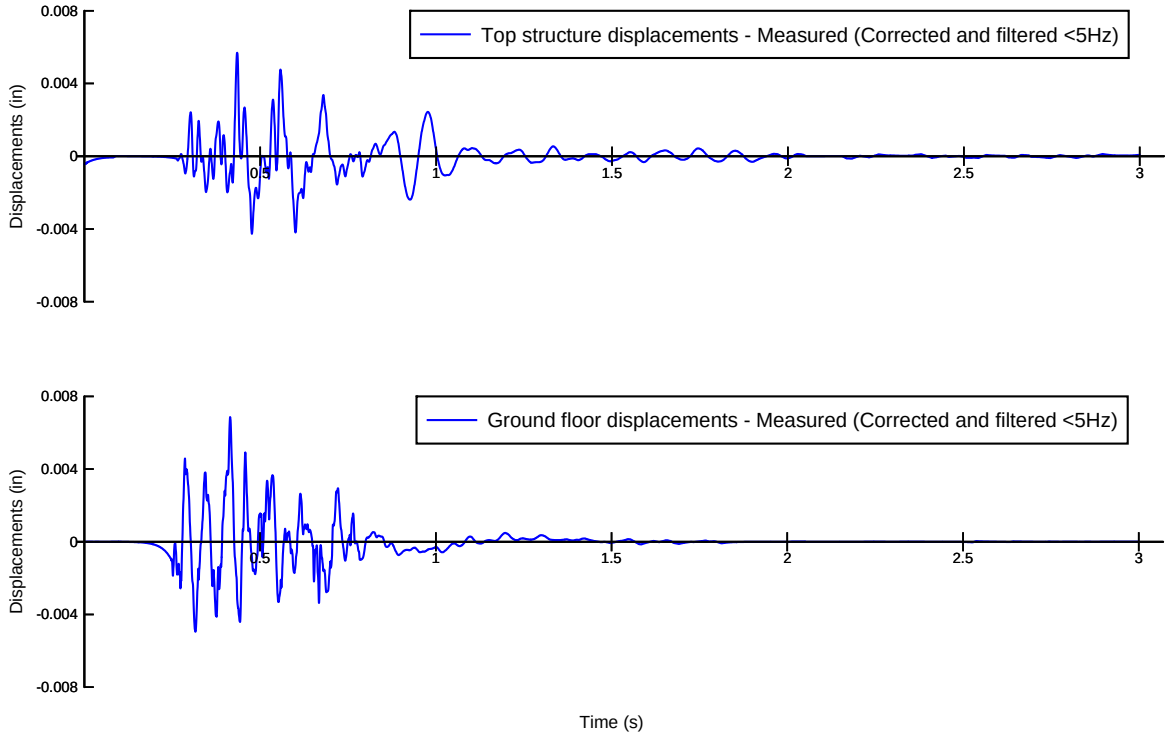

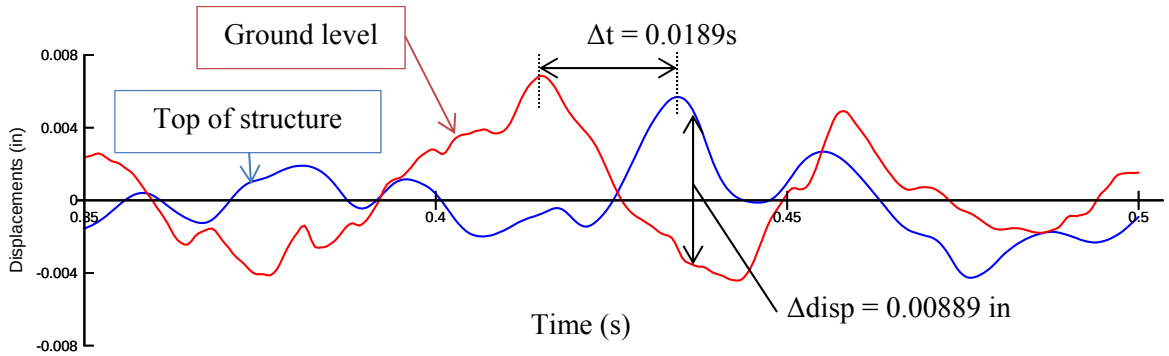

Global shear strain calculation:

$\Delta d =$ Maximum differential displacement = 0.00889in

$\varepsilon =$ Global shear strain $= \dfrac{\Delta d}{\Delta H} = \dfrac{0.00889in}{780in}$

$\varepsilon = 11.4 \times 10^{-6} = \underline{11.4 \mu strains}$

Propagation delay:

$\Delta t = 0.0189s$

$\Delta H = 780in = 65\ ft$

$C_c = \dfrac{65\ ft}{0.0189s} = \underline{3440\ ft/s}$

Figure IV-17 - Global shear strain calculation from measured displacements and wave propagation phenomenon in the structure

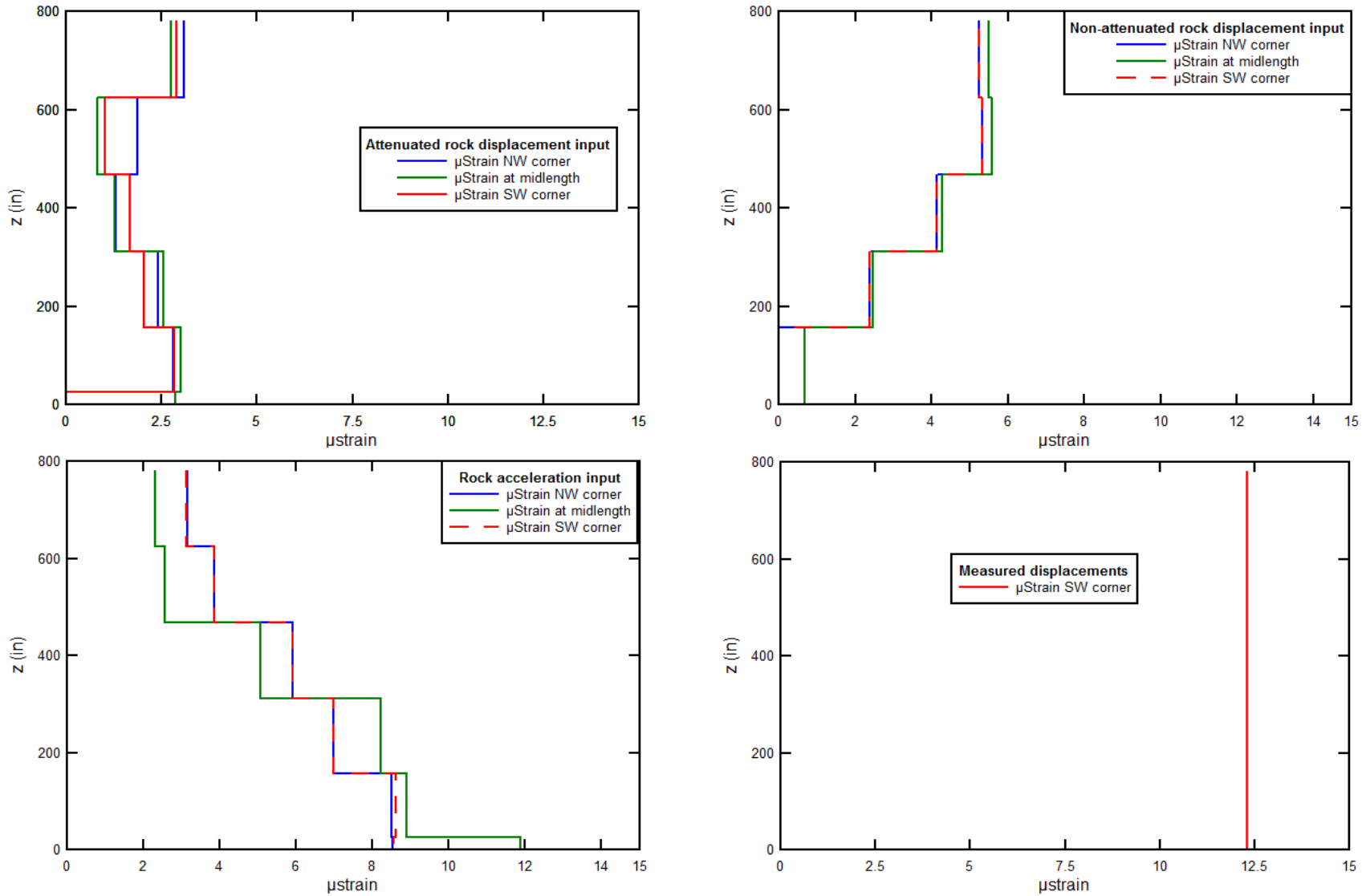

Figure IV-18 - Comparison of inter-story shear strains from different models with measured global strains

DISCUSSION

This study was possible only through the foresight of the Aimone-Martin Associates, the blasting contractor, and construction manager. Even though the data provided are not ideally comprehensive, they do represent several steps forward in instrumentation in urban environments. Velocity time histories were measured "in-rock" as well as on the building, both at the "ground floor" level and at the top. Normally compliance measurements are made only at the ground level in the building. In urban environments with immediately adjacent rock excavation, there are very limited safe, maintainable locations at which to measure ground motions without placing velocity transducers in bore holes.

Special, recoverable transducers had to be employed to measure the "in-rock" motion. The same set of transducers could be employed at different locations adjacent to the building as the blasting progressed through the site. In addition extra holes for the instrumentation had to be drilled ahead of time. All of this activity required coordination above and beyond that normal in compliance monitoring.

Building response transducers had to be emplaced on the adjacent buildings, which are not normally owned by those excavating the rock. Thus "ground floor" level transducers were placed on the outside wall of the structure. Top transducers were placed at the bottom of the exterior parapet wall to avoid penetrating the roof membrane. These location restrictions prevented the transducers to be placed at precise, structurally defined locations.

If a similar study were to be conducted, a number of steps could be taken to improve the measurement coverage. An array of geophones in the rock should be used to observe the dispersion and attenuation of rock motions with distance between 10 and 100ft away from the blast. Thus measured motions could replace those that were estimated. Amplification of the basement wall motions measured at the "ground level" could also be studied more precisely by placing

transducers along the structure at this mid-wall level. Finally, the exact location of the blast should be defined relative to the "in-rock" transducer location. This lack of blast to transducer information is not critical because the in-rock transducer measures excitation motions, no matter the location of the blast.

Modeling presented in the second part of this report could also be improved by adjusting the 3D model parameters to match the measured displacements at the top of the structure and at mid-wall locations. No attempt was made to fit model results to measured displacements. Model properties were assumed employing standard estimating technique without knowledge of the structure specifics. It also appears necessary to investigate the reason for the difference in model response between acceleration and displacement excitation. The need for only one acceleration time history implies that the excitation is applied for the structure as a whole without regard to traveling wave phenomena. Calculating the variation of the maximum strains in an appropriate 3D model as a function of peak particle velocity from 0.5 to 4 in/s (so far studied with PPV=1.5in/s) might provide valuable information on the building behavior.

CONCLUSIONS

The measurements presented in this report show that the amplification patterns in the ground and the structure match that of the US Bureau of Mines (Siskind, Stagg, Kopp, & Dowding, 1980). They decrease with increasing PPV, and are in the mid- to lower range of those measured by the USBM. The amplification values observed in this case of close-in blasting in a dense urban area are also lower than the ones found in the US Bureau of Mines report. The global transverse shear strains found by differentiating ground floor and top displacements were calculated to be 12 micro-strains.

The relative displacement response of the various models excited by rock motions show that non-attenuated displacement excitation and acceleration excitation most closely match the relative displacements calculated by differentiating ground level and top motions. The maximum inter-story transverse shear strains in the modeled structure were found through the acceleration excitation and were less than 12μstrains for a 1.5ips rock motion, and declined with elevation. The inter-story transverse shear strains calculated with rock displacement input were less than half that found with the acceleration excitation.

Chapter V- CONCLUSIONS

This thesis summarizes micro-inch crack response to environmental phenomena and blast-induced ground motions from an aggregate quarry in Illinois, and to road compaction using vibratory rollers in New Mexico. It also compares measured and 3D model simulation of a building response to close-in blasting in a dense urban area. These structures were instrumented and studied as part of the Autonomous Crack Monitoring [ACM] research effort at the Infrastructure Technology Institute [ITI] at Northwestern University in Evanston, Illinois.

Responses of the Illinois house have been measured for more than two years and were presented and analyzed in Chapter II. More than 28 months of continuous crack response have been recorded, including several periods of many months without blasting, thus showing that large crack response occurs without blasting. The unusually long monitoring period allows observation of two maximum, climatologically induced peak crack responses, and as such represents one of the longest periods of continuous observation in the literature. These once a year peak climatological responses are compared with unusually intensive ground motions in excess of that allowed by regulation.

As has been observed before, crack response to environmental variations was shown to be overwhelmingly larger than that produced by blast induced ground motion and associated air overpressure pulses. Seasonal variations and even the passing of weather fronts can produce crack response that is larger by at least an order of magnitude. Turning off the heat inside the house in the fall can cause crack response of that order of magnitude larger as well, but over periods of time as short as a week. Observation of occupant activity and wind gust events shows that both can produce crack response as large as that produced by blast induced, typically annoying ground motions.

The response of the New Mexico adobe house to construction vibrations during road compaction was measured for only a short period of a week. Structure displacements and existing crack displacements were measured and employed to calculate strains. Results were presented in Chapter III. Construction-induced dynamic crack displacements were compared to that induced by changes in temperature and humidity.

Measured structural and crack response over a period of a week during which vibratory rollers were used to compact an adjacent road showed that the influence of temperature and humidity is more than 15 times greater than any motion that occurred during vibration work, even though one event produced peak particle velocity of nearly 0.5ips. The strain study demonstrated that the minimum factor of safety against cracking from vibrations is 20. Thus large weather-induced changes in crack width are the greatest contributing factor to crack extension and widening over time.

Chapter IV presented the dynamic response measurements and analysis of a 5-story building to very-high frequency excitation from blasting vibrations originating from a contiguous excavation. Velocity transducers, which were located in the rock and on the structure were used to measure the dynamic displacement response of the building to blasting. A 3D model was used to compare computed displacements and strains to measured results.

Measurements presented in this chapter showed that the amplification patterns at the ground level and top of the structure match or are lower than that observed by the US Bureau of Mines (Siskind, et al., 1980). They decrease with increasing PPV. From the measurements, the global transverse shear strains found by differentiating ground floor and top displacements were calculated to be 12μstrains.

Relative displacement response of the various model produced by various modes of excitation show that non-attenuated displacement excitation of the base and acceleration excitation most closely match the relative displacements calculated by differentiating first floor and top motions. The maximum inter-story transverse shear strains calculated with the model were found through the acceleration excitation and were less than 12μstrains for a 1.5ips rock motion. The inter-story transverse shear strains calculated with rock displacement input were less than half that found with the acceleration excitation.

REFERENCES

Aimone-Martin, C. T. (2011). *Structure Response of the Conroy Honors Center to Construction Vibrations.* Socorro, NM: Aimone-Martin Associates LLC.

Dowding, C. H. (1985). *Blast Vibration Monitoring and Control.*

Dowding, C. H. (1996). *Construction Vibrations.*

Dowding, C. H. (2008). *Micrometer Crack Response to Vibration and Weather.* International Society of Explosives Engineers.

Dowding, C. H., Kotowsky, M., & Koegel, T. (2011). *Field Qualification of Inexpensive Wireless System to Monitor Micro-Inch Crack Response for Structural Health Monitoring.* Technical report, ITI - Northwestern University, Evanston, IL.

Koegel, T. (2011). *Comparative Field Qualification of ACM and ACSM Systems at Sycamore, IL.* ITI - Northwestern University, Evanston, IL.

Kosnik, D. E. (2008). *Autonomous Crack Displacement Monitoring of a Residence Near a Limestone Quarry, Naples, Florida.* Technical Report, ITI - Northwestern University, Evanston, Illinois.

Meissner, J. E. (2010). *Autonomous Crack Monitoring of Residential Structure – Sycamore, IL.* Installation Report, ITI - Northwestern University, Evanston, Illinois.

Meissner, J. E., & Dowding, C. H. (2009). *Response of a Concrete Block Structure to Quarry Induced Ground Motion and Weather.* Technical report, ITI - Northwestern University, Evanston, Illinois.

Siebert, D. (2000). *Autonomous Crack Comparometer.* MS Thesis, Northwestern University, Evanston, IL.

Siskind, D. E., Stagg, M. S., Kopp, J. W., & Dowding, C. H. (1980). *RI8507 - Structure Response and Damage Produced by Ground Vibration From Surface Mine Blasting.* U. S. Bureau of Mines.

Snider, M. L. (2003). *Crack Response to Weather Effects, Blasting, and Construction Vibrations.* Evanston, IL: Northwestern University.

Welsby, S. D., & Hitz, T. (1997). *True Position Measurement with Eddy Current Technology.*

APPENDIXES TO CHAPTER III

Appendix A - Time correlation between structure vibration data and crack response

Appendix B - Calculation of Structure Wall Strains

Appendix C - Vibration compaction events

APPENDIX A - TIME CORRELATION BETWEEN STRUCTURE VIBRATION DATA AND CRACK RESPONSE

Due to the use of two different devices to record the structure dynamic response and the crack opening, in some rare cases there is an uncertainty in the time-correlation between the recordings. In such a case, as shown in **Figure A1**, a given crack response could be positioned differently in time depending on the trigger point that was used as a starting signal for the recording device. In this case, a choice was made to correlate signals using the very first triggering point of every event, as shown with the Correlation 1 in **Figure A1**. However, since the time bases are different between the two devices, it is safer to perform this verification for every event.

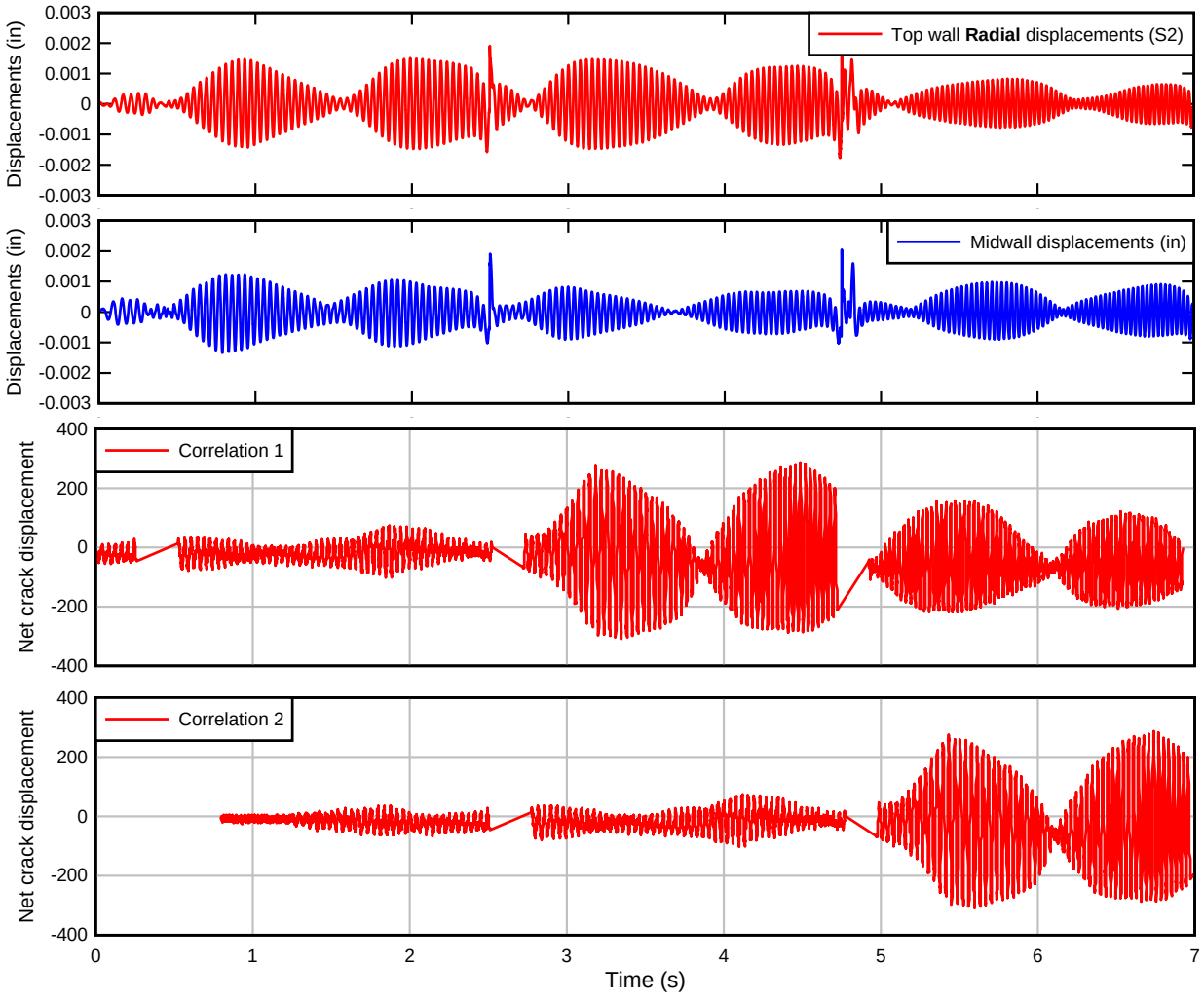

Figure A1 - Manual time-correlation between crack opening and dynamic vibration time histories

APPENDIX B - CALCULATION OF STRUCTURE WALL STRAINS

Strains Calculated for Structure Walls

The magnitude of induced strains in structure components ultimately determines the likelihood of cosmetic cracking in residences. Global or whole structure shear strains leading to in-plane tensile wall strains and mid-wall bending strains arise from corner distortions and wall flexure as illustrated in **Figure B1**. It is the practice to use gypsum core drywall board material as the representative construction material that would first show signs of distress when structures are subjected to high dynamic blasting strains. This "threshold" material is thus associated with "threshold" cracking potential. Therefore, wall strains are computed for the largest external excitation (e.g., the excitation that generates the highest horizontal ground motion) and strains are compared with failure strain levels required to crack existing wall materials.

In-plane Tensile Strains

Wall materials crack in tension caused by wall shearing distortions in which the diagonal dimension, L, is "stretched" by ΔL as shown in **Figure B1**. Shear strains may be estimated from differential structure corner motions calculated from the difference in displacements at the upper, S2, and lower, S1, corners in a direction parallel with the plane of the wall of interest. In other words, for a structure with walls parallel with the north and west directions, ground motions that cause the south wall to flex, drive shear distortions in the east wall and visa-versa.

Velocity time histories measured at structure corner locations S1 (lower corner) and S2 (upper corner) are integrated to obtain displacement time histories. The difference between the time histories are computed and the largest time-correlated difference, δ_{max}, between corner responses (S2 minus S1) are found.

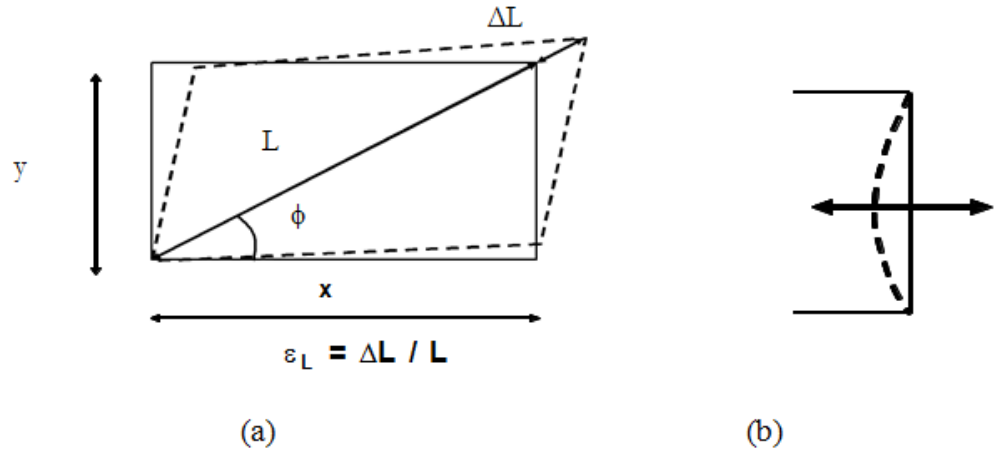

Figure B1 - In-plane tensile strain, ε_L (a) and out of plane mid-wall bending (b)

Global shear strain is determined by the following:

$$\gamma_{max} = \frac{\delta max}{L}$$

where

γ_{max} = global shear strain (micro-strains or 10^{-6})
δ_{max} = maximum differential displacement, S2 – S1 or S3 - S1 (in)
L = height of the wall subjected to strain, or the difference in height between upper and lower corner sensors (in)

In-plane tensile strains, important in the assessment of wall cracking potential, are a function of the wall dimensions. The maximum tensile strain, ε_{Lmax}, is calculated from global shear strain by the equation:

$$\varepsilon_{Lmax} = \gamma_{max} (\sin\theta)(\cos\theta)$$

where θ is the interior angle of the longest diagonal of the wall subjected to strain with reference to a horizontal. Theta, θ is calculated by taking the inverse tangent of the ratio of wall height to wall length.

Bending Strains

Bending strains in walls are computed using the mid-wall sensors. Walls of structures, which approximate flexible plates, tend to flex in a direction perpendicular to the plane of the wall with maximum displacements in the first mode of response at the middle of the wall as shown in **Figure B1** (b). Such wall flexure is directly related to the bending strain induced in the walls and is modeled as a beam fixed at both ends, e.g., at the lower corner or often the foundation (S1) and upper corner or the roof (S2).

It has been determined that foundations are well coupled to the ground, or "fixed". However, the roof can be modeled with varying degrees of "fixity", ranging from relatively unconstrained to highly fixed. Bending strain is most conservatively estimated with the fixed-fixed analogy because this model predicts the highest strains in walls per unit of maximum relative displacement at the mid-point height of a wall.

$$\varepsilon_L = \frac{6\, d\, \Delta\delta max}{L^2}$$

where

ε_L = bending strain in walls (micro-strains or 10^{-6})
d = the distance from the neutral axis to the wall surface, or one half the thickness of the wall subjected to strain (in.)

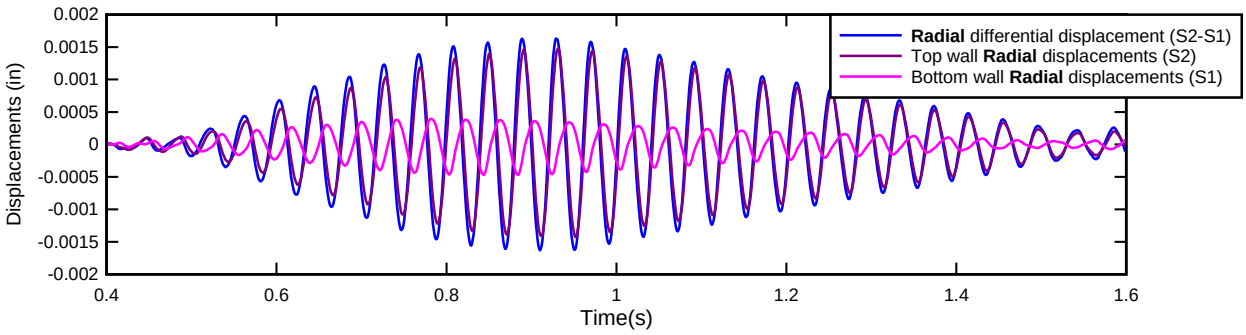

Figure B2 - Peak differential displacement during Event #1

Figure B2 presents the way the differential displacements were computed, plotted and used in order to compute the strains. The absolute displacements at the bottom of the wall (S1) were subtracted from the absolute displacements at the top of the wall (S2), thus giving the value of the differential displacements. The structure strains are then obtained from these differential displacements, using the adequate direction, radial or transverse.

Figures B3 and B4 present an example of the displacement study that was performed, for event #1. The structure displacements (top S2, bottom S1 and mid-wall) as well as the ground displacements are plotted, along with the differential displacements (S2-S1 and midwall–average(S1,S2)).

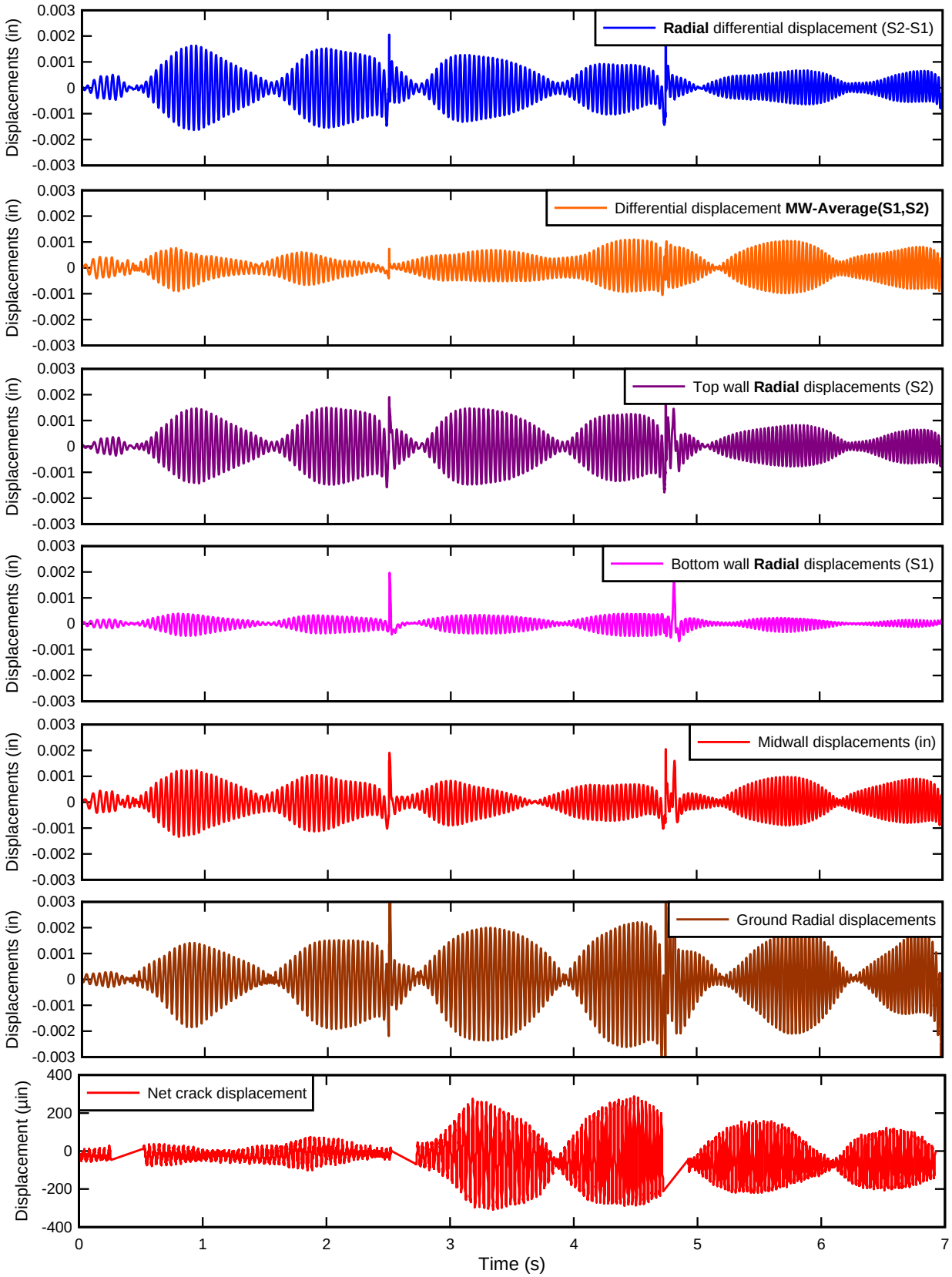

Figure B3 - Event #1 displacements study – Radial direction

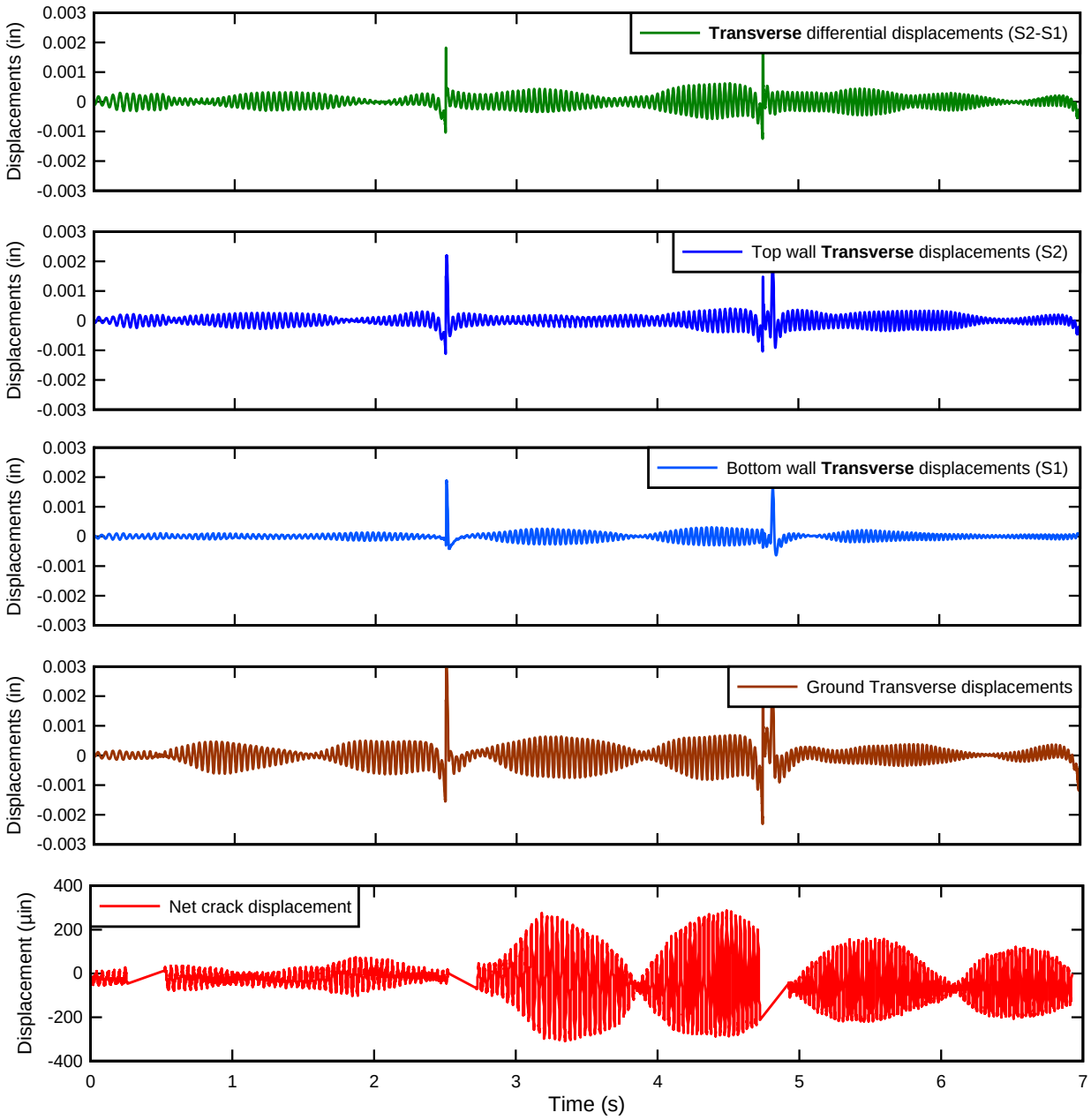

Figure B4 - Event #1 displacements study – Transverse direction

APPENDIX C - VIBRATION COMPACTION EVENTS

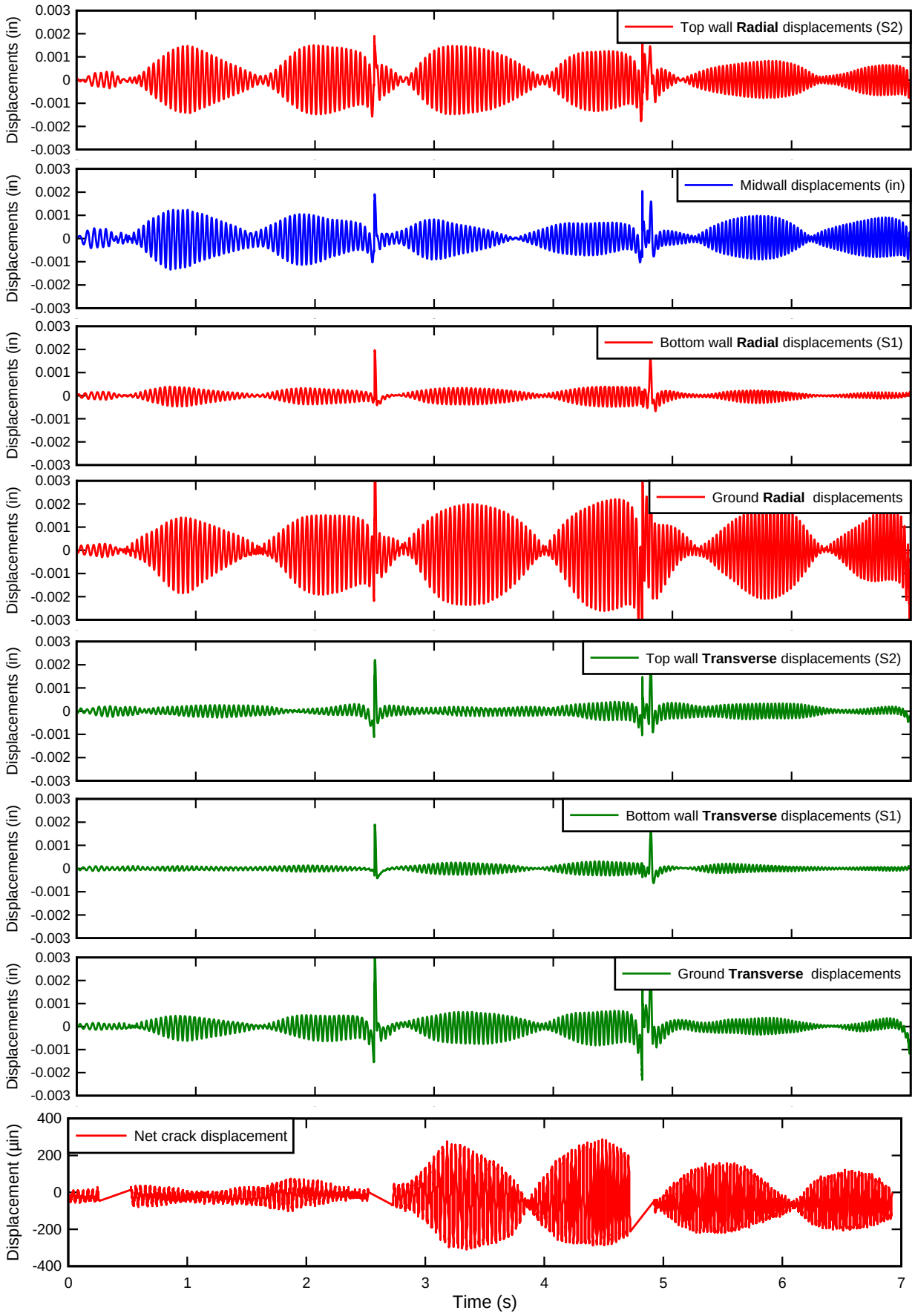

Figure C1 - Displacements time-histories for Event #1 - 10:40am on 04/18/2011

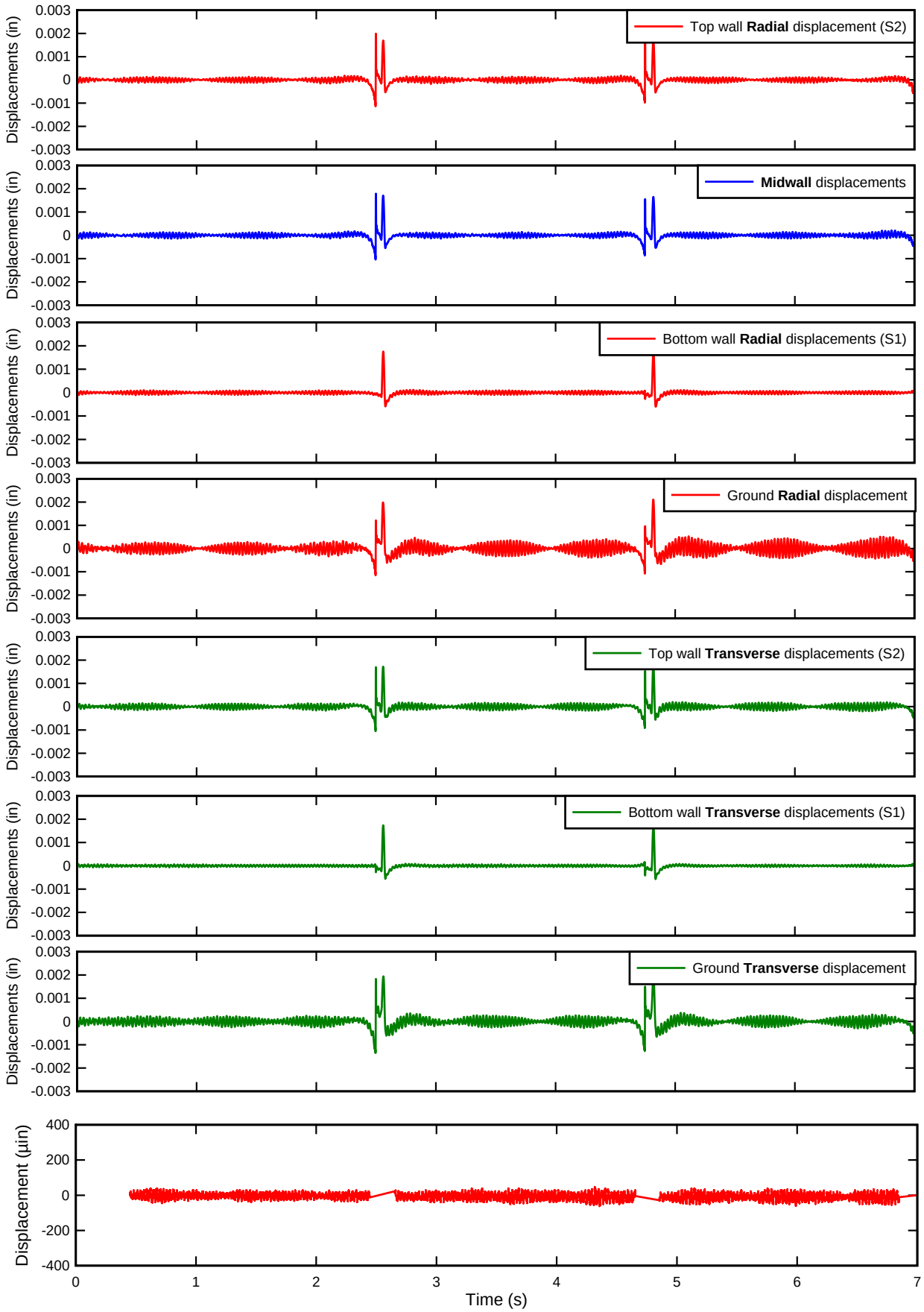

Figure C2 - Displacements time-histories for Event #2 - 10:47am on 04/18/2011

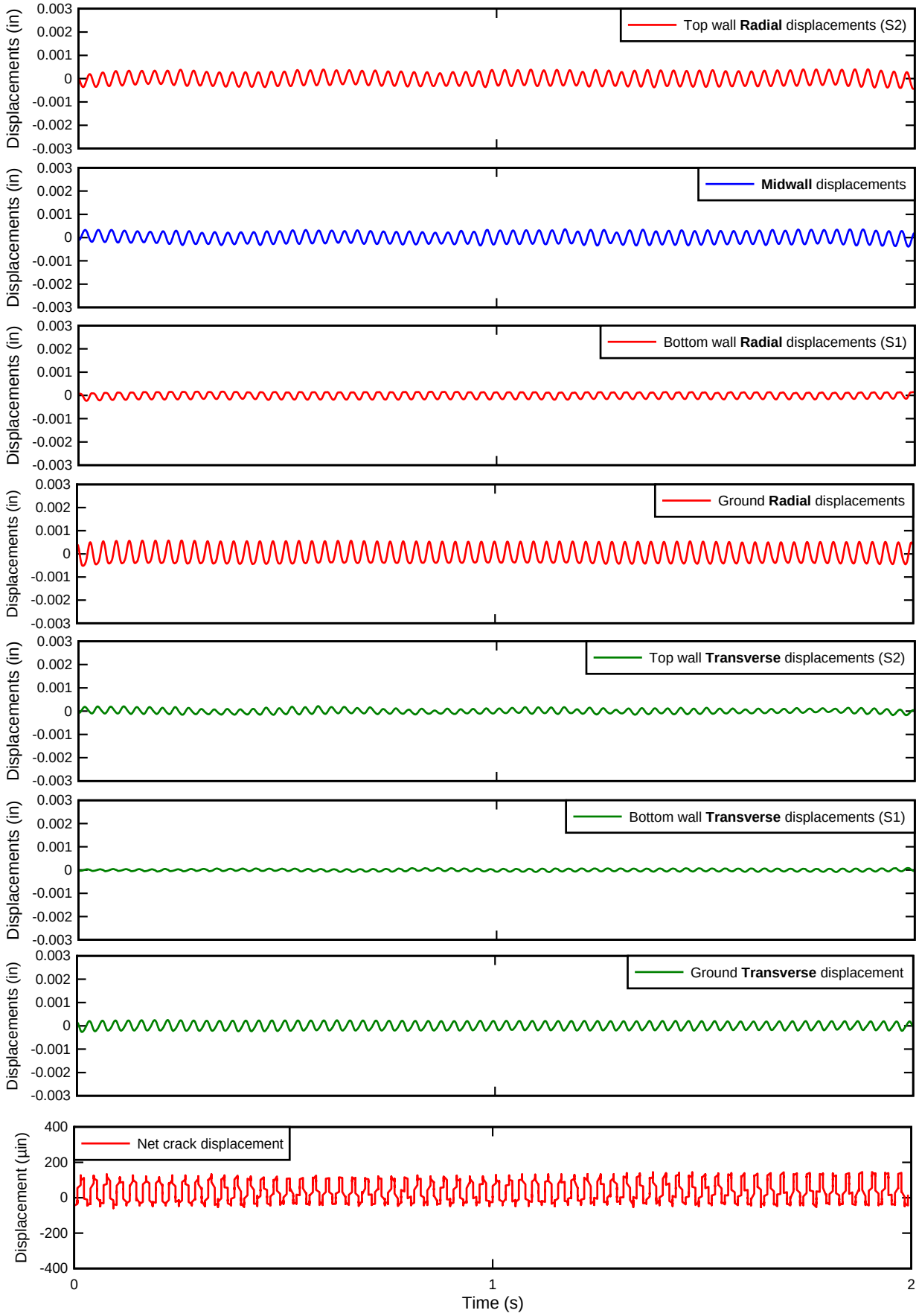

Figure C3 - Displacements time-histories for Event #3 – 12:40pm on 04/14/2011

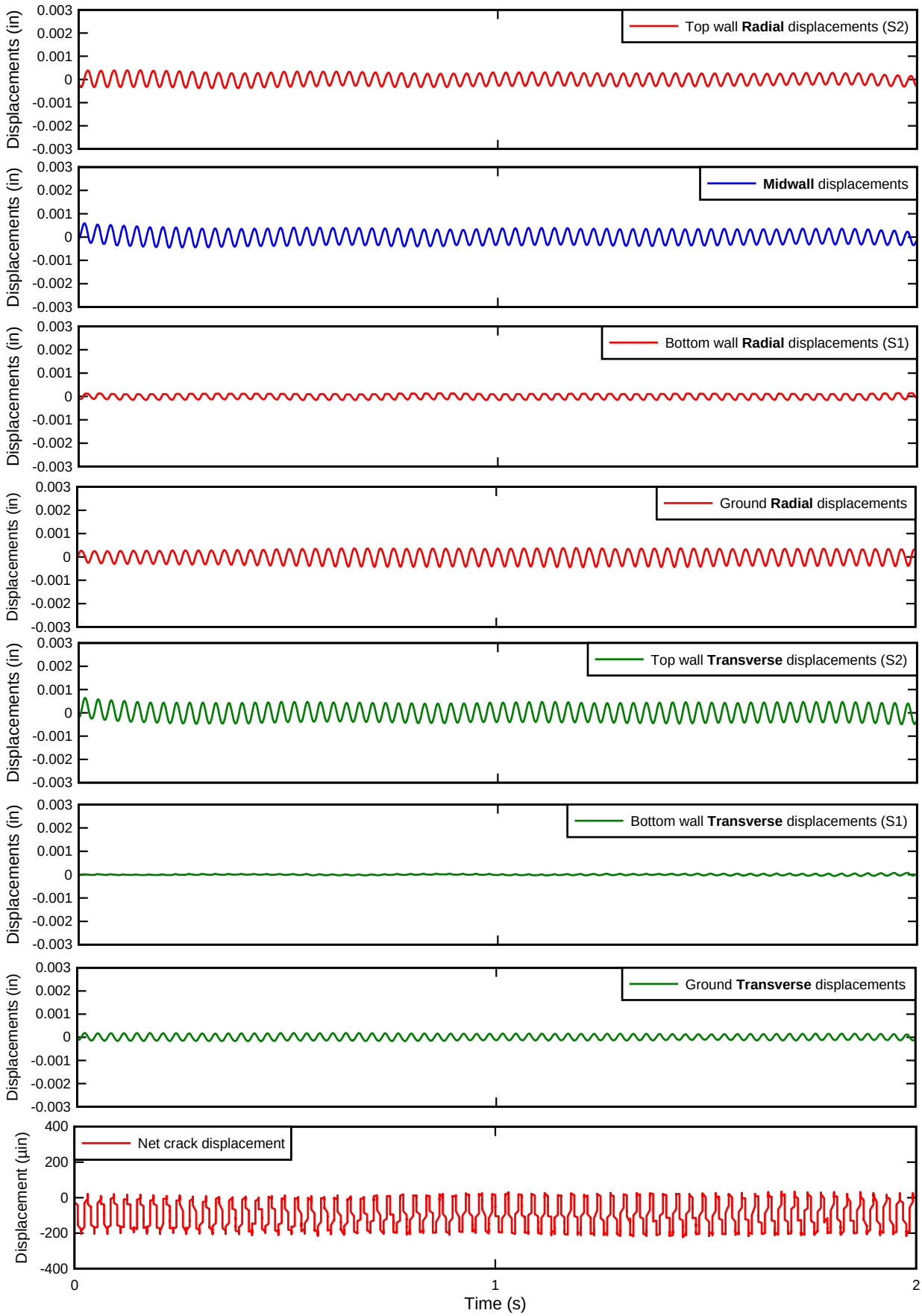

Figure C4 - Displacements time-histories for Event #4 – 12:47pm on 04/14/2011

APPENDIX D – RECORDED VELOCITY TIME HISTORIES IN THE TRANSVERSE DIRECTION

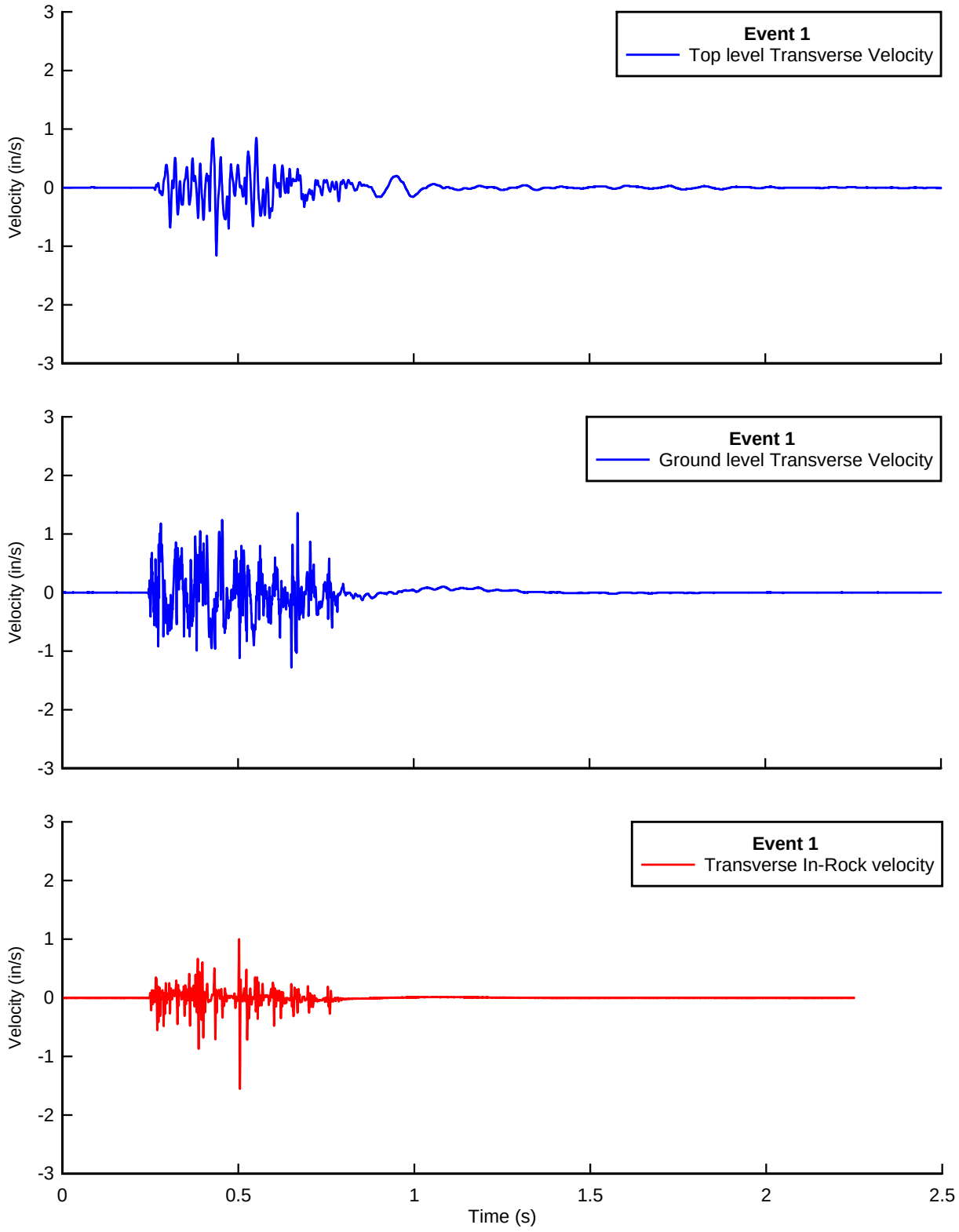

Figure D-1 - Recorded Velocity time histories in the Transverse Direction, in the rock and on the structure at ground level and top level, during Event #1

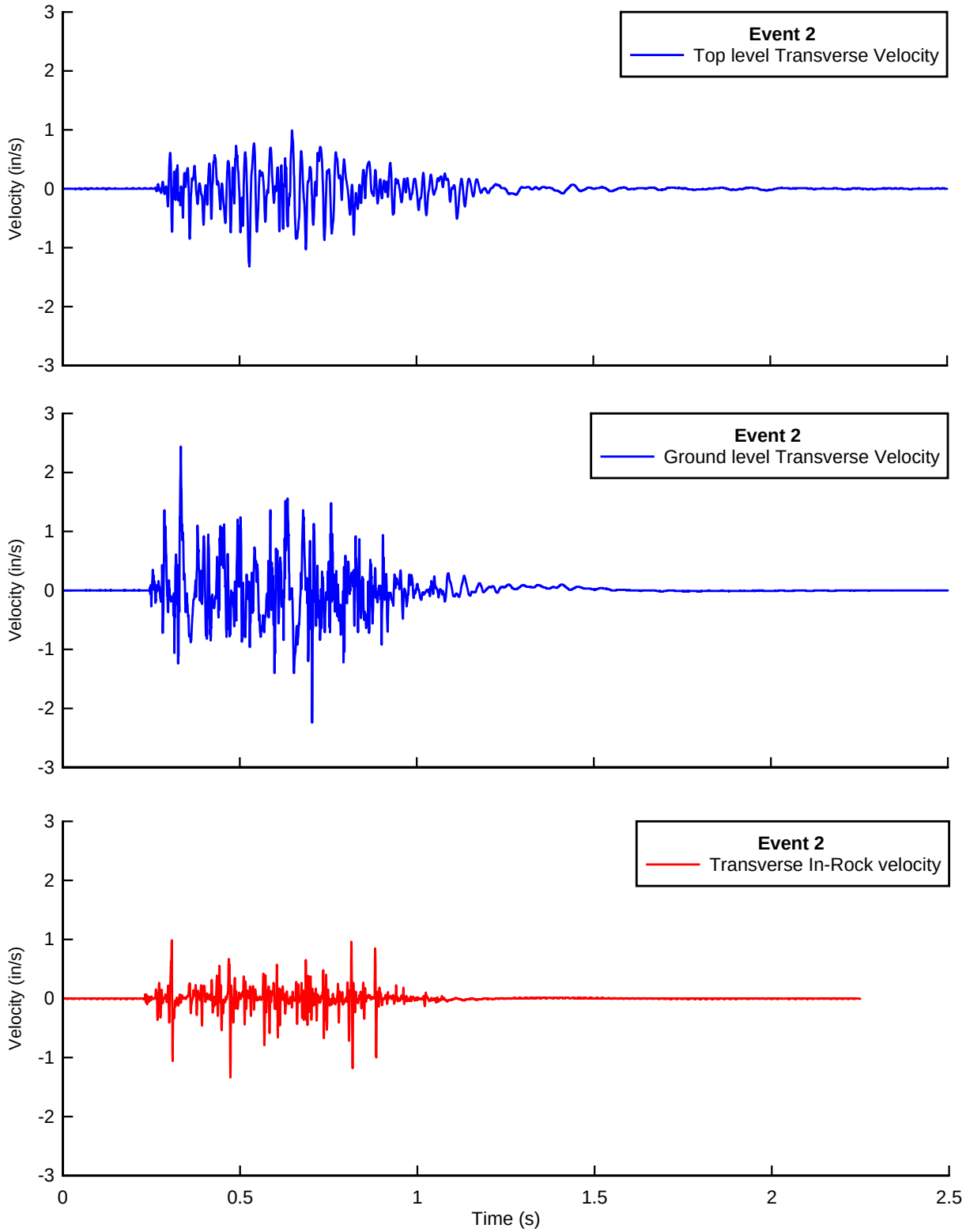

Figure D-2 - Recorded Velocity time histories in the Transverse Direction, in the rock and on the structure at ground level and top level, during Event #2

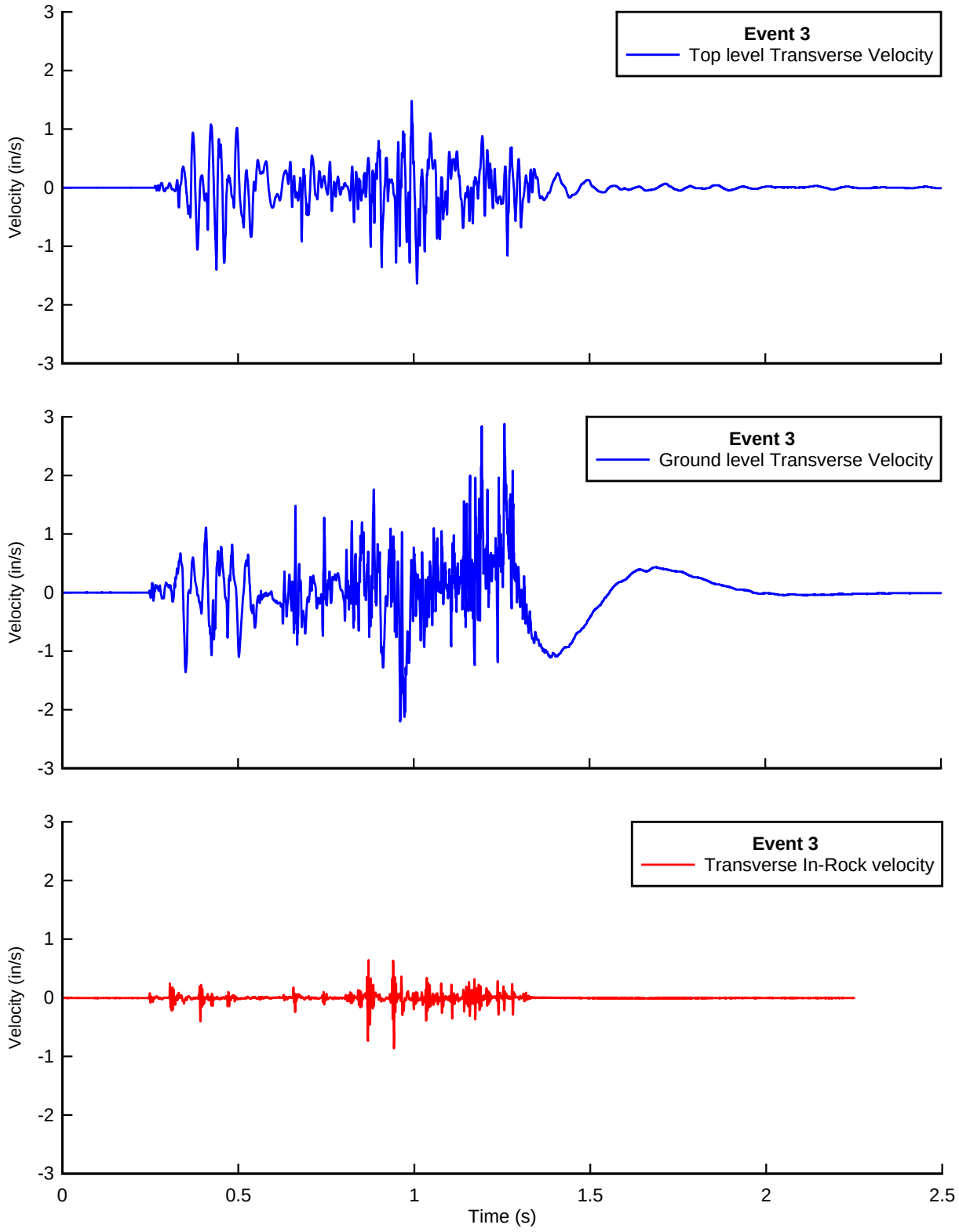

Figure D-3 - Recorded Velocity time histories in the Transverse Direction, in the rock and on the structure at ground level and top level, during Event #3

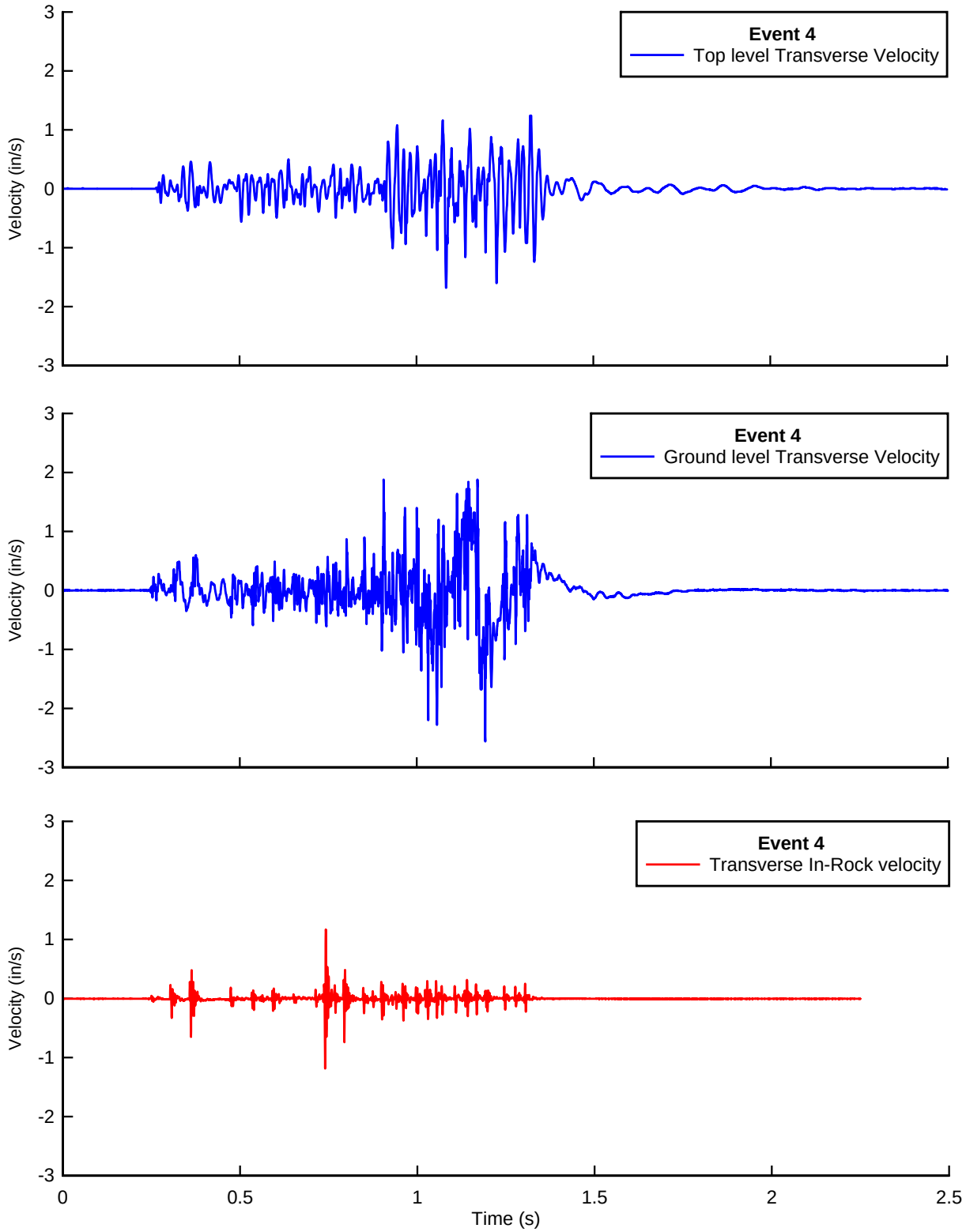

Figure D-4 - Recorded Velocity time histories in the Transverse Direction, in the rock and on the structure at ground level and top level, during Event #4

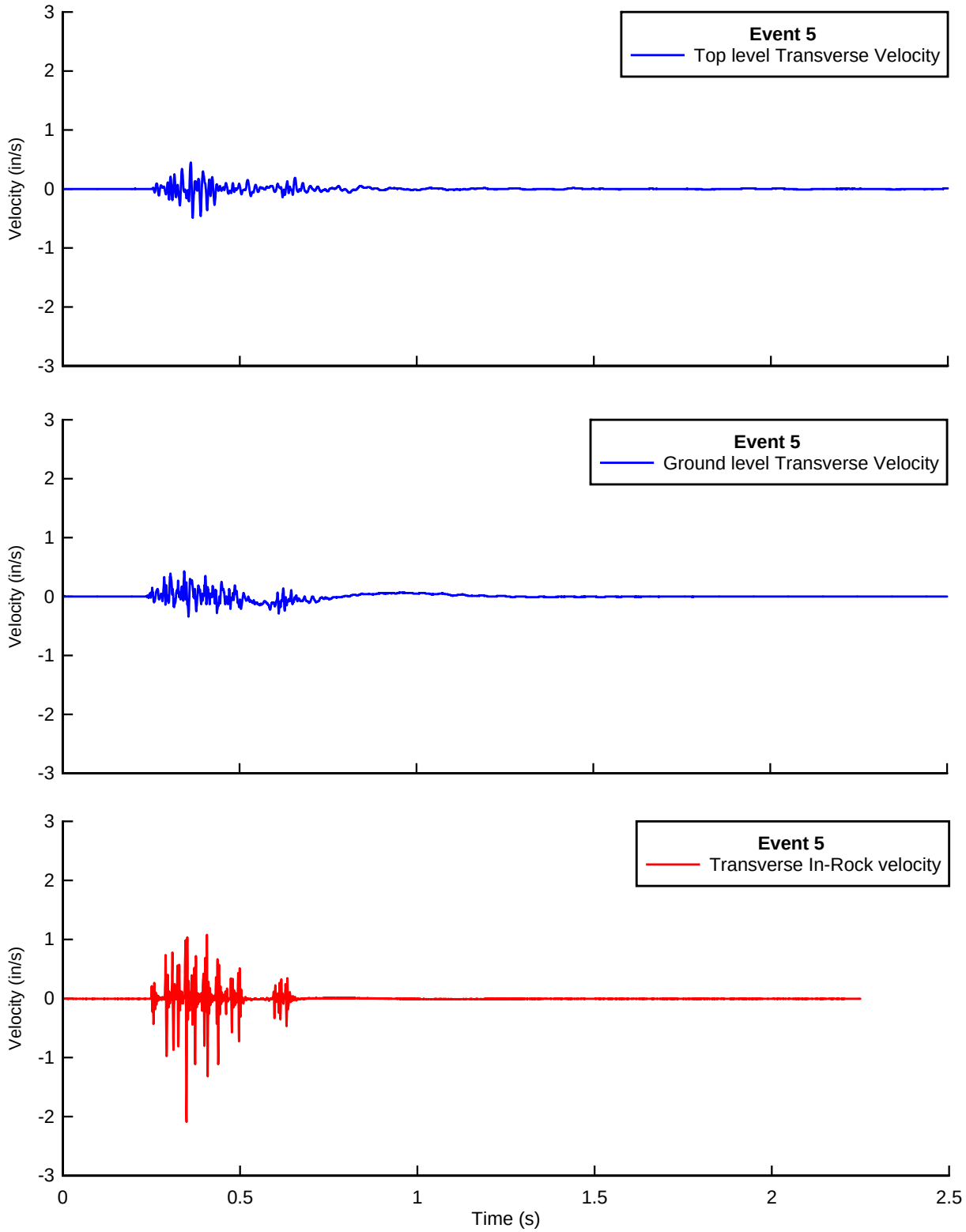

Figure D-5 - Recorded Velocity time histories in the Transverse Direction, in the rock and on the structure at ground level and top level, during Event #5

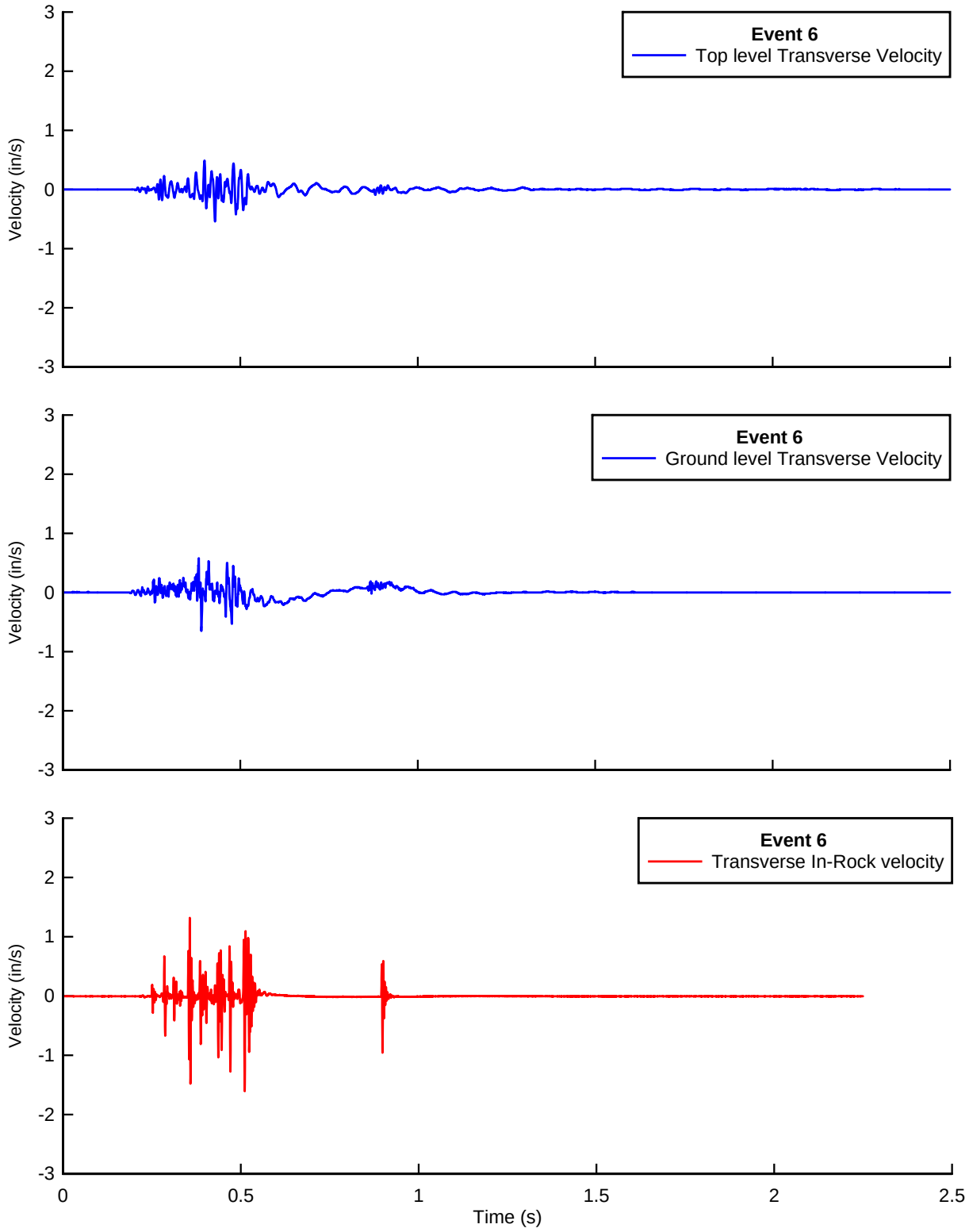

Figure D-6 - Recorded Velocity time histories in the Transverse Direction, in the rock and on the structure at ground level and top level, during Event #6

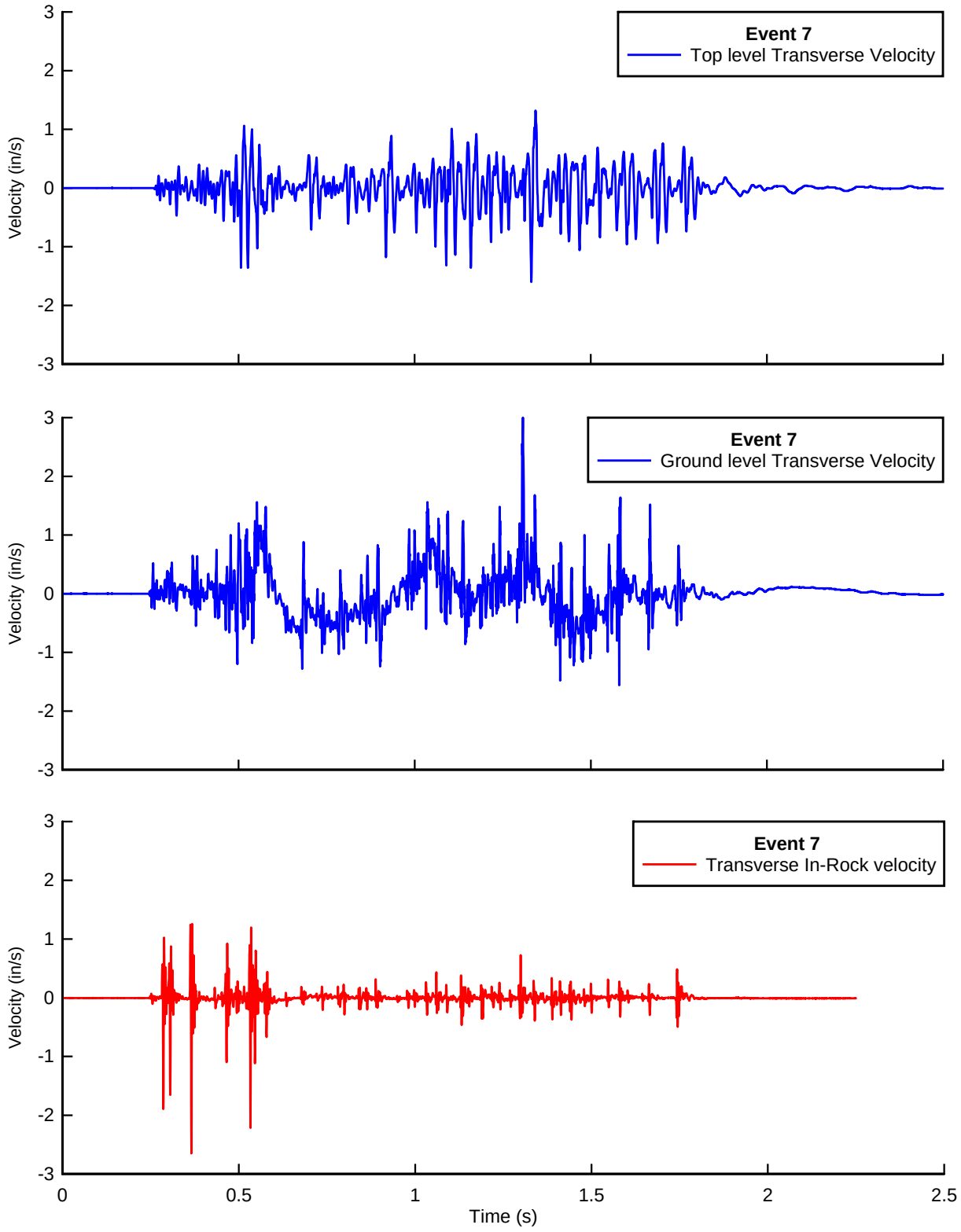

Figure D-7 - Recorded Velocity time histories in the Transverse Direction, in the rock and on the structure at ground level and top level, during Event #7

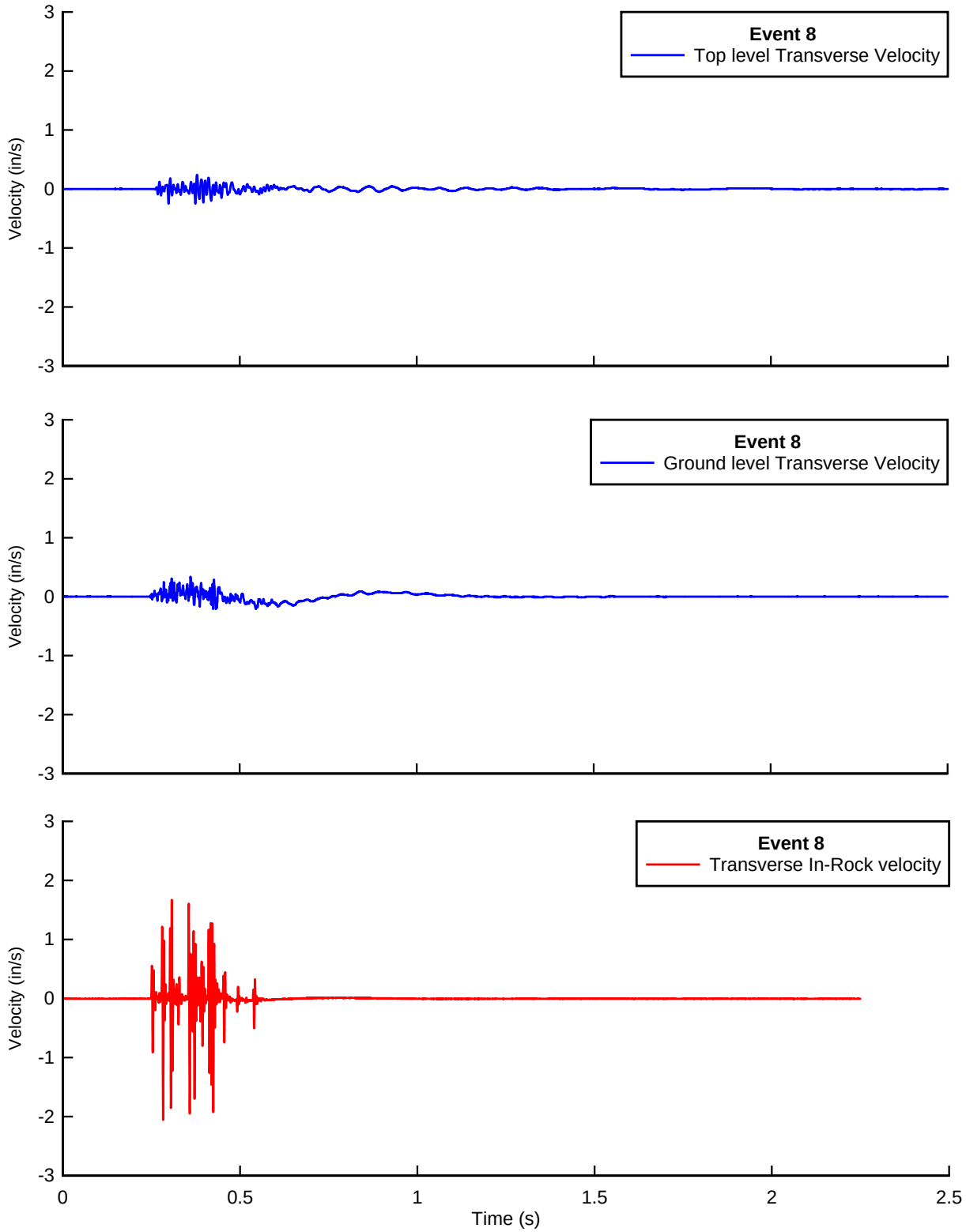

Figure D-8 - Recorded Velocity time histories in the Transverse Direction, in the rock and on the structure at ground level and top level, during Event #8

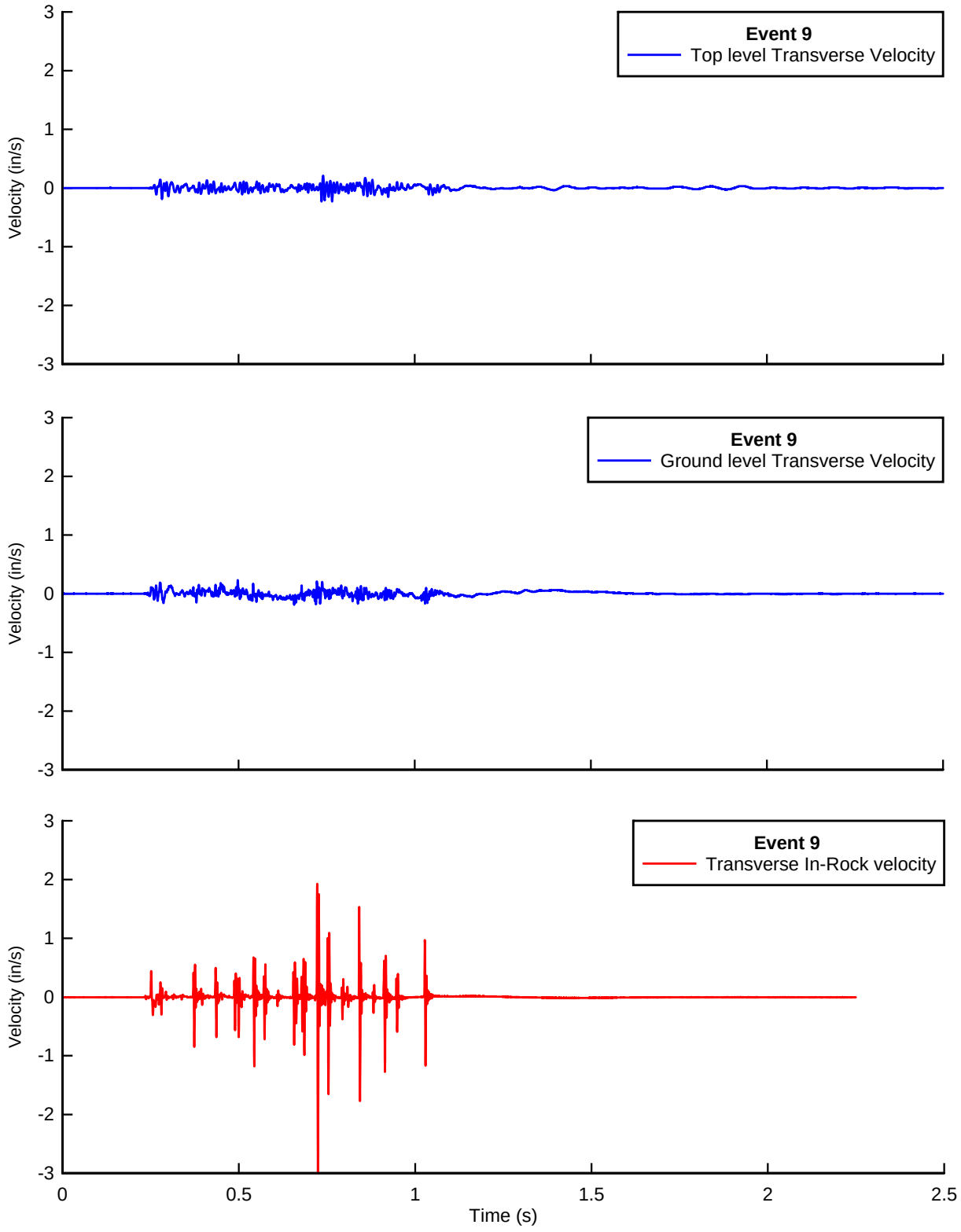

Figure D-9 - Recorded Velocity time histories in the Transverse Direction, in the rock and on the structure at ground level and top level, during Event #9

APPENDIX E – FREQUENCY AND AMPLIFICATION ANALYSIS FOR EVENTS 1, 3 AND 9

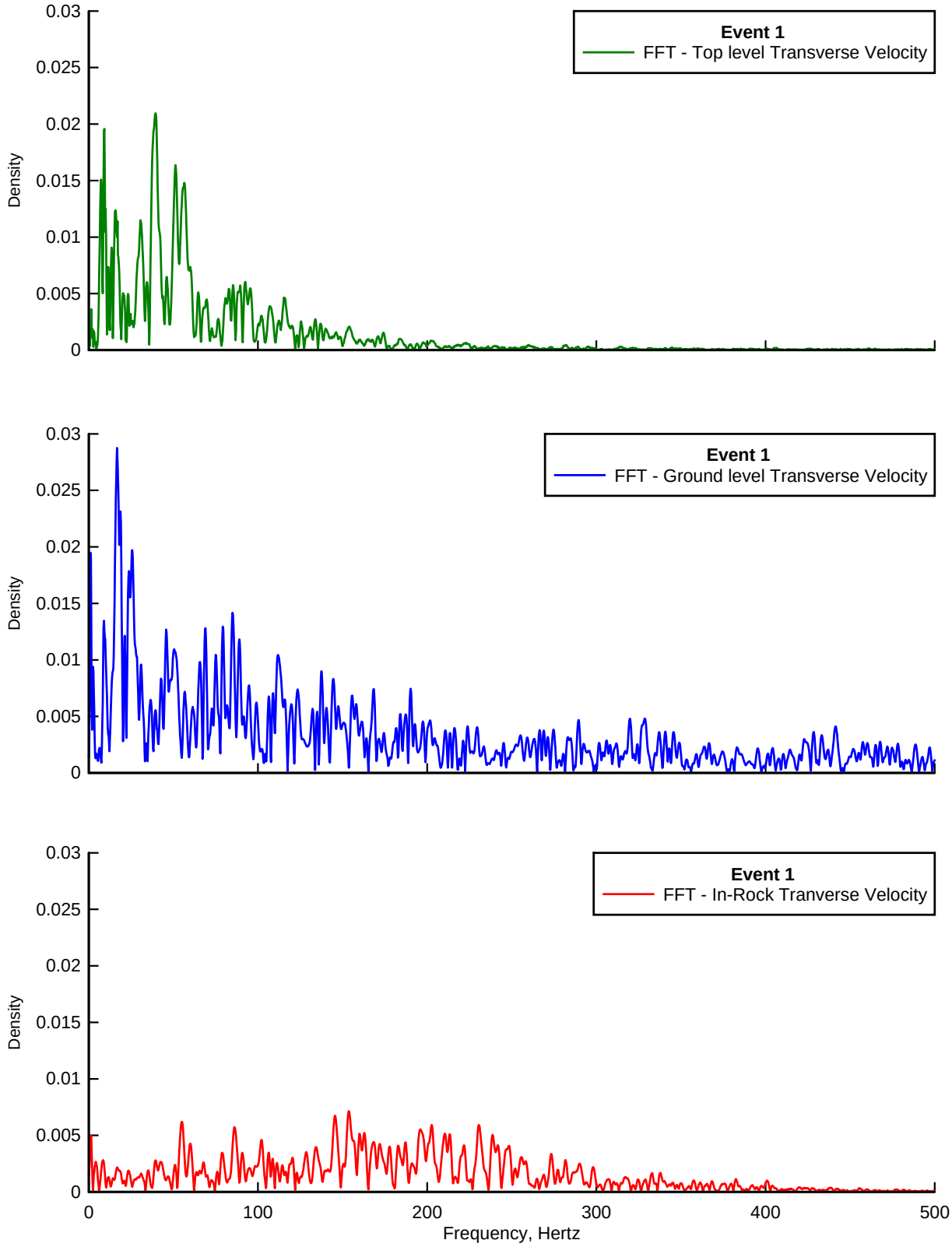

Figure E-1 - Fourier Frequency Analysis of Recorded Transverse Velocity time histories, on the structure and in the rock for Event #1

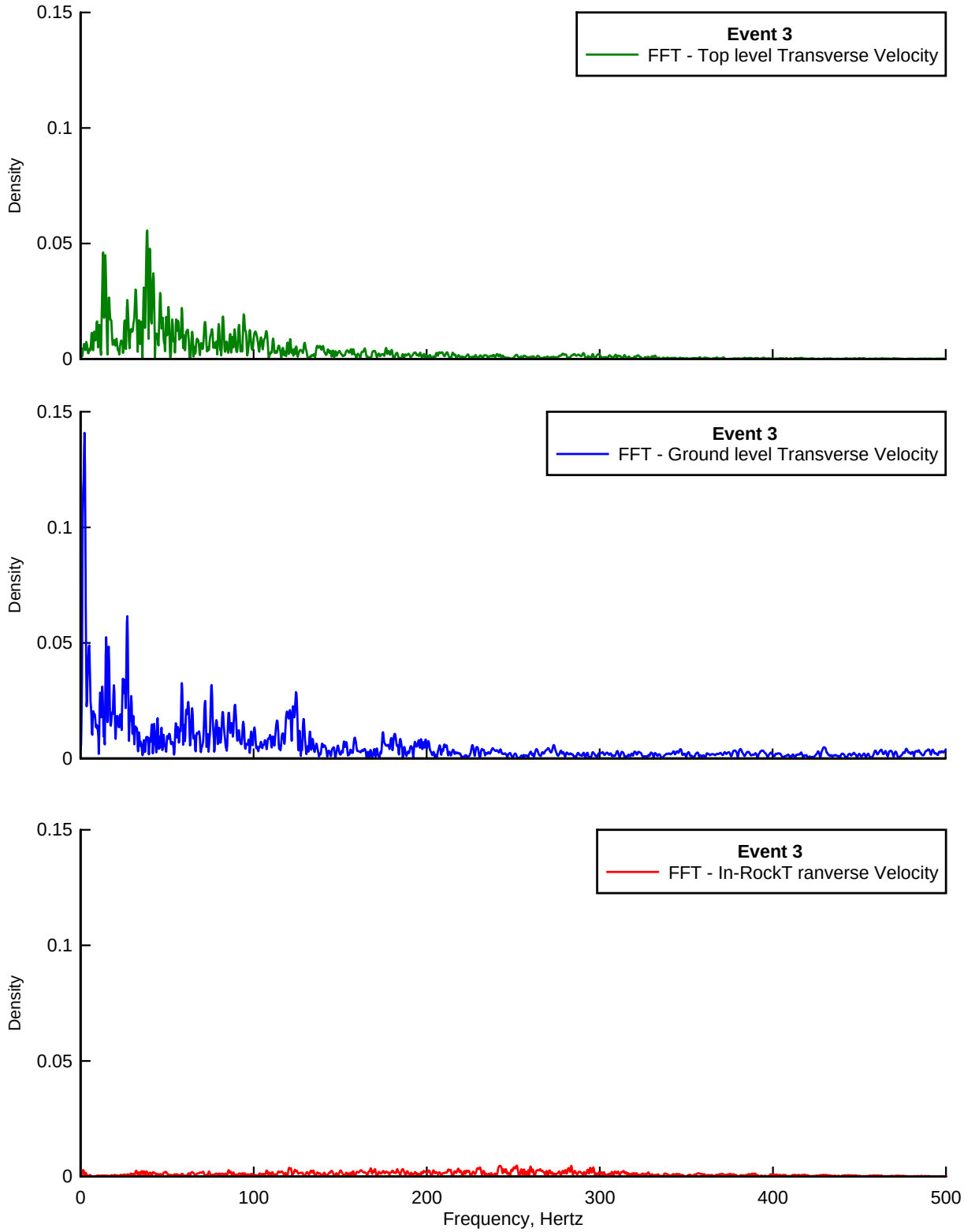

Figure E-2 - Fourier Frequency Analysis of Recorded Transverse Velocity time histories, on the structure and in the rock for Event #3

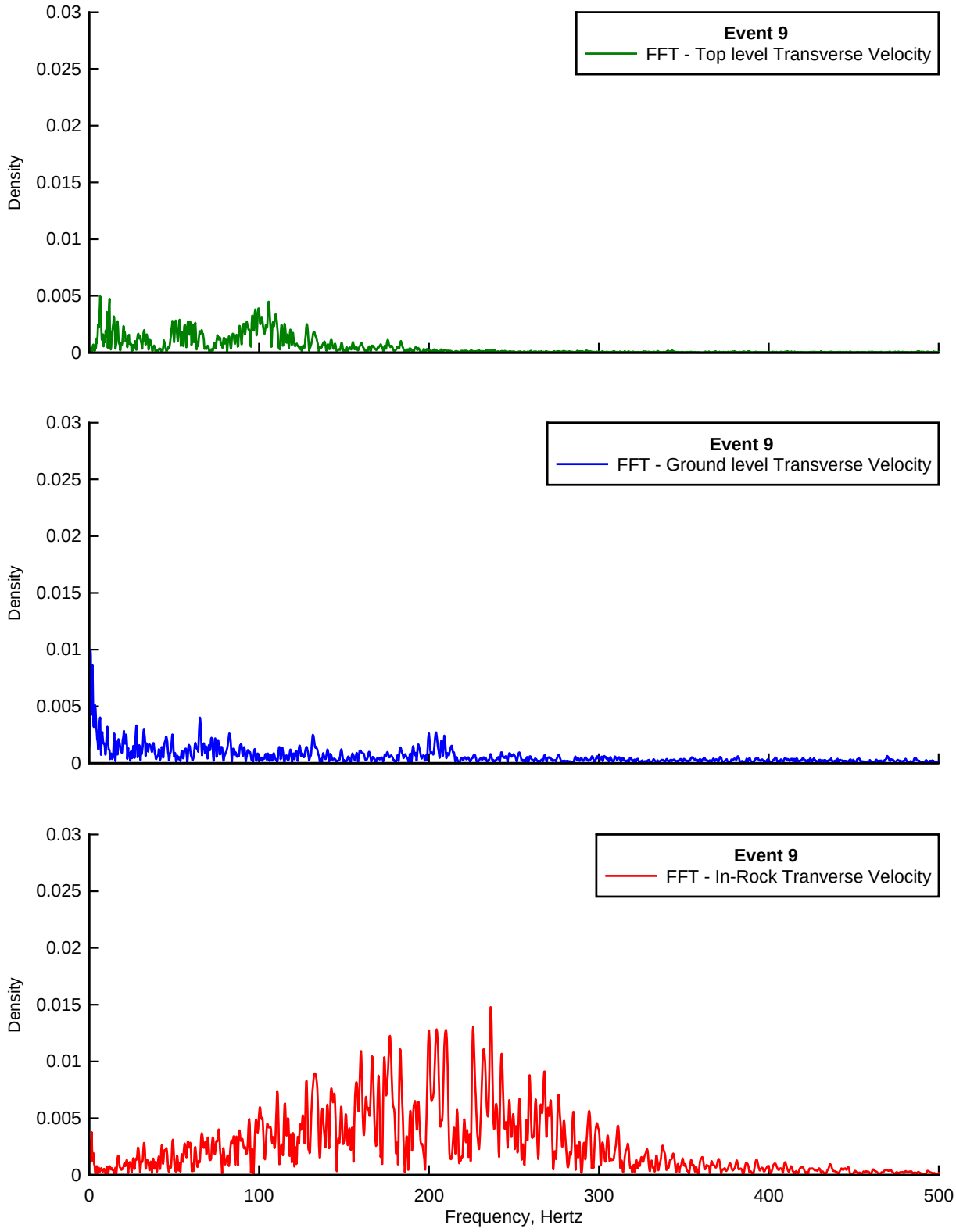

Figure E-3 - Fourier Frequency Analysis of Recorded Transverse Velocity time histories, on the structure and in the rock for Event #9